SYNTHESIS AND SYSTEMATIC EVALUATION OF ALTERNATING PYRIDINE–THIOPHENE OLIGOMERS

Dissertation zur Erlangung
der naturwissenschaftlichen Doktorwürde
(Dr. sc. nat.)

vorgelegt der
Mathematisch-naturwissenschaftlichen Fakultät
der Universität Zürich

von
Silvia Veleirinho de Oliveira Rocha
aus Brasilien

Promotionskomitee:
Prof. Dr. Jay S. Siegel (Vorsitz)
PD Dr. Nathaniel S. Finney (Leitung der Dissertation)
Prof. Dr. Kim K. Baldridge
Prof. Dr. Karl-Heinz Ernst
Prof. Dr. Nathan W. Luedtke

In memoriam patris.

ABSTRACT OF THE DISSERTATION

Synthesis and Systematic Evaluation of Alternating Pyridine–Thiophene Oligomers

by

Silvia Veleirinho de Oliveira Rocha

University of Zurich, 2012

Organic materials containing conjugated polymers have attracted a lot of attention in the past years, and have found many applications in photovoltaics, organic field effect transistors and emitting devices. The control of the bandgap magnitude in conjugated molecules is a very sought after capability, as it would be beneficial for a number of applications of these materials. In particular, a reduction of the bandgap would enhance the thermal population of the conduction band, increasing the number of charge carriers, which has the potential to improve the performance of such materials in electronic and optoelectronic devices. One approach to reducing the bandgap is known as the donor-acceptor (D–A) strategy, where the interaction between the donor and the acceptor units give rise to an increased double bond character between them, resulting in a more extended conjugation and therefore a smaller bandgap.

The use of polythiophenes and thiophene-containing polymers and oligomers has been a major subject in this field and although the combination of thiophene with electron-poor heterocycles in an alternating donor–acceptor manner has been significantly studied, pyridine-containing molecules are not abundant. In this thesis, the use of pyridine and thiophene as acceptor and donor moieties, respectively, will be discussed.

The synthesis of two series of oligomers and a series of dendrimers is described in this work. The two oligomeric series differ in the regiochemistry across the pyridine ring; a 2,6-disubstitution around the pyridine moiety characterizes the first series, called *2,6-series* throughout the thesis, while a 2,5-disubstitution pattern across the pyridine ring is the feature present in the second series, *2,5-series*. The dendrimeric series has a 2,4,5-trisubstituted pyridine ring as the core and branching points of the dendrimers. It is interesting to highlight that all the aryl–aryl bond formation reactions were done *via* Negishi cross coupling reaction, which proved to be the most successful for this system. Another noteworthy feature of the synthesis is the iterative approach that was applied in the preparation of the oligomers.

All the compounds had their photophysical properties characterized and a red shift is observed with increasing chain length for both the absorption and the emission spectra. In the case of the dendrimeric series, a particularly significant observation is the concentration-dependent absorption and emission spectra, where a red shift is observed with increasing concentration.

An interesting feature of pyridine-containing conjugated molecules is the fact that each pyridine unit provides a well-defined site for postsynthetic modification. Through protonation or Lewis acid coordination, a modulation of the optical properties can be obtained, since these affect the electronic properties of the pyridine unit, affording a moiety with better π-electron acceptor character. In fact, all the compounds were qualitatively characterized in their protonated form, and a red shift is observed in all cases for both absorption and emission properties.

Another interesting feature of the oligomeric series is their electrochemical behavior. Only the reduction of the species was observed in cyclic voltammetry experiments performed in THF, and it is remarkable that the longer oligomer in the *2,5-series* is capable of accepting up to five electrons.

ZUSAMMENFASSUNG

Synthese und systematische Evaluation von alternierenden Pyridin–Thiophen Oligomeren

von

Silvia Veleirinho de Oliveira Rocha

Universität Zürich, 2012

Organische Materialien basierend auf konjugierten Polymeren haben in den vergangenen Jahren zunehmend an Bedeutung gewonnen. Zu den Anwendungsbereichen gehören unter anderem Photovoltaikanlagen, Feldtransistoren und lumineszierende Materialien wie Leuchtdioden. Bis zum jetzigen Zeitpunkt ist es jedoch für eine Vielzahl von Anwendungen nicht möglich die Bandlückenenergien von solchen konjugierten Molekülen zu kontrollieren. Insbesondere eine Erniedrigung der Bandlückenenergie würde die Besetzung des Leitungsbandes fördern und die Anzahl an Ladungsträgern erhöhen. Folglich könnte dadurch die Effizienz von diesen Materialien in elektronischen und optoeletronischen Anwendungen potenziell verbessert werden. Eine Herangehensweise zur Reduktion der Bandlückenergie ist die sogenannte Donor-Akzeptor-Strategie. Dabei entstehen zwischen den Donor- und Akzeptor-Einheiten Wechselwirkungen, die Doppelbindungscharakter haben. Dies wiederum führt zu einer erweiterten Konjugation und schliesslich zu einer niedrigeren Bandlückenenergie.

Die Verwendung von Polythiophenen und Polymeren sowie Oligomeren, die Thiophene enthalten, nimmt in der Donor-Akzeptor-Strategie eine zentrale Stellung ein. Auch die alternierende Kombination von Thiophenen mit elektronenarmen Heterozyklen ist dabei Gegenstand der Forschung. Studien über die Applikation von Pyridin in Kombination mit Thiophen sind jedoch bis anhin selten. In dieser Arbeit wird der Gebrauch von Pyridin und Thiophen als Akzeptor- und Donor-Einheiten untersucht. Hierzu wurden zwei Serien von Oligomeren und eine Serie von Dendrimeren synthetisiert.

Die zwei Oligomer-Serien unterscheiden sich regiochemisch betrachtet bezüglich der Substitution am Pyridinring. Die erste Serie zeichnet sich durch Substitutionen an 2. und 6. Position aus (im folgenden 2,6-Serie genannt), wobei die zweite Serie Substitutionen an 2. und 5. Position aufweist (2,5-Serie). Die Dendrimer-Serie beinhaltet im Kern einen dreifach substituierten Pyridinring an 2., 4. und 5. Position sowie unterschiedliche Verzweigungen an

den Verknüpfungsstellen. Für alle Serien erwies sich dabei die Negishi-Kreuzkupplung als die geeignetste Reaktion zur Bildung der Aryl-Aryl Bindungen. Erwähnenswert ist ausserdem die iterative Herangehensweise zur Synthese der Oligomere.

Die Charakterisierung der photophysikalischen Eigenschaften der verschiedenen Verbindungen führte zur Beobachtung einer rot-Verschiebung mit zunehmender Kettenlänge der Oligomere. Dies gilt sowohl für die Absorptions- als auch Emissions-Spektren. Die Dendrimer-Serie zeigte eine Konzentrations-Abhängigkeit der Absorptions- und Emissions-Spektren, wobei eine rot-Verschiebung mit zunehmender Konzentration festgestellt wurde.

Eine interessante Besonderheit von konjugierten Molekülen mit Pyrdin ist die Möglichkeit von gezielten Veränderungen am Pyridinring nach der Synthese. Durch Protonierung oder Koordination einer Lewis-Säure können die Akzeptoreigenschaften des Pyridinrings verbessert werden, wodurch die optischen Charakteristika angepasst werden können. Demzufolge wurden alle Verbindungen in ihrer protonierten Form qualitativ charakterisiert und es wurde eine rot-Verschiebung für die Absorptions- und Emissionseigenschaften eruiert.

Ein weiteres interessantes Merkmal der Oligomer-Serie ist deren elektrochemisches Verhalten. Die durchgeführten Experimente mit zyklischer Voltammetrie in Tetrahydrofuran als Lösungsmittel führten zur Erkenntnis, dass nur Reduktionen beobachtet wurden. Es ist auch erwähnenswert, dass das längere Oligomer in der 2,5-Serie die Fähigkeit besitzt, bis zu fünf Elektronen aufzunehmen.

ACKOWLEDGEMENTS

Before I begin to describe the scientific work, I would like to thank the people that help me achieve this degree. First, I would like to thank PD Dr. Nathaniel Finney, my advisor, for accepting me in his group and for his constant and immense support and trust. I have definitely learned a lot from his experience, curiosity and creativity.

I would also like to thank Professor Jay Siegel, for his support and ideas throughout the course of my PhD and for being the chair of my thesis. In this sense, I would like to acknowledge Professor Kim Baldridge and Professor Nathan Luetdke for being in the committee of my thesis, and Professor Benjamin King for being the external reviewer and for his suggestions and comments on my work.

I am also grateful for the great infrastructure provided by the Institute of Organic Chemistry of the University of Zurich, in particular the NMR facilities and Professor Oliver Zerbe and the MS facilities led by PD Dr. Laurant Bigler, they were always very helpful in the moments of need.

Special thanks to Ylenia and Anna Veron for believing that it was a good idea to do a master based on my project; I am sorry if I did not help you more, but I did my best and I hope you enjoyed working with me.

Throughout the years as a PhD student, the people that taught me the most were my lab-mates and I am very thankful to have met all of them, because each had a special contribution to my development as a chemist and as a person: Amit, Anna, Arif, Ashley, Benno, Caroline, Daphne, Davide, Derik, Eoin, Fabiene, Fitore, Lee, Marek, Martin, Michael, Mireille, Nelli, Paola, Rahul, Roman, Simon, Swen, Yazmin. Also thanks to the people that were not directly in the lab but that have contributed to my life in the OCI: Anne, Becky, Mike, Ronaldo, Tereza, Yohann. In particular I would like to thank Ronaldo for his immense help in the beginning of my studies in Zurich.

I have definitely made friends for life during the time I spent in Zurich, so I would like to thank Davide, my Italian brother, for all his support during the hardest moments; Eoin, also known as the leprechaun, for all the laughs, the coffees chugged and the Guinness' cakes; Roman, gäu?!, for teaching me some Swiss German and for the encouragement at end; Derik, for helping me in the lab when I first arrived, teaching me to like beer more than I should and for his friendship even when I did not deserve it; Simon, for showing me the proper way of

working in a laboratory and for the shared glasses of wine; Paola, she was always there when you needed her and for being a great company at the aquafit class.

I also would like to thank the love of my life, Michi, meeting him was the best thing that happened to me in Zurich and now I could not imagine living without him.

Last but not least I would like to thank my family! My brothers Ricardo and Felipe, who, although sometimes silently, always encouraged me to pursue my studies. My Aunt, Rosa, and my Grandma, Izaira, who were constantly worried about my safety and health and super supportive. And to my parents, Silvina and Basilio (*in memory*) who have sacrificed a lot in order for me to study and be where I am; I hope I did not disappoint you, I am extremely grateful for all you have done for me and I will continue to make you proud.

TABLE OF CONTENTS

LIST OF FIGURES

LIST OF SCHEMES

LIST OF TABLES

CHAPTER 1

1 INTRODUCTION AND BACKGROUND – CONJUGATED SYSTEMS

As defined in the IUPAC Gold Book, *a conjugated system is a molecular entity whose structure may be represented as a system of alternating single and multiple bonds*;[1] the interaction between the *p*-orbitals in these systems gives rise to a delocalization of the bonds and is most commonly described by quantum mechanics. Delocalized π-bonds became especially important in the discovery of the conductance of polyacetylene in the late 70's, which later, in 2000, granted the Nobel Prize in Chemistry to Shirakawa, MacDiarmid, and Heeger.[2] Ever since, the fields of conjugated organic polymers, oligomers, and small molecules have attracted a lot of attention. Conjugated molecules are great candidates for applications as conducting and semiconducting materials because of their outstanding processability compared to the inorganic counterparts, and such materials were employed in the development of organic field-effect transistors (OFETs), organic light-emitting diodes (OLEDs), solar cells, and sensors.[3–6] π-Conjugated systems can be described by Hückel Molecular Orbital theory (HMO), which is a simple method that provides a remarkable understanding of the structure and properties of conjugated organic molecules and will be discussed in the following section.

1.1 Hückel Molecular Orbital Theory

The Hückel Molecular Orbital model was first reported in the early 30's and it describes the molecular orbitals of conjugate systems.[7,8] The theory assumes that the molecule is planar and that all the atoms are sp^2 hybridized and with one atomic *p* orbital left available for conjugation. Consequently, the sp^2-hybridized atoms are seen as a rigid framework where all the σ-C–C bonds are equal, and the hydrogen atoms are not taken into consideration. In other words, the model assumes that the σ and π systems can be treated separately and that σ and π bonds do not interact.

In the Hückel model, only the π system is considered and the atomic *p* orbitals are combined through a process know as linear combination of atomic orbitals, LCAO, to produce *delocalized* molecular π orbitals. Therefore, the *i*th molecular orbital, ψ_i, of a molecule

possessing k atoms can be written as in equation 1, where ϕ_k is the wave function for the p orbital in the kth carbon and c_k is a constant. Although the notion that there is a conservation of the total number of orbitals in the atomic and molecular systems might be intuitive, it is important to emphasize that the combination of n atomic orbitals gives rise to n molecular orbitals.[9,10]

$$\psi_i = c_1\phi_1 + c_1\phi_2 + \cdots + c_k\phi_k = \sum_{\mu=1}^{k} c_\mu\,\phi_\mu \tag{1}$$

The constant c_k conveys the contribution of each of the individual p atomic orbitals to the final molecular π orbital ψ_i; finding the contributions of each individual p atomic orbital allows us to depict the corresponding molecular orbitals. In the HMO theory, we assume that the Hamiltonian, $\mathcal{H}$, of the system is known and that the only components missing are the coefficients c_k. If the energy of the system is then minimized with respect to c_k by taking the partial derivatives of E with respect to all the c_k, one at a time,[i] the best possible estimate for the energy of the system according to this model is obtained.[11]

Using ethene as a simple model system, we can write a general π molecular orbital, ψ_π, as:

$$\psi_\pi = c_1\phi_1 + c_2\phi_2 \tag{2}$$

Using the modified version of the Schrödinger equation ($\mathcal{H}\psi = E\psi$) shown in equation 3 and substituting equation 2 in it, we get equation 4. When all the terms are multiplied and expanded we arrive at equation 5.

$$E = \frac{\int \psi^* \mathcal{H}\psi d\tau}{\int \psi^2 d\tau} \tag{3}$$

$$E = \frac{\int (c_1\phi_1 + c_2\phi_2)\mathcal{H}(c_1\phi_1 + c_2\phi_2)d\tau}{\int (c_1\phi_1 + c_2\phi_2)^2 d\tau} \tag{4}$$

$$E = \frac{\int (c_1\phi_1\mathcal{H}c_1\phi_1 + c_1\phi_1\mathcal{H}c_2\phi_2 + c_2\phi_2\mathcal{H}c_1\phi_1 + c_2\phi_2\mathcal{H}c_2\phi_2)d\tau}{\int (c_1^2\phi_1^2 + 2c_1c_2\phi_1\phi_2 + c_2^2\phi_2^2)d\tau} \tag{5}$$

[i] This is what is called the variational method, and its details will not be discussed here. See reference 11.

At this point it is useful to introduce some abbreviations and simplifying assumptions to the terms that appear in equation 5. It is also important to recognize that the Hamiltonian operator is Hermitian and therefore: $\int c_i\phi_i\mathcal{H}c_j\phi_j = \int c_j\phi_j\mathcal{H}c_i\phi_i$.

$$\int \phi_i \mathcal{H} \phi_i d\tau = H_{ii} \quad \text{Coulomb integral} \tag{6}$$

$$\int \phi_i \mathcal{H} \phi_j d\tau = H_{ij} \quad \text{resonance integral} \tag{7}$$

$$\int \phi_i \phi_i d\tau = S_{ii} \quad \text{normalization integral for identical atoms} \tag{8}$$

$$\int \phi_i \phi_j d\tau = S_{ij} \quad \text{overlap integral} \tag{9}$$

The Coulomb integral, H_{ii}, gives the energy of an electron in an isolated p orbital. This energy is estimated to be identical for all the atoms and its value is given as α, a negative number, since the reference (zero) value is an empty p orbital and an electron at infinite separation.

The resonance integral, H_{ij}, is as estimation of the extra stability when an electron is placed between the two p orbitals in consideration, in other words it represents the "strength of the π-electron bond between these atoms".[12] When the atoms considered are σ-bonded, this stabilization, a negative number, is given the symbol β and it is assumed to have the same value for all the atoms directly bonded. When the atoms are not directly bonded, the estimation of H_{ij} is a more difficult problem, and we can assume that it is in the range between 0 and β. In HMO theory, H_{ij} is defined as zero ($H_{ij} \equiv 0$) for all atoms that are not directly σ-bonded. This is an approximation that simplifies the analysis to a great extent, making it possible to apply the HMO method for a wide variety of molecules.

S_{ij} designates the overlap integral and it represents the overlap of the atomic p orbitals centered in atoms i and j. When $i = j$, the term S_{ii} is nothing more than the normalization integral and its value is defined as 1 for normalized atomic orbitals ($S_{ii} \equiv 1$). In the case where $i \neq j$, the overlap varies with the distance as well as the orientation of the two orbitals, and assigning a value for this term would be arbitrary in most of the cases, since the distances vary in

different molecules. Furthermore, assigning any value different than zero would complicate the treatment of the problem, so in the HMO method S_{ij} is defined as zero ($S_{ij} \equiv 0$).

Although some physical meaning was given to the assumptions given above, it is hard to justify such approximations nowadays, since the advances in computers and the development of computational methods make it possible to evaluate very complicated systems applying *ab initio* calculation methods. Nevertheless, the use of HMO utilizing all the approximations is a remarkably powerful educational tool in the understanding and visualization of conjugated systems molecular orbitals and trends within a class of compounds are generally correctly described.

Continuing with the ethene example, we can apply the variational method and compute $\frac{\partial E}{\partial c_1} = 0$, which gives us equation 10 after rearrangements and substitutions.[ii] Carrying out the same partial derivative with respect to c_2 gives us equation 11.

$$c_1(H_{11} - ES_{11}) + c_2(H_{12} - ES_{12}) = 0 \tag{10}$$

$$c_1(H_{21} - ES_{21}) + c_2(H_{22} - ES_{22}) = 0 \tag{11}$$

As stated before, in the HMO theory it is assumed that the only unknown values are c_1 and c_2. Therefore, possessing two equations and two unknowns allows us to write a secular determinant of the coefficients of the unknown variables, equation 12; it is important to note that the trivial solution ($c_1 = c_2 = 0$) has no physical meaning.

$$\begin{vmatrix} H_{11} - ES_{11} & H_{12} - ES_{12} \\ H_{21} - ES_{21} & H_{22} - ES_{22} \end{vmatrix} = 0 \tag{12}$$

The secular determinant in equation 12 can be rewritten applying the approximations discussed earlier, namely: $H_{ii} = \alpha$, $H_{ij} = \beta$ (for σ-bonded atoms), $H_{ij} = 0$ (for atoms not σ-bonded), $S_{ii} = 1$, $S_{ij} = 0$.

$$\begin{vmatrix} \alpha - E & \beta \\ \beta & \alpha - E \end{vmatrix} = 0 \tag{13}$$

Solving the determinant, two values for the energy of the molecular orbitals are found $E = \alpha + \beta$ and $E = \alpha - \beta$.[iii] This values can then be substituted in equations 10 and 11 and we

[ii] For detailed treatment please refer to reference 11.

find $c_1 = c_2$. Applying the normalization condition for the molecular orbital, $\int \psi_\pi^* \psi_\pi d\tau = 1$, where $\psi_\pi = c_1\phi_1 + c_2\phi_2$, gives us the values for the coefficients. The solution for ethene is completed and we can write the two molecular orbitals with the corresponding energy values, equations 14 and 15. A depiction of the molecular orbitals for ethene and other linear conjugated systems is shown in **Figure 1.1**. The illustration of the molecular orbitals is accomplished from the atomic p orbitals coefficients, c_k, obtained after applying the HMO method described above utilizing the *Simple Hückel Molecular Orbital Calculator* tool available online as a Java plugin.[13,iv]

$$\psi_1 = \frac{1}{\sqrt{2}}\phi_1 + \frac{1}{\sqrt{2}}\phi_2 \qquad E_1 = \alpha + \beta \tag{14}$$

$$\psi_2 = \frac{1}{\sqrt{2}}\phi_1 - \frac{1}{\sqrt{2}}\phi_2 \qquad E_2 = \alpha - \beta \tag{15}$$

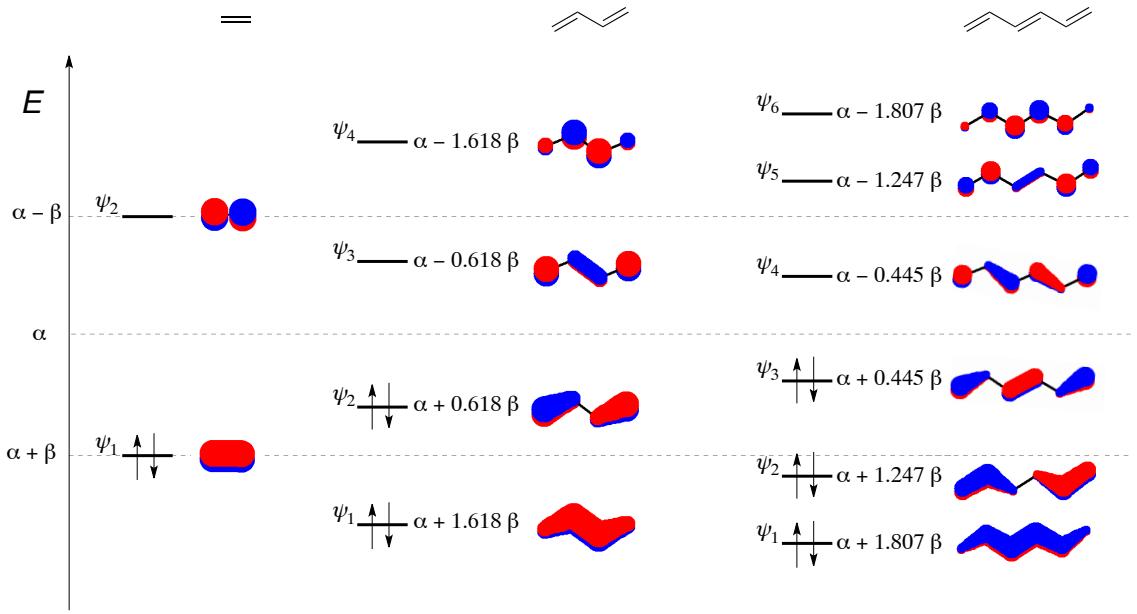

Figure 1.1: *Depiction of the molecular π orbitals for ethene, 1,3-butadiene and 1,3,5-hexatriene. The orbital plots and relative energies were calculated using HMO theory through the SHMO Calculator tool available online as a Java plugin.*[13]

[iii] A useful strategy to solve the determinant in equation 13 is to divide all the terms by β and to represent $\frac{\alpha - E}{\beta} = x$, arriving at the determinant $\begin{vmatrix} x & 1 \\ 1 & x \end{vmatrix} = 0$. Solving the latter for x and introducing the solutions into the definition of x gives the energy values mentioned.

[iv] The SHMO Calculator tool is based on the theoretical description from Chapters 3 and 5 of reference 10.

For a general linear conjugated system containing *k* atoms, the secular determinant can be written as shown in equation 16. To illustrate the secular determinant for longer systems after applying the HMO definitions and approximations, an example for 1,3,5-hexatriene in equation 17 is presented.

$$\begin{vmatrix} H_{11} - ES_{11} & \cdots & H_{1k} - ES_{1k} \\ \vdots & \ddots & \vdots \\ H_{k1} - ES_{k1} & \cdots & H_{kk} - ES_{kk} \end{vmatrix} = 0 \tag{16}$$

$$\begin{vmatrix} \alpha - E & \beta & 0 & 0 & 0 & 0 \\ \beta & \alpha - E & \beta & 0 & 0 & 0 \\ 0 & \beta & \alpha - E & \beta & 0 & 0 \\ 0 & 0 & \beta & \alpha - E & \beta & 0 \\ 0 & 0 & 0 & \beta & \alpha - E & \beta \\ 0 & 0 & 0 & 0 & \beta & \alpha - E \end{vmatrix} = 0 \tag{17}$$

In fact, the essence of the Hückel Molecular Orbital theory is depicted in **Figure 1.1**; since it delineates the relative energy levels with respect to α and β as well as it illustrates the corresponding molecular orbitals. In the HMO method it is also found that for systems containing only carbon atoms, the bonding and anti-bonding orbitals are symmetrically placed bellow and above the non-bonding energy level ($E = \alpha$), respectively. Another interesting aspect of this theory is that the number of nodes increases with increasing energy level, and for a linear system containing an even number of carbons, the molecular orbital ψ_n will show $n - 1$ nodes. All of these aspects of the HMO theory make it possible to predict the general features of conjugated systems even without performing all the calculations.

1.1.1 Cyclic Conjugated Systems: Benzene

Applying the HMO method to cyclic conjugated systems like benzene provides different patterns in the energy levels. Analyzing the secular determinant for benzene, expressed in equation 18, we can see that in this case the anti-diagonal has two additional entries when compared to the linear system in equation 17. This is the case in benzene because atoms 1 and 6 are σ-bonded and therefore H_{16} and H_{61} cannot be neglected anymore.

$$\begin{vmatrix} \alpha - E & \beta & 0 & 0 & 0 & \beta \\ \beta & \alpha - E & \beta & 0 & 0 & 0 \\ 0 & \beta & \alpha - E & \beta & 0 & 0 \\ 0 & 0 & \beta & \alpha - E & \beta & 0 \\ 0 & 0 & 0 & \beta & \alpha - E & \beta \\ \beta & 0 & 0 & 0 & \beta & \alpha - E \end{vmatrix} = 0 \qquad (18)$$

Solving the determinant in equation 18 and applying the normalization conditions for the molecular orbitals allows us to draw **Figure 1.2**, where a depiction of the orbitals as well as their relative energy levels are shown. It is interesting to note that two sets of degenerate orbitals are found, this is the case because of the symmetry of the system. Benzene belongs to the $\mathbf{D}_{6h}$ point group and, in fact, its secular determinant can be factored into two 1×1 and two 2×2 determinants when the irreducible representations of the set of atomic orbitals is used. This set of irreducible representations of the atomic orbitals is directly reflected on the symmetry and energy levels of the molecular orbitals.[14]

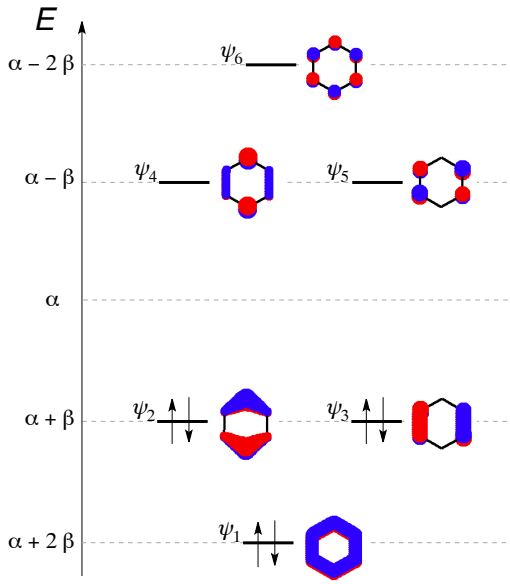

Figure 1.2: *Representation of the molecular orbitals of benzene and their relative energy levels. Calculated using HMO theory through the SHMO Calculator tool available online as a Java plugin.*[13]

1.1.2 Introduction of Heteroatoms

The HMO theory can also be applied to conjugated systems containing heteroatoms and it is done so treating the heteroatom as a perturbation to the system. The constants α and β are defined for carbon atoms and they represent the core energy of an electron localized in a $2p$

atomic orbital and the energy associated with the interaction of an electron with two neighboring carbon $2p$ atomic orbitals, respectively. These constants can then be modified to represent heteroatoms and this is achieved with the definition of parameters that depend on the type of heteroatom as well as on its coordination number. The heteroatomic parameters are given the symbols h_X and k_{XY}; h_X is specific for each heteroatom and its corresponding coordination number (for the atoms where this is applicable) and k_{XY} concerns the interaction of two different atoms. The expressions for α_X and β_{XY} are shown in equations 19 and 20.

$$\alpha_X = \alpha + h_X|\beta| \tag{19}$$

$$\beta_{XY} = k_{XY}|\beta| \tag{20}$$

A list of semiempirical parameters for heteroatoms based on Pariser-Parr-Pople calculations was developed in the early 80's and is shown for selected atoms in **Table 1.1**.[15] Although interactions between heteroatoms can also be considered, the values on **Table 1.1** are shown only for interactions between a carbon center and a heteroatom.

Table 1.1: *List of parameters h_X and k_{XY} for selected heteroatoms.*[15]

X	number of electrons	h_X	k_{XC}
C[a]	1	0.00	−1.00
N2[b]	1	−0.51	−1.02
N3[a]	2	−1.37	−0.89
O1[c]	1	−0.97	−1.06
O2[b]	2	−2.09	−0.66
S1[c]	1	−0.46	−0.81
S2[b]	2	−1.11	−0.69
F[c]	2	−2.71	−0.52
Cl[c]	2	−1.48	−0.62

a) tricoordinated, planar geometry; b) dicoordinated; c) monocoordinated.

When the values in **Table 1.1** are examined, it is possible to observe that the value for tricoordinated nitrogen $k_{N3C} = -0.89$ and for dicoordinated oxygen $k_{O2C} = -0.66$ are smaller compared to the value for a carbon atom $k_{CC} = -1.00$, this is a reflection of the size of the orbitals, which are smaller in the case of the heteroatoms due to their greater electronegativity; this is also reflected in the h_X parameter, which increases in absolute value with increasing electronegativity. If the two parameters k_{N2C} and k_{N3C} for nitrogen centers are considered, a dicoordinated center shows a greater value than a tricoordinated center, which is a reflection of

the reduced effective electronegativity in the former, since there are more remaining nonbonded electrons in *p* orbitals.

In the context of this work, the two most relevant conjugated heterocycles are pyridine and thiophene and there is an enormous amount of applications of molecules containing these building blocks. The molecular orbitals of these heterocycles can be computed applying the HMO method utilizing the heteroatom parameters described above, which allows us to draw **Figure 1.3**, where a depiction of the orbitals and their respective energy level is shown.

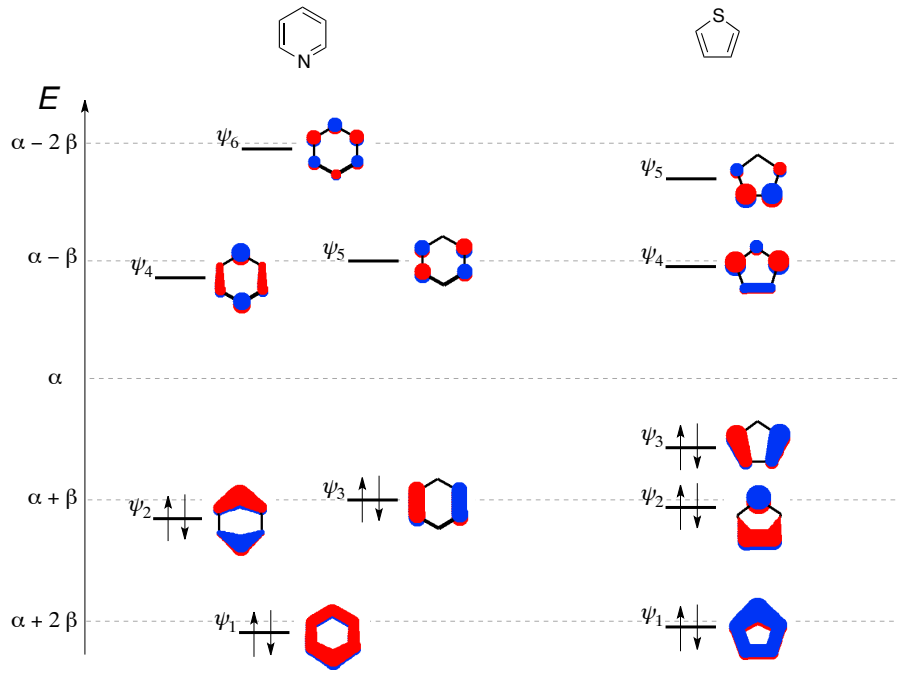

Figure 1.3: *Representation of the molecular orbitals and their relative energy levels for pyridine and thiophene. The orbital plots and energies were calculated using HMO theory through the SHMO Calculator (Simple Hückel Molecular Orbital Calculator) tool available online as a Java plugin.*[13]

It is important to note that the orbitals for pyridine resemble in many aspects the orbitals found for benzene, but many differences are also found. The first similar aspect is the shape of the orbitals, and the differences seen here are the coefficients for the different atoms, in special the coefficient for the nitrogen atom is bigger compared to the carbon atoms in the case ψ_1 and smaller in the case of ψ_6. Another important difference is the fact that now the symmetry of the molecule is $\mathbf{C}_{2v}$ (which is lower compared to $\mathbf{D}_{6h}$ for benzene) and therefore the molecular orbitals do not appear as two degenerate pairs anymore. In addition, the introduction of the heteroatoms causes the LUMO to be at a lower level when we compare the

heterocycles to the all-carbon counterparts; pyridine is compared to benzene while thiophene is compared to cyclopentadienyl anion.[v]

With this basic notion of the molecular orbitals in conjugated systems, a discussion of conjugated oligomers and their properties will be carried out in the next sections.

1.2 Conjugated Organic Materials

Conjugated organic molecules are great candidates for applications as conducting and semiconducting materials and polythiophenes are amongst the most employed conjugated polymers.[16] This is a reflection of the stability of polythiophenes as well as the ease with which their optical, electronic and material properties can be tuned by structural modifications.[17] It must be pointed out that predicting which structural modifications lead to desired changes in properties is very difficult and most often this is done experimentally by arduous synthesis followed by characterization.

The energy levels of conjugated polymers are similar to those of inorganic semiconductors; both have the electrons distributed in bands rather than in discrete levels. The interaction between the π orbitals of the monomers leads to the formation of the band structures in conjugated polymers; this can be seen in the illustration of the molecular orbitals of oligothiophenes, **Figure 1.4**.

[v] The levels for cyclopentadienyl anion (Cp^-) are not shown here, but can be found in reference 9. Its LUMO is at $E_{\mathrm{LUMO}}^{\mathrm{Cp}^-} = \alpha - 1.618\,\beta$ while the LUMO for thiophene is at a lower energy $E_{\mathrm{LUMO}}^{\mathrm{TH}} = \alpha - 0.967\,\beta$.

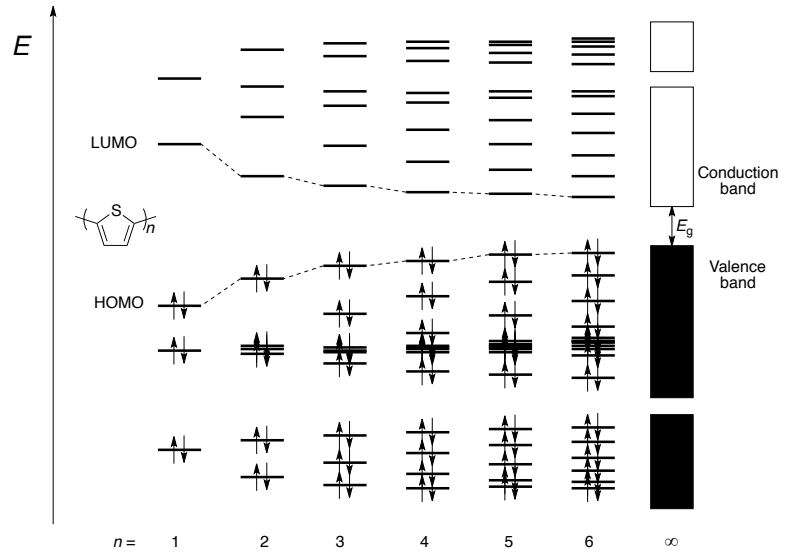

Figure 1.4: *Relative energy levels of oligothiophenes. Calculated using HMO theory through the SHMO Calculator.*[13]

With increasing oligomer length, a clustering of the orbitals is observed and this leads to the formation of the bands at infinite length and idealized conjugation. The relative energy levels shown in **Figure 1.4** were calculated through the HMO method. The band that is derived from the HOMO of the monomers is called valence band and it is an electron-filled band in the final polymer, the band derived from the LUMO of the monomers is called conduction band; these names were adopted to correspond to the inorganic semiconductors nomenclature. Likewise, the band gap in conjugated polymers is given the symbol E_g, and it symbolizes the energy difference between the conduction and the valence band. Although the terms used in band theory are going to be used in this thesis, a theory that better explains electrical conductivity and semiconductivity properties is the Mott–Hubbard model,[18] which will not be discussed here.

The control of the bandgap magnitude in conjugated polymers is a very sought after capability, as it would be beneficial for a number of applications of these materials. In particular, a reduction of the bandgap would enhance the thermal population of the conduction band, increasing the number of charge carriers, which has the potential to improve the performance of such materials in electronic and optoelectronic devices.[19]

To achieve a smaller band gap in conjugated polymers, a maximization of the conjugation across the backbone is crucial, and this can be accomplished utilizing alternating donor and acceptor building blocks, also referred to as π-electron rich and π-electron deficient conjugated moieties, respectively. One case where this has been demonstrated is in thiophene

polymers where there are two alternating thiophene units, one possessing a donor and the other an acceptor functional group.

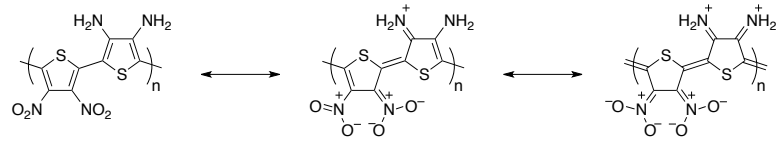

1

Scheme 1.1: *Donor–acceptor (D–A) polymer and its mesomeric structures showing the backbone conjugation between the units.*[20]

The backbone conjugation of donor–acceptor (D–A) polymer **1** can be demonstrated through the mesomeric structures that can be written for this molecule, **Scheme 1.1**.[20] In this example, the nitro group acts as the acceptor unity while the amino group serves as the donor moiety. In accordance with the mesomeric structures, the authors state that a large zwitterion character is present in the polymer, since experimental evidence such as unusually small optical band gap of 1.4 eV in solution and lack of fluorescence, combined with a high solubility in polar solvents such as THF and DMF points towards that assumption. HMO theory can be used to assess the band gap of this system and the impact of the donor and acceptor subunits; indeed, when the HMO method is applied to oligomer **2**, representing polymer **1**, a lower HOMO/LUMO gap is observed when donor and acceptor building blocks are present in the same structure in contrast to unsubstituted thiophene **3** and donor-only **4** or acceptor-only **5** oligomers, **Table 1.2**. In fact, the HMO results show the same trend as reported for the experimental optical band gaps, since the value for the D–A polymer is smaller than for the unsubstituted thiophene case.

Table 1.2: *Energy levels for donor–acceptor thiophene oligomers, calculated using SHMO; and the experimental bandgap for the respective polymers.*

Oligomer	HOMO and LUMO energies	ΔE	$E_g{}^a$ / eV
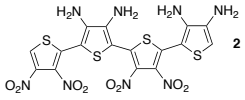 2	$E_{\mathrm{LUMO}} = \alpha - 0.277\,\beta$ $E_{\mathrm{HOMO}} = \alpha + 0.196\,\beta$	$0.473\,\beta$	1.4 [20]
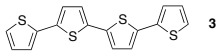 3	$E_{\mathrm{LUMO}} = \alpha - 0.517\,\beta$ $E_{\mathrm{HOMO}} = \alpha + 0.151\,\beta$	$0.668\,\beta$	1.94 [21]
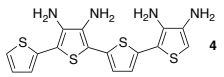 4	$E_{\mathrm{LUMO}} = \alpha - 0.582\,\beta$ $E_{\mathrm{HOMO}} = \alpha + 0.041\,\beta$	$0.623\,\beta$	–
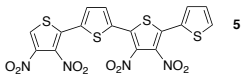 5	$E_{\mathrm{LUMO}} = \alpha - 0.241\,\beta$ $E_{\mathrm{HOMO}} = \alpha + 0.280\,\beta$	$0.521\,\beta$	–

a) experimental band gap estimated from the onset of the absorption spectra of the corresponding polymers in solution.

The D–A concept has been widely applied in polymers,[22] not only as alternating subunits but also in block copolymers consisting of donor and acceptor block polymers where they are linked by a third conjugated polymeric unit.[23] In general, the behavior of the resulting polymer in fabricated devices, either a p-type (hole transporter) or an n-type (electron transporter) component, is highly dependent on the acceptor unit utilized,[24,25] and the exact characteristics of an acceptor unit which will lead to certain properties are still unclear. An important measure is the electron affinity of the acceptor unit, as this is correlated to how susceptible each unit is to accept electrons.

In terms of molecular orbitals, the donor and the acceptor portions differ on the energy levels of the frontier orbitals. The energy level of the donor HOMO is at a higher level when compared to the corresponding acceptor HOMO, while the acceptor LUMO is at a lower energy level compared to the analogous donor orbital, **Figure 1.5**. As a result, the hybridization of the D and A individual orbitals gives rise to a molecule (D–A) that exhibits a lower HOMO/LUMO gap. Elongation of the chain utilizing this D–A unit would then afford a polymer that has a low bandgap.[26]

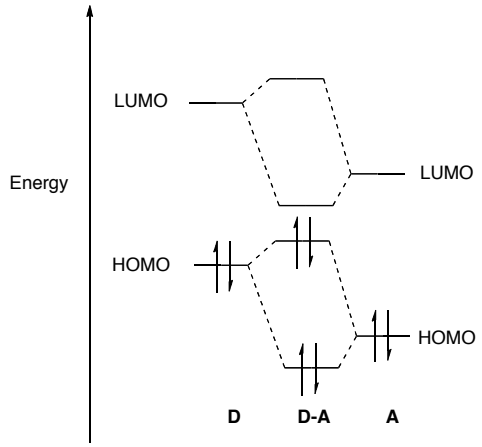

Figure 1.5: *Depiction of the hybridization between a donor (D) and an acceptor (A) unit. The resultant D–A unit has a smaller HOMO/LUMO gap.*[26]

The introduction of nitrogen-containing heterocycles as the acceptor unit has proven to be one of the most effective strategies in the construction of D–A polymers,[27,28] since they are, in general, electron poor conjugated units.[vi] The use of pyridine, the simplest N-containing conjugated heterocycle, has been demonstrated in many examples.[29,30] Pyridine is a unique building block, since it can be easily protonated or used as a ligand in the construction of metal complexes, both strategies have been applied in the studies of pyridine–containing conjugated polymers and a variety of hybrid conjugated and redox materials have been reported.[31–34]

Recently, Izuhara and Swager reported conjugated polymers that incorporate pyridine units in its charged form, as a pyridinium ion.[35,36] The polymers reported are shown in **Table 1.3**, and the pyridinium polymers, **6-8b**, were found to be electron-accepting (n-type) materials exhibiting high electrical conductivity. Analyzing the structure of the polymers, we can consider that the electron-accepting unit in the polymers is the pyridine phenylene, for series **a**, and the pyridinium phenylene, for series **b**. In the case of polymers **7a-b**, the presence of a thiophene unit in an alternating D–A manner leads to a red shift in the absorption maxima and a decrease of the bandgap in comparison to the other polymers in the same series.

[vi] One exception is pyrrole, which is a N-containing conjugated heterocycle but is electron-rich. This is the case because the nitrogen atom has no direct π-bond to the neighboring carbon atoms and therefore contributes with two electrons to the π-system.

Table 1.3: *Phenylene piridinium polymers and the respective representative properties.*[35]

Polymer	λ_{max}[a] / nm	E_g[b] / eV	Polymer	λ_{max}[c] / nm	E_g[b] / eV
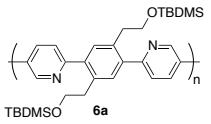 **6a**	322	3.49	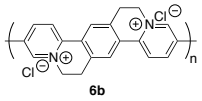 **6b**	431	2.56
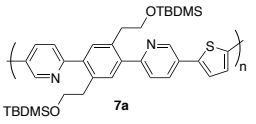 **7a**	373	3.02	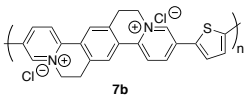 **7b**	483	2.16
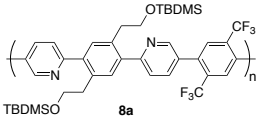 **8a**	300	3.62	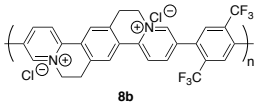 **8b**	376	2.95

a) solution in THF; b) experimental band gap estimated from the onset of the absorption spectra of the corresponding polymer in solution; c) solution in methanol.

An additional aspect of polymers **6-8** that should be highlighted is the fact that a lower bandgap as well as a red shift in the absorption maxima are observed when the pyridinium units are introduced. Although the authors argue that this is due to the fact that the ethylene bridges force a planar conformation across the pyridinium phenylene moiety, a complementary argument should be considered. The pyridium unit is a much better electron acceptor when compared to pyridine; the conjugation across the whole backbone when a D–A system is in place should therefore increase in the presence of the pyridinium subuntis, and this is what is observed for polymer **7b**, which exhibits the lowest bandgap among all the polymers. Furthermore, the bandgap reported for **7a** is comparable to the one of **8b**, leading us to reason that the D–A aspect of polymers **7** has a bigger impact in the properties.

Although the use of conjugated polymers is important in a variety of applications,[6,37] the intrinsic polydisperse character of polymers, together with processability issues associated with large polymer chains, results in difficulties to consistently prepare materials with the same characteristics. The use of oligomers has emerged as a general tendency in the field of conjugated materials.[38] Although the preparation of oligomers is more laborious compared to polymers, their defined structure and modisperse character are attractive features in the fabrication of films for solar cells, OFETs and OLEDs.[39]

One of the advantages of the study of oligomers series is the employment of systematic analyses that correlate the structure, many times length, to the properties observed.[40,41] The benefit associated with such studies is a deeper understanding of how the structure relates to properties and it assists in attempts to rationalize modifications that could be performed to the structure and would lead to specific designed characteristics. More details about studies correlating photophysical properties to oligomer length are given in Chapter 3.

Another trend in the field of conjugated materials has been the use of branched three-dimensional molecules called dendrimers.[42–45] The term dendrimer is derived from "δενδρον", which is the Greek word for tree; this name was given because of the branched structure of this class of molecules, which resembles the branches of a tree. In general, dendrimers are symmetrical around the core, which is surrounded by branches, and each branch also has branching points, which can be of the same kind as the core or of different nature. Each branching point is given a generation number, the core is called generation zero (G0) and the successive branching points are given consecutive numbers, which are relative to their distance from the core; therefore, a generation two (G2) branching point is one branching point away from the core.

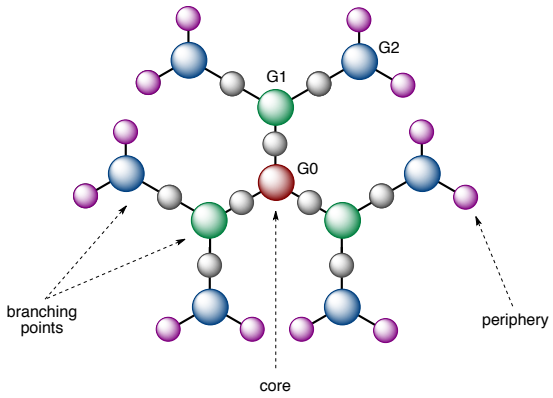

Figure 1.6: *Representation of a general dendrimer and the respective names used to define the different features of the structure.*

Dendrimers exhibit some of the same characteristics of oligomers: both are monodisperse species, in contrast to the polydispersity present in polymers, but differ in the three-dimensional aspect of the structure; while oligomers are one-dimensional linear species, dendrimers have more complicated shape, a three-dimensional primary structure.[46] Oligomers and polymers can also adopt a secondary three-dimensional assembly, but the nature of the primary structure is linear. The three-dimensional aspect of dendrimeric structures is of great

importance, and in dendrimers composed of conjugated building blocks, the molecular size has been proven to cause great impact in the properties.[47–50]

1.3 Utilizing Pyridine and Thiophene as Building Blocks in Conjugated Oligomers

Considering that pyridine and thiophene are the most common conjugated heterocycles, it was astonishing to realize that although there are several reports on conjugated polymers containing either pyridine or thiophene as building blocks,[51–55] few reported the use of both in an alternated manner,[56–61] and no systematic study of oligomer systems consisting of the two heterocyclic building blocks were available when this project was conceptualized. Since we began the investigations described in this work, the syntheses of some pyridine-thiophene containing oligomers have been reported.[62–64] However, few consider structure-properties relationships.[65,66] This work was not only instigated by the lack of reports on pyridine-thiophene oligomers, but also by the knowledge of the group on how to prepare 2,6-biarylpyridines, which were found to be useful fluorophores in the context of chemosensor development.[67–69]

The essential idea behind the use of pyridine and thiophene as the building blocks for the conjugated systems examined here is the electronic nature of this molecules, since it is well-stablished that pyridine is a π-electron deficient and thiophene is a π-electron rich heterocycle.[70] These characteristics are reflected in the energy levels of the molecular orbitals of the two units, as illustrated using the Hückel molecular orbitals, **Figure 1.3**; the HOMO of the thiophene is at a higher energy level when compared to the pyridine analogous orbital, while the pyridine LUMO is at a lower energy level in comparison to the thiophene LUMO. To examine the effect of the electronic nature of this heterocycles in conjugated oligomers, three series of molecules were designed. All the series have in common the alternation of pyridine and thiophene units, the first two series consist of linear oligomers while the third comprises branched dendrimeric molecules.

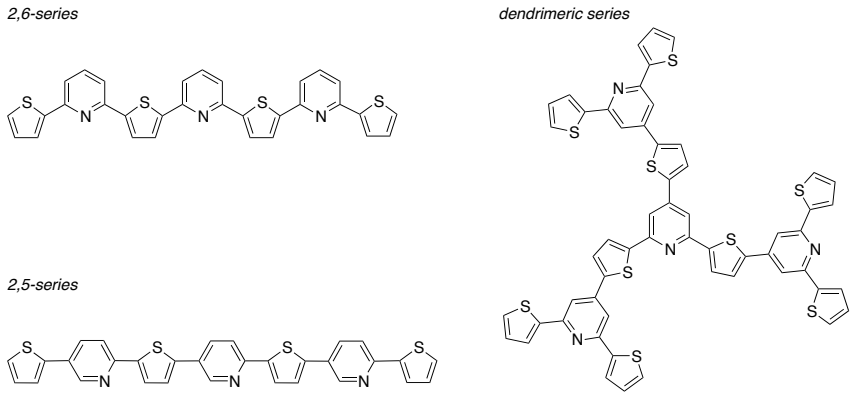

***Figure 1.7**: General structures of the series of compounds that are the main focus of this work.*

The first oligomeric series is characterized by a 2,6-disubstitution around the pyridine moiety, while the second features a 2,5-disubstitution pattern across the pyridine ring. **Figure 1.7** shows the generic structure of the oligomer series and the respective generic names that will be used throughout this work, the series names were chosen to correspond to the regiochemistry around the pyridine moieties; the structure of the actual compounds that were prepared and characterized is given in the next chapter. A generic structure of the dendrimeric series is also shown in **Figure 1.7**, and it consists of tri-substituted pyridine rings that constitute the core of the dendrimer as well as the branching points.

Analyzing the structures of the two oligomeric series, a higher conjugation between the individual heterocycles is expected in the *2,5-series* and two models can be considered in the justification of this interpretation.

The first one deals with resonance structures, it is well known in benzene systems that the *ortho* and *para* positions relative to a substituent are related through resonance structures. One of the most common ways to look at this phenomenon is through the reactivity of substituted benzenes, and a common example is the electrophilic bromination of phenol, where the reaction occurs at the *ortho* and *para* positions relative to the OH group;[71] this is what is called the resonance effect or also known as mesomeric effect.[72,73] The same effect applies to pyridine systems and the resonance structures for oligomers belonging to the *2,6-series* and the *2,5-series* can be written as shown in **Scheme 1.2**. It is clear that the conjugation is extended through the whole structure in the case of the *2,5-series*, while this does not happen in the *2,6-series*, since the substituents are *meta* relative to each other.

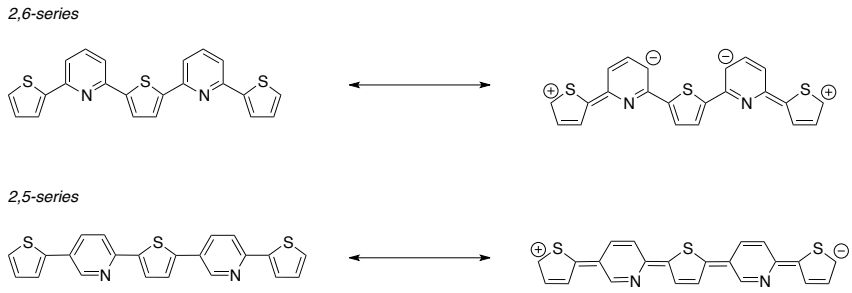

Scheme 1.2: *Resonance structures that can be written for oligomers of the* 2,6- *and* 2,5- *family series. Although more structures can be written, only one is shown as example for each of the series.*

The second model to be considered is the frontier molecular orbitals that can be found for these oligomers, here, the Hückel molecular orbitals will be considered. If we look at the LUMO of the molecules presented in **Figure 1.8**, it is evident that the *2,5-series* exhibits a higher degree of conjugation. The LUMO orbitals in the case of the *2,6-series* molecules does not contain the molecule as a whole, but is rather present in localized regions; in contrast, the LUMO in the *2,5-series* molecules is delocalized throughout the whole structure. The delocalization of the LUMO in the *2,5-series* is reflected in a lower relative energy of this orbital if compared to the same oligomer length in the *2,6-series*. This aspect observed in the HMO orbitals predicts a lower bandgap for an oligomer belonging to the *2,5-series* when compared to an oligomer of the same length in the *2,6-series*.

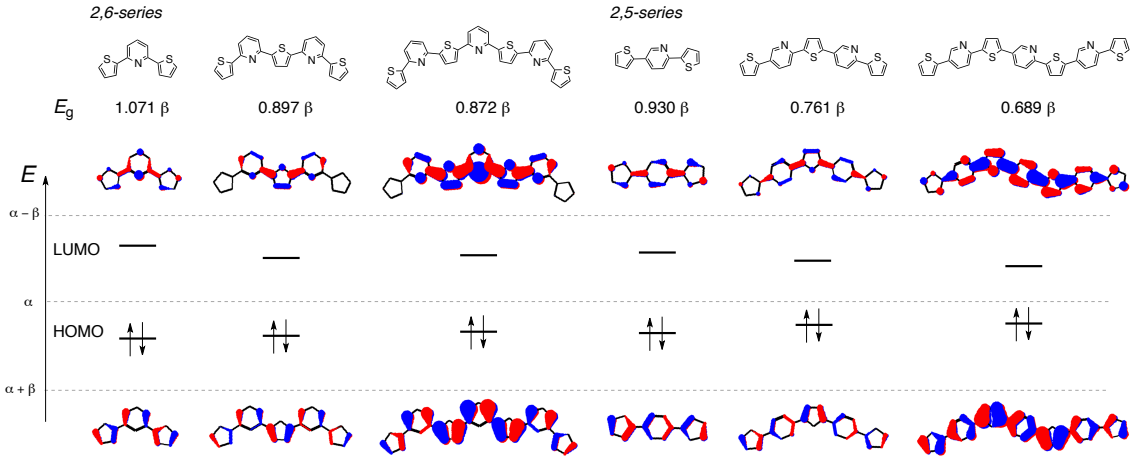

Figure 1.8: *Hückel molecular orbitals for the HOMO and the LUMO of analogue structures of the* 2,6-series *and the* 2,5-series. *The orbitals and relative energies were calculated using HMO theory through the SHMO Calculator.*[13]

When the same Hückel molecular orbital analysis is carried out for the dendrimeric series, **Figure 1.9**, it is found that in this case, since the same *meta* pattern is present, the bandgap is higher when compared to the *2,5-series*, but smaller when compared to the *2,6-series*, which is most likely due to the presence of a higher number of conjugated units. Furthermore, the HOMO energy levels are lower for this system when compared to either linear series and although the LUMO for the largest dendrimer analyzed is at a very similar energy level compared to the largest oligomer for the *2,5-series*, the stabilization of the HOMO in the case of the dendrimer, reflected in a localization of that orbital, leads the system to have a larger HOMO/LUMO gap (E_g = 0.818 β for a dendrimer containing 13 heterocyclic units *vs.* 0.761 β for a *2,5-oligomer* containing 5 units).

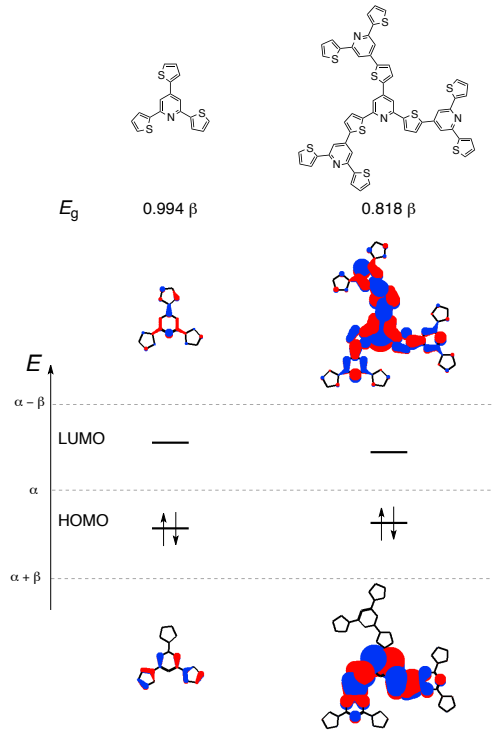

Figure 1.9: *Hückel molecular orbitals for the HOMO and the LUMO of molecules belonging to the dendrimeric series. The orbitals and relative energies were calculated using HMO theory through the SHMO Calculator.*[13]

All of the aspects of conjugated organic molecules, in special oligomers and dendrimers, discussed in the present chapter are of utmost importance in the analyzes of the properties found for the series of molecules reported in this work. None of this work is possible without preparing the actual compounds; accordingly, in Chapter 2 a discussion of the different routes considered for the synthesis and the synthetic routes used are presented, the detailed experimental procedures and characterization of the compounds are given in Chapter 5. In

Chapter 3, an overview of the general aspects of the photophysical properties of organic molecules is given, followed by a discussion of the properties found for the series of compounds that are the focus of this work and an analysis of their respective structure-properties relationship. Chapter 4 focuses on other significant properties, such as cyclic voltammetry and titrations.

CHAPTER 2

2 SYNTHESIS

In the context of the synthesis of conjugated oligomers and polymers, the majority of the C–C bond formation reactions employs transition metal-catalyzed cross-coupling reactions. The advancement in this field has been enormous ever since the first reports by Kumada, Heck, and Sonogashira in the early 1970's, and its importance was recognized in 2010 when Heck, Negishi and Suzuki won the Nobel Prize in Chemistry.[74,75] Although cross-coupling reactions are frequently employed in the field of conjugated oligomers, the classical condensation reactions to form pyridines and the thiocyclizations to form thiophenes deserve consideration, as they are historically important in the field of heteroaromatics. In this chapter, a brief discussion of the classical condensation and cyclization reactions will be presented, followed by a discussion on the palladium-catalyzed cross-coupling reactions and finally the presentation of the synthesis employed in the preparation of the target molecules.

2.1 Classical Synthesis of Pyridines and Thiophenes

2.1.1 Pyridine Rings: Condensation Reactions

The classical synthesis of pyridine rings involves condensation of aldehydes and ketones with ammonia. **Scheme 2.1** shows the generic Hantzsch pyridine synthesis, which was first reported in 1881.[76] In this reaction, one equivalent of an aldehyde, two equivalents of 1,3-dicarbonyl and ammonia are condensed to yield a symmetrical dihydropyridine that can be oxidized to the pyridine. The esther groups can then be removed through saponification followed by decarboxilation to give a trisubstituted pyridine ring. Many modifications to give unsymmetrical pyridines have been implemented, but since this is not the focus of the thesis, they will not be discussed.

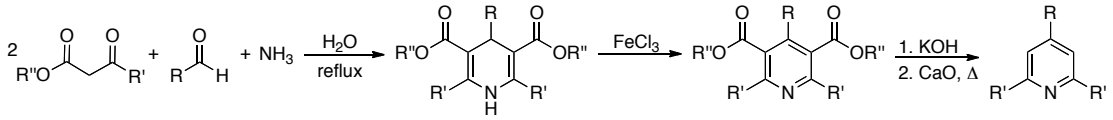

Scheme 2.1: *General Hantzsch pyridine synthesis reaction.*

Another example of pyridine ring-formation reaction is the Tschitschibabin pyridine synthesis.[77] It involves the condensation of any combination of aldehydes, ketones or α,β-unsaturated carbonyl compounds, **Scheme 2.2**. The steps involved in the reaction are: base-catalyzed aldol condensation, imine formation and a Michael addition in the ring-forming step. One limiting factor of the condensation reactions in the formation of pyridine rings is the fact that they are low yielding and can give many side products.

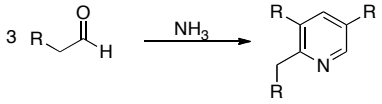

Scheme 2.2: *General Tschischibabin pyridine formation reaction.*

2.1.2 Formation of Thiophenes

One of the classical methods employed in the preparation of thiophenes is the Paal-Knorr reaction, which involves the cyclization of 1,4-diketones with phosphorus pentasulfide and an acid catalyst;[78,79] modifications to the classical Paal-Knorr conditions involve the use of Lawesson's reagent or the use of hydrogen sulfide, **Scheme 2.3**-A.[80] Another classical approach is the Hinsberg thiophene ring synthesis,[81] where a Claisen-type condensation between a 1,2-diketone and a thiodiacetate takes place, **Scheme 2.3**-B; this reaction is quite general and can also be used in the preparation of furans, selenophenes, and pyrroles.[80] Intramolecular reductive coupling has been shown to be very successful in the formation of sterically demanding 3,4-disubstituted systems. In this manner, 3,4-di-*tert*-butylthiophene can be prepared in the presence of low-valent titanium followed by acid-catalyzed dehydration, **Scheme 2.3**-C.[80]

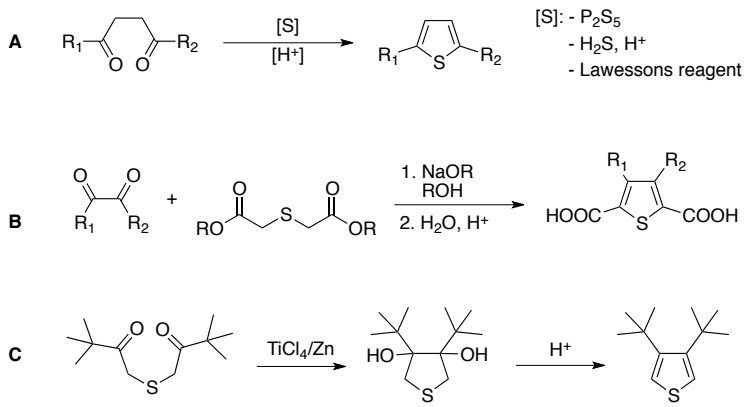

Scheme 2.3: *Classical reactions for the formation of thiophenes. General Paal-Knorr reaction using 1,4-diketones, **A**; Hinsberg thiophene ring synthesis, **B**; low-valent Titanium intramolecular reductive coupling, **C**.*

Another method that has been used in the synthesis of thiophene rings, in special thiophene oligomers[82] and thiophene-containing macrocycles,[83] is the thiocyclization of 1,3-diynes. In this reaction, hydrogen sulfide or sodium sulfide readily reacts with the diyne moiety to give the 5-membered heterocycle. De Meijere and coworkers[83] have used this method to prepare a series of macrocycles containing alternating thiophene and spirocyclopropane rings in remarkably good yields, **Scheme 2.4**. Altough cyclization reactions are important in the formation of thiophene rings, they are not the most commonly used to access the building blocks necessary for the many applications of thiophene precursors.

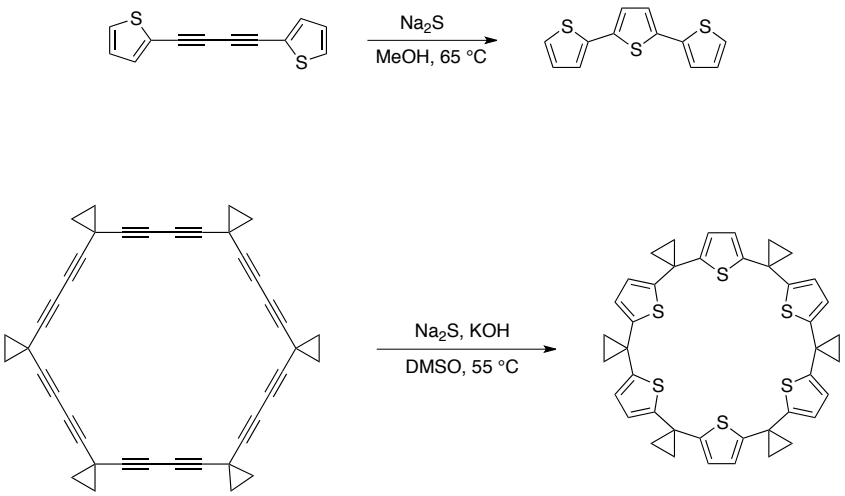

Scheme 2.4: *Thiocyclization of 1,3-diynes employed in the synthesis of oligothiophenes, top, and thiophene-containing macrocycles, bottom.*

2.1.2.1 Bromo- and Alkylthiophene Derivatives

Alkylthiophenes are undoubtedly the most important building blocks in the preparation of oligomers and polymers for materials applications. This is the case because the use of unsubstituted thiophene rings leads to materials of very sparing solubility and are therefore difficult to process, isolate and characterize. While the synthesis of thiophene rings from cyclization reactions is very important, it has not been used very often in the preparation of alkyl-thiophene precursors for oligomers and polymers application. Transition-metal catalyzed alkylation reactions using halogenenated thiophenes as starting materials are the most employed pathways. In that sense, it is worth discussing the bromination of thiophene rings and the commonly employed alkylation methods. While the direct alkylation through Friedel-Crafts alkylation is possible, it affords α-substitution, and for most applications, the alkyl-thiophene is required to be unsubstituted at the α-positions.

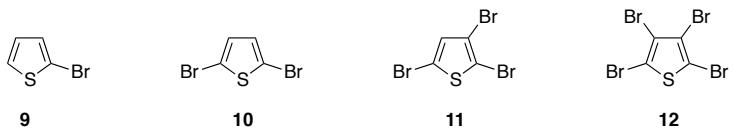

9 **10** **11** **12**

Figure 2.1: *Bromothiophenes, 2-bromothiophene (**9**), 2,5-dibromothiophene (**10**), 2,3,5-tribromothiophene (**11**), and tetrabromothiophene (**12**).*

Starting from thiophene, brominated derivatives can be easily prepared by the reaction with bromine in acetic acid, and 2-bromo- (**9**), 2,5-dibromo- (**10**), 2,3,5-tribromo- (**11**), and tetrabromothiophene (**12**), **Figure 2.1**, can be prepared depending on how many equivalents of bromine are used. The α-positions (2 and 5) of the ring are brominated first due to the higher electron density at those sites; and 3-bromo (**13**) and 3,4-dibromothiophene (**14**) can only be prepared by the debromination of the tri- and tetrabromo precursors, respectively. There are two main routes used in the reduction/debromination of the α-position of thiophenes. The first one uses Zn powder in acetic acid and the second uses lithium-halogen exchange, normally with butyllithium, followed by hydrolysis of the organometallic intermediate, **Scheme 2.5**.

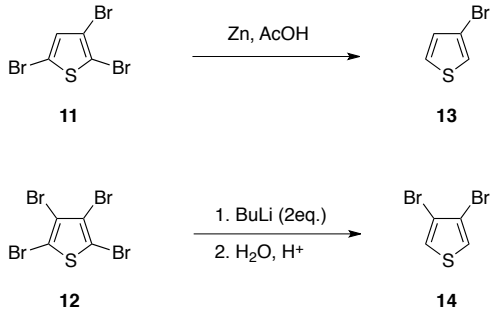

Scheme 2.5: *Preparation of 3-bromo and 3,4-dibromothiophene requires an overbromination followed by reduction.*

The brominated thiophenes can then be submitted to transition metal-catalyzed alkylation, normally Kumada-type, applying nickel as the metal catalyst and a Grignard alkyl reagent. In this fashion, different alkyl thiophenes can be prepared and there is a large number of examples in the literature applying this methodology. **Scheme 2.6** shows the synthesis of 3-hexylthiophene (**15**), one of the most used alkylthiophene building blocks in the preparation of polythiophenes.

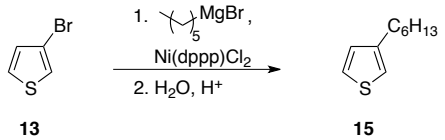

Scheme 2.6: *A representative example of the preparation of 3-alkylthiophenes, employing Kumada cross-coupling with a Grignard reagent.*

2.2 Palladium-Catalyzed Cross-Coupling Reactions

The general reaction referred to as *cross-coupling* involves the formation of a C–C bond between an organometallic reagent (R^1–M) and an organic electrophile (R–X) catalyzed by a transition metal, typically palladium or nickel. Depending on the nature of the organometallic reagent employed, the reaction is given a different name, associated with the scientist that first described it. A summary of the most common types of cross-coupling reactions and their respective names and general conditions is shown in **Table 2.1**. The commonly accepted mechanism for this type of reaction will be discussed in detail later, using the palladium-catalyzed Negishi cross-coupling as a representative case.

Table 2.1: *General scheme for the transition metal-catalyzed cross coupling reaction and the most commonly used organometallic reagents and the respective names given to the reaction.*

$$\mathbf{R^1}\text{–X} \;+\; \mathbf{R^2}\text{–M} \xrightarrow[\text{additive}]{\text{catalyst}} \mathbf{R^1}\text{–}\mathbf{R^2} \;+\; \text{sideproduct}$$

for all the reactions, X = Cl, Br, I, OTf

Name	–M	Catalyst	Additive	Sideproduct
Kumada	–Li or –MgX'	Ni(0) or Pd(0)	–	XM
Negishi	–ZnX'	Ni(0) or Pd(0)	–	XZnX'
Stille	$-SnR_3$	Pd(0)	–	$XSnR_3$
Hiyama	$-SiR_3$	Pd(0)	Nu^-	$[XSi(Nu)R_3]^-$
Suzuki	$-BX'_2$	Pd(0)	base	$HOBX'_2$

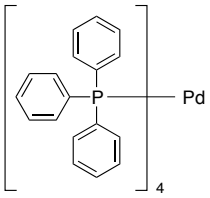

16

Many advances regarding this family of reactions have been reported, and they have significantly extended their scope and practical application. In this regard, it is important to highlight that great effort has been devoted to the development of new pre-catalysts and ligands. By far, phosphine ligands are the most commonly used in cross-coupling reactions, and tetrakis(triphenylphosphane)palladium(0) (also called *palladium tetrakis* or simply *tetrakis*) (**16**) is one of the most frequently used pre-catalysts. However, with the development of N-heterocyclic carbene (NHC) ligands in the early 2000's, not only the scenario of catalysts employed in cross-coupling reactions changed, but also the scope of educts that could be subjected to these reactions; since these type of ligands enabled the effective use of aryl chlorides as the electrophile counterpart. The general structure of N-heterocyclic carbenes (**17**) is shown in **Figure 2.2**; some of the classic NHC ligands are *IPr* (**18**), *SIPr* (**19**) and *IPent* (**20**).

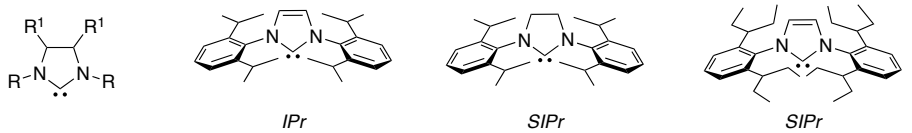

17 *IPr* **18** *SIPr* **19** *SIPr* **20**

Figure 2.2: *General structure of N-heterocyclic carbenes and the most frequently used derivatives.*

2.2.1 Negishi Cross-Coupling Reaction

The Negishi cross-coupling reaction was first reported in 1977[84] and has found many applications in the intervening decades.[85,86] It comprises the cross-coupling between an organozincate as the organometallic partner and an organic electrophile capable of undergoing oxidative addition at a Pd(0) center. In the beginning of the investigation of this reactivity, mostly aryl and alkenyl functional groups were employed, but nowadays, with the development of new ligands and catalyst systems, the scope of the reaction has been enlarged to encompass the use of allyl, benzyl, propargyl, alkyl, and acyl groups.[87] In particular, the use of alkyl electrophiles should be highlighted, as it was considered very difficult to achieve. For this work, the coupling of aryl moieties is important and that is what will be considered in the further discussion.

The accepted mechanism of transition metal-catalyzed cross-coupling reactions involves the following steps: *oxidative addition*, *transmetallation*, *tran-cis isomerization* and *reductive elimination*.[88] The catalytic cycle for the palladium-catalyzed Negishi cross-coupling is illustrated in **Figure 2.3**. The first step in the catalytic cycle is the *oxidative addition*, which involves the addition of the organic electrophile R–X bond to the active palladium catalyst center with the concomitant oxidation of the metal, going from Pd(0) to Pd(II). For this step, the nature of X, either a halogen, Cl, Br, I, or pseudo-halogen, OTf, plays a very important role, since the oxidative addition is faster for X = I > Br ~ OTf >> Cl.

The next step in the catalytic cycle is the *transmetallation*, which involves the exchange of ligands between two metal centers, the catalyst and the organometallic reagent. In the case of the Neshishi variation, the organometallic partner is an organozincate, and it is important to highlight that organozincades are among the most efficient partners for the transmetallation at a palladium center.[89]

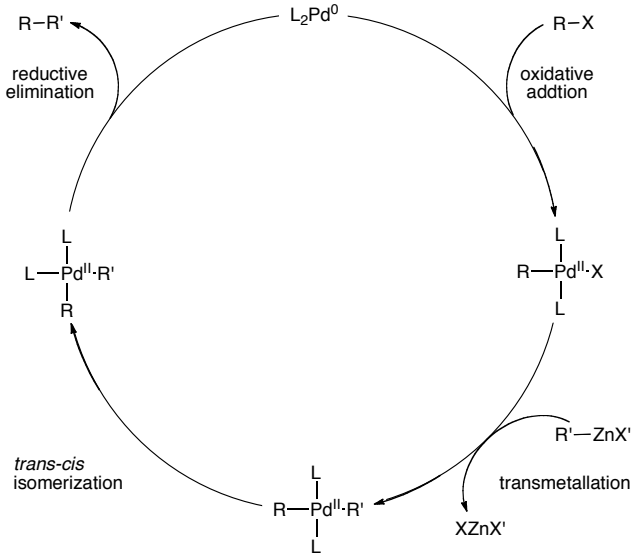

Figure 2.3: *General catalytic cycle for the Palladium-catalyzed Negishi cross-coupling reaction.*

The final two steps are comprised of a *trans-cis isomerization* and *reductive elimination*. The *trans-cis* isomerization is crucial for the further reductive elimination, which cannot occur in the *trans* isomer. If the ligand used is bidentate, there is no opportunity for formation of a *trans* complex and this step is neglected. The *reductive elimination* is the reverse of the oxidative addition, and it is through this process that the new carbon-carbon bond is formed and the catalyst center is regenerated to the valence zero state. This last step is favored by bidentate ligands or ligands exhibiting a large bite angle; the latter is the case for NHC ligands, which makes them remarkably good ligands in these reactions.

2.3 Examples of Conjugated Oligomers

There are several examples in the literature of oligomers comprised of thiophene and nitrogen-containing heterocycles, and the synthesis of relevant examples will be discussed in this session.

Thiophene-diazine oligomers were prepared using Pd-catalyzed Stille cross-coupling.[90] Starting from 5,5'-bis(tributylstannyl)-2,2'-bithiophene (**21**) and 4,6-dichloropyrimidine (**22**) using standard Stille coupling conditions, mono-coupling of the pyrimidine site was achieved to yield 70 % of oligomer **23**, which was further reacted with 2-(tributylstannyl)-thiophene to yield oligomer **24** in 50 % yield. Pyridazine oligomer **25** was obtained in a similar fashion with a 43 % overall yield starting from the 3,6-dichloropyridazine, **Scheme 2.7**. The low yield of the longer oligomers can be attributed to poor solubility.

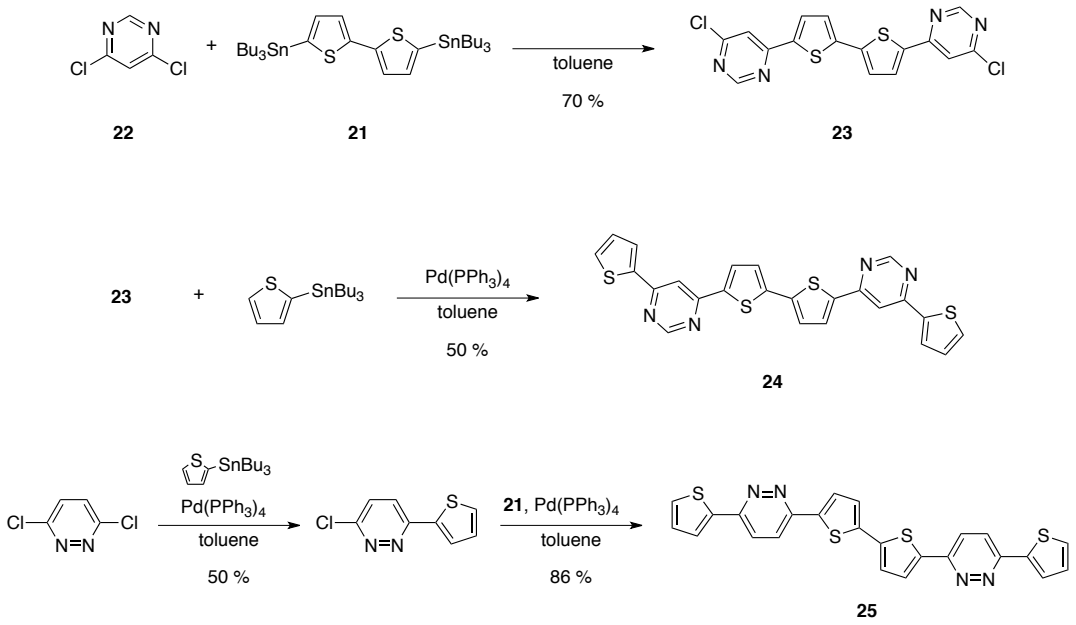

Scheme 2.7: *Synthesis of thiophene-diazine oligomers* via *Stille cross-coupling reaction.*[90]

N-alkylated isoindigo has also been utilized as the nitrogen-containing heterocycle acceptor unit to prepare donor–acceptor–donor (D–A–D) and acceptor–donor–acceptor (A–D–A) oligomers with bithiophene.[91] The synthesis employs Palladium-catalyzed Suzuki cross-coupling reaction between 6-bromo- (**26**) and 6,6'-dibromoisoindigo (**27**) and the corresponding bithiophene boronic acid pinacol ester, **Scheme 2.8**. In the preparation of the A–D–A oligomer (**28**), 2,2'-bithiophene-5,5'-diboronic acid bis(pinacol) ester (**29**) was employed and in the case of the D–A–D oligomer (**30**), the monoboronic acid pinacol ester (**31**) was used, to yield the final oligomers in 57 % and 83 % yield, respectively.

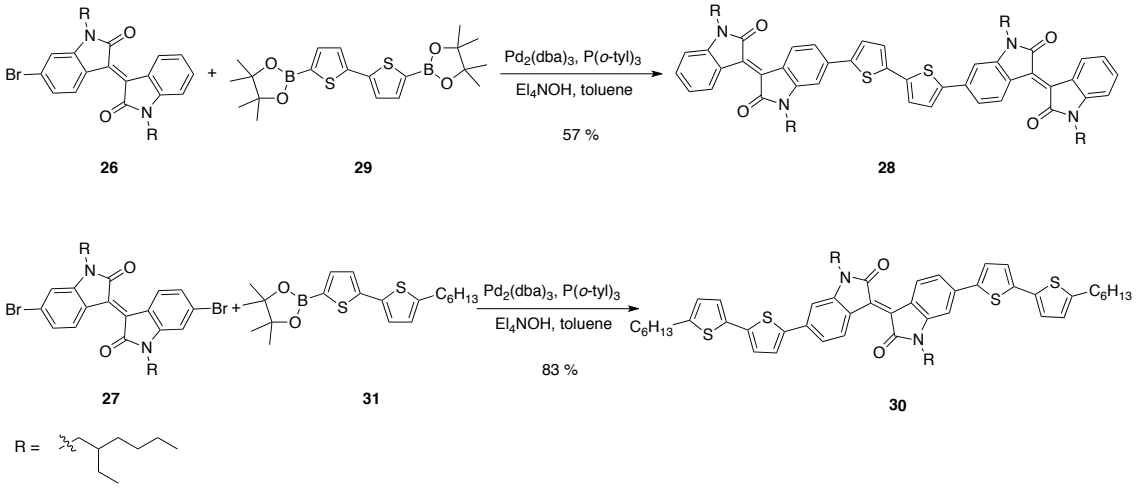

Scheme 2.8: *Synthesis of isoindigo-containing thiophene oligomers by palladium-catalyzed Suzuki cross-coupling.*[91]

Another nitrogen-containing heterocycle that has often been used is 2,1,3-benzothiadiazole, and it has been employed in the study of donor-acceptor oligomers containing thiophene as the donor unit.[92] The synthesis of the oligomers starts with Stille cross-coupling between 4,7-dibromo-2,1,3-benzothiadiazole (**32**) and 2-(trimethylstannyl)thiophene (**33**) in the presence of a palladium catalyst to give oligomer **34** in 56 % yield, and further lithiation followed by stannylation afforded **35**, which was homocoupled under oxidative conditions to furnish oligomer **36** in 15 % yield, **Scheme 2.9**. Oligomer **37** was prepared by the coupling of **32** and 5-(trimethylstannyl)-2,2'-bithiophene (**38**) in 14 % yield. In the publication, the authors comment on the poor solubility of oligomers **36** and **37**, which could be one of sources of poor yield in their preparations.

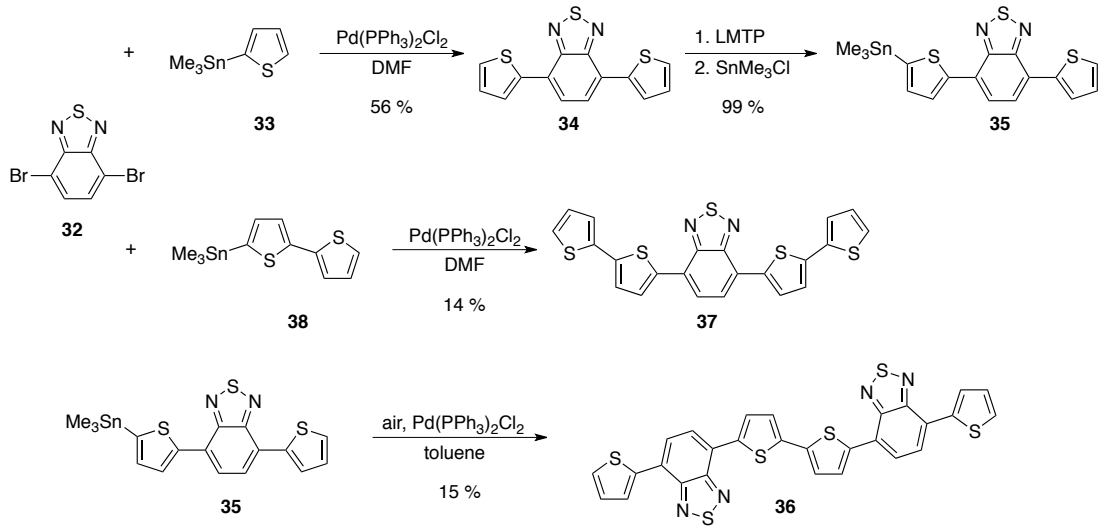

Scheme 2.9: *Synthesis of oligomers containing 2,1,3-benzothiadiazole and thiophene units.*

Only few examples of oligomers containing thiophene and pyridine are present in the literature, the synthesis of the most significant ones will be considered. The first approach, utilizes the thiocyclization of a 1,4-diketone to form the thiophene ring, **Scheme 2.10**.[93] The thiocyclization proceeds by the treatment of the appropriate pyridyldiketone with Lawesson's reagent to afford three-ring oligomers, **39**, **40**, and **41**, with a central thiophene ring and varying regiochemistry across the pyridine. A three-ring oligomer containing a central pyridine substituent (**42**) was also reported by the same authors. There was no mention of photophysical of electrochemical properties for these systems.

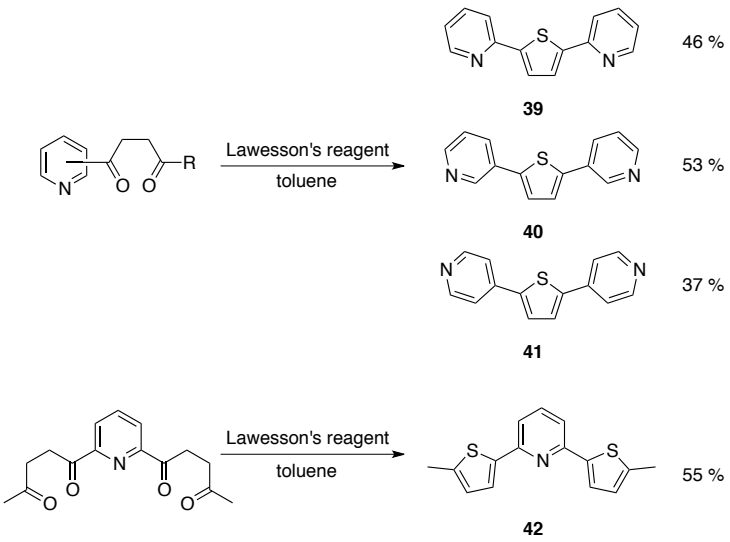

Scheme 2.10: *Synthesis of three-ring thiophene-pyridine systems through thiocyclization of 1,4-diketones.*[93]

Another report demonstrates the synthesis and optical properties of pyridine end-capped oligothiophenes.[29] The synthesis again illustrates the utility of transition metal-catalyzed cross-coupling reactions, in particular Stille and Kumada couplings. Three pyridine end-capped oligothiophenes were reported, **43**, **44**, and **45**; in addition, two other oligomers, one of alternating thiophene-pyridine **46** and the other a dimer of an alternating system comprised of a bithiophenyl central moiety, **47**, **Scheme 2.11**.

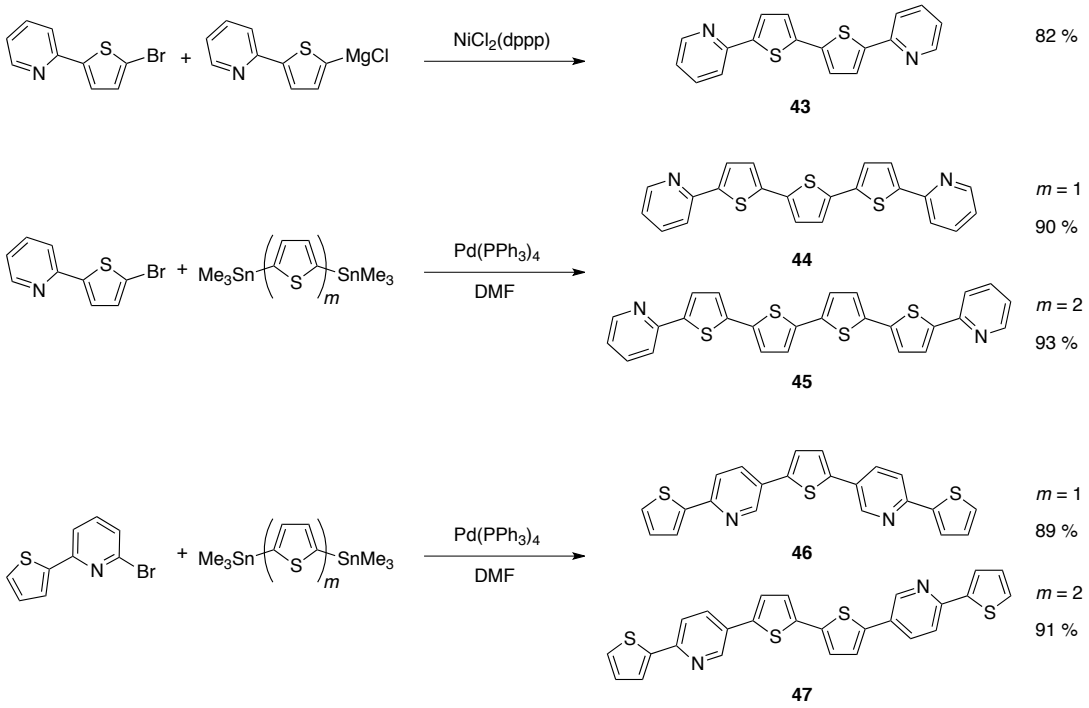

Scheme 2.11: *Synthesis of pyridine end-capped oligothiophenes and other derivatives.*[29]

2.4 Retrosynthetic Analysis of the Target Molecules

The primary purpose of this project was to carry out a systematic study of a series of oligomers and dendrimers comprised of alternating thiophene and pyridine moieties; regarding the synthetic pathway to complete the synthesis, one can imagine not only different retrosynthetic disconnections but also different regiochemistry connecting the units.

In a very general manner, if we analyze the disconnections between the heterocycles in the oligomers, there are mainly two approaches that could be followed, one considering two reactive sites in one of the reactants, pathway **A**, and the other considering only one reactive site at each reactant, pathway **B**, **Scheme 2.12**. At a first glance, pathway **A** might seem to be more attractive, since it would afford longer oligomers in fewer steps, but having two reactive sites in one of the reactants carries the issue of incomplete reaction, forming mono- and di-coupled products.

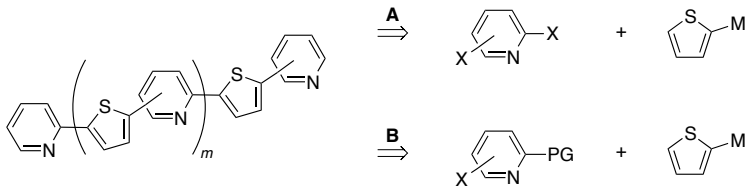

Scheme 2.12: *General retrosynthetic scheme for a generic representation of the target oligomers.*

When the dendrimeric series is considered, there are two main approaches that could be followed, divergent or convergent, **Figure 2.4**.[94] The divergent pathway begins with the core of the dendrimer. Here, an exponential increase of the peripheral reactive sites is achieved with each generation, which demands a large excess of reactant to drive the reaction to completion. The convergent strategy starts on what will be become the periphery of the dendrimer and it is based on the construction of dendrons, species that possess only one reactive site. On one hand this facilitates the control of the reaction but on the other this makes it difficult for the reaction to occur with increase of generations due to the fact that the reactive site becomes sterically crowded.

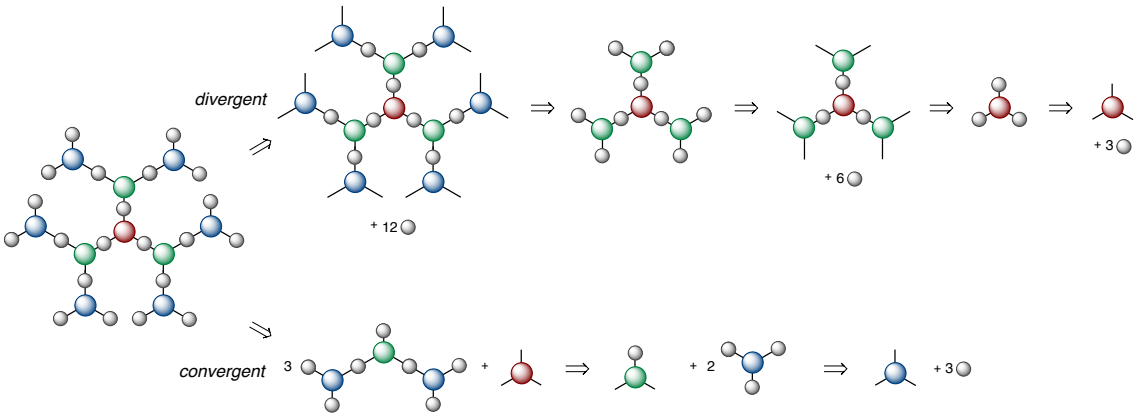

Figure 2.4: Retrosynthetic pathway of a dendrimer showing the two main approachs, divergent and convergent. The coloring represents the different generations, red – generation zero, green – first generation, blue – second generation.

2.4.1 Oligomers: Pathway A – di-Coupling Approach

The first retrosynthetic approach considered was pathway **A**. This path is particularly attractive for the *2,6-series*, since the regiochemistry of the connections afford a symmetric molecule possessing a pyridine unit in the center and two equivalent thiophene units, **Scheme 2.13**. In contrast, this path is not a good choice when the *2,5-series* is considered, as di-coupling furnishes a three-ring intermediate that does not possess a mirror plane passing through the central pyridine ring, resulting in non-equivalent α-positions of the peripheral thiophenes, which makes it difficult for further regioselective functionalization.

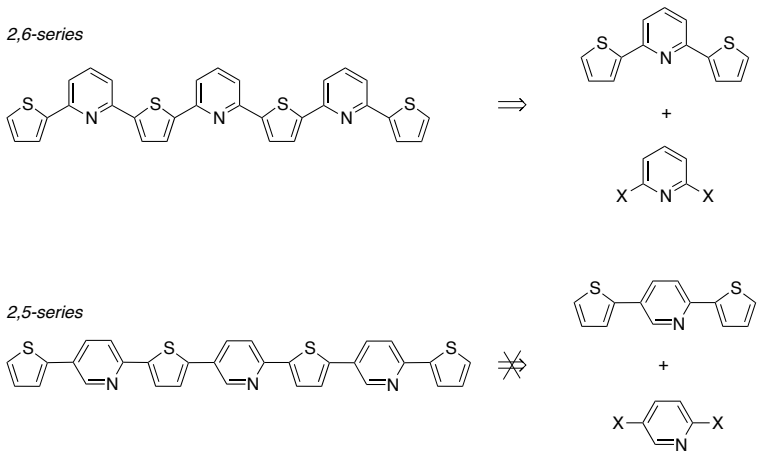

Scheme 2.13: Detailed pathway A. Applying this pathway for the 2,6-series *affords a symmetrical molecule where the two flanking thiophene rings are equivalent. If this approach is considered for the* 2,5-series, *it is clear that a mixture of regioisomers would be obtained, since the peripheral thiophene rings are not equivalent.*

Another difficulty regarding this pathway is the number of reactive sites. If the reaction does not go to completion, a mixture of mono- and di-coupled material is obtained and this could pose complications in the purification process. In this regard, pathway **B** decreases the number of reactive sites from two to one, giving rise to only one major possible product.

2.4.2 Oligomers: Pathway B – Iterative Approach

This approach was designed to not only comprise fewer reactive sites and therefore afford less possible products, but also to give access to only one regioisomer of each oligomer in both series, as well as to be an iterative strategy to the synthesis of conjugated alternating oligomers. The oligomer chain growth is unidirectional and a two-ring extension can be achieved in each step, **Scheme 2.14**. Correspondingly, the synthesis is based on two two-ring building blocks of complementary reactivity, one possessing a protecting group at the pyridine 2-position and the other a group that can undergo oxidative addition in cross-coupling reactions. This last building block is then employed iteratively on the reaction of longer oligomers, always having the available thiophene alpha-position of the protected oligomers as the reactive partner.

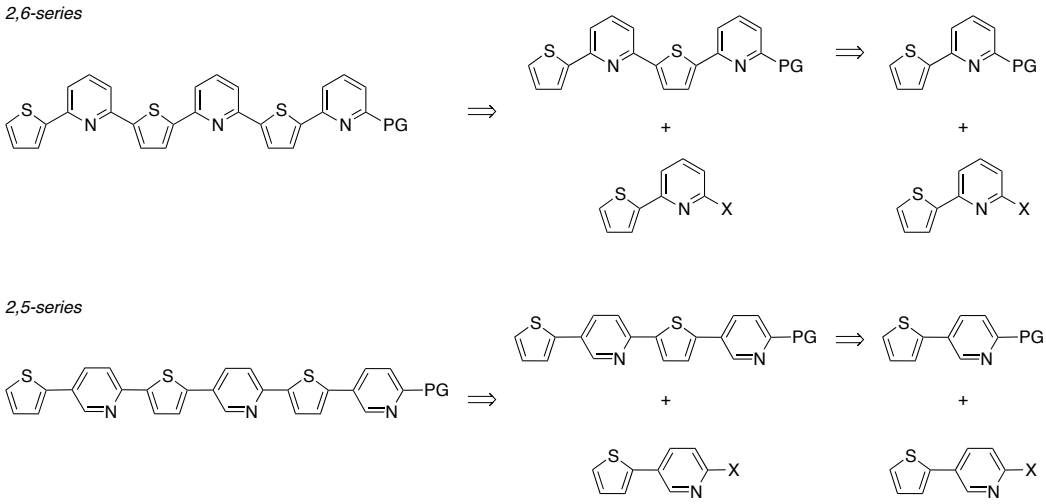

Scheme 2.14: *Detailed pathway* ***B****. The oligomer chain growth is unidirectional and is based on a two-ring extension at each step.*

The synthesis of the fundamental two-ring building blocks takes advantage of the straightforward conversion of the protected compound, **2Ring-PG**, into its activated version, **2Ring-X**, **Scheme 2.15**. The preparation of the protected pyridine coupling partner is based on the reactivity of the 2-position of the pyridine ring towards nucleophilic aromatic substitution;

this point is particularly important in the *2,5-series*, where the regiochemistry of the substitution is crucial.

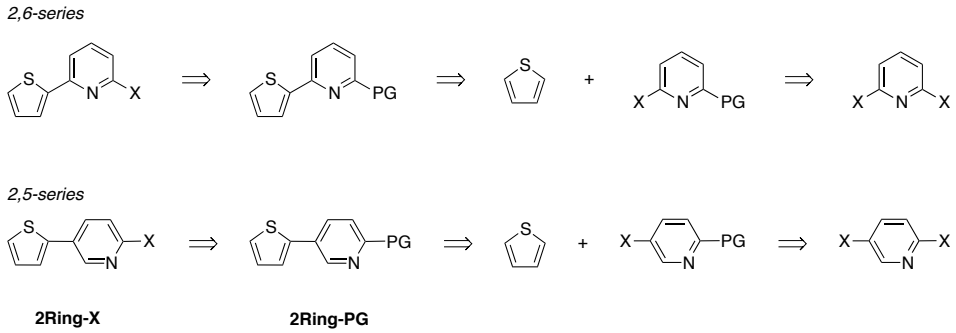

Scheme 2.15: *Retrosynthesis of the two-ring building blocks.*

When mono-alkylated thiophene coupling partners are considered, it is important to note that this unidirectional iterative pathway is very appropriate, since setting the regiochemistry of the building blocks guarantees a regioisomeric oligomer.

2.4.3 Dendrimers: Divergent Approach

The divergent retrosynthetic pathway of dendrimer **48** is based on the construction of a core, **49**, that can be recursively reacted with the pyridine and thiophene building blocks to give the dendrimer, **Scheme 2.16**. In this design, the pyridine building block, **50**, must have two different reactive groups to provide a regioselective coupling with the corresponding thiophene to form **51** as one regioisomer. The M-thiophene is designed to be active in palladium cross-coupling reactions and an activation step is required to get to **49** after the initial coupling between tri-halopyridine and the metalothiophene.

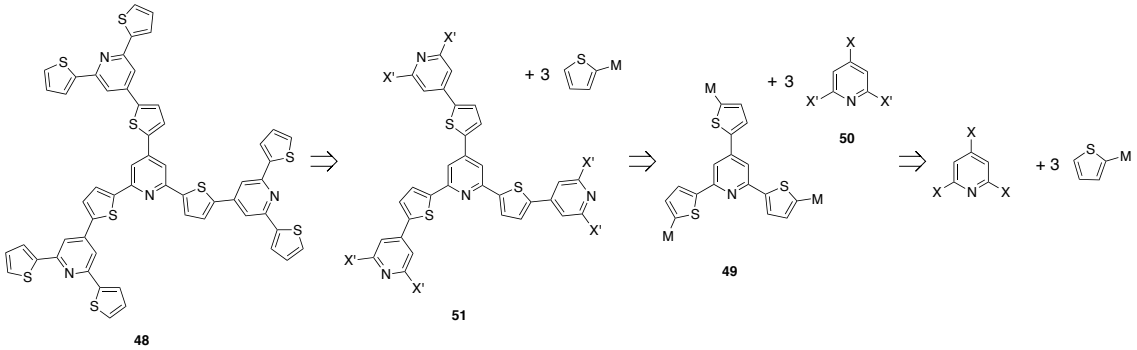

Scheme 2.16: *Divergent retrosynthetic pathway of alternating pyridine–thiophene dendrimer **48**.*

2.4.4 Dendrimers: Convergent Approach

In this pathway, the core is brought together as the last step and the synthesis focuses on the preparation of dendron **49a**. The regioselective activation to give metallated **49a** is of utmost importance, since it will ensure that only one regioisomer of the final dendron is formed in the subsequent step.

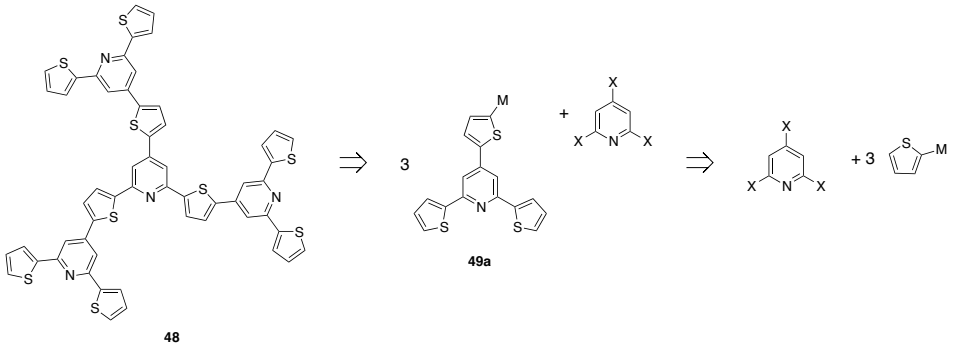

*Scheme 2.17: Convergent retrosynthetic pathway of alternating pyridine–thiophene dendrimer **48**.*

2.5 Synthesis of the 2,6-Series

2.5.1 Early Synthesis Using 3,4-Dibutylthiophene

The beginning of these studies started with the synthesis of the *2,6-series* employing the synthetic pathway **A** and a doubly-alkylated thiophene derivative. The synthesis began with the lithiation of 3,4-dibutylthiophene using butyllithium at –78 °C and subsequent transmetalation with zinc chloride to prepare **52** in situ, which was reacted with 2,6-dibromopyridine, **53**, in the presence of palladium tetrakis to afford three-ring compound **54** in 79 % yield, **Scheme 2.18**. Elongation of **54** was performed by its deprotonation followed by transmetalation with zinc chloride and further reaction with **53** using the same conditions to give seven-ring **55** in 21 % yield.

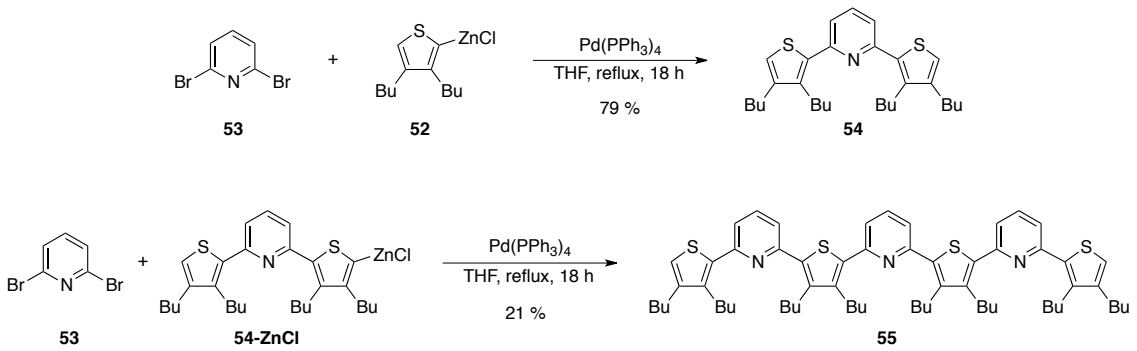

Scheme 2.18: *Synthesis of members of the* 2,6-series *using 3,4-dibutylthiophene as the donor unit.*

Analysis of the calculated conformation of **55** after energy minimization shows a twisted conformation between the aromatic subunits, **Figure 2.5**. The main factor contributing to this non-planar conformation seems to be the presence of the di-alkyl chain in the thiophene rings, which hinders the coplanar conformation because of steric interactions. For simplicity, the calculation was performed considering 3,4-dimethylthiophene instead of 3,4-dibutylthiophene used in the synthesis.

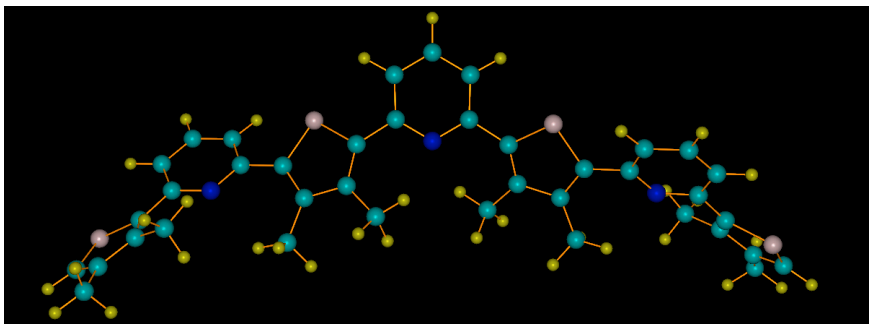

Figure 2.5: *Calculated conformation of 55 shows that the rings are not coplanar.*

2.5.2 Synthesis Using 3-Butylthiophene

Considering the calculated conformation for the dibutyl derivative **55**, and literature precedents for the conformation of aryl moieties, it was evident that a mono-alkylated thiophene would be a more suitable candidate as a coupling partner. The synthesis of the oligomers was then performed using 3-butylthiophene as the donor unit.

3-Butylthiophene, **56**, was prepared according to standard literature procedures, but it will be shown here for completion. The reaction of 3-bromothiophene, **13**, and butylmagnesium bromide, **57**, in the presence of dichloro(1,3-bis(diphenylphosphino)propane)nickel ($Ni(dppp)Cl_2$) catalyst afforded 3-butylthiophene, **56**, in

91 % yield, **Scheme 2.19**-I. The pyridine coupling partner was prepared by nucleophilic aromatic substitution utilizing potassium *tert*-butoxide as the nucleophile. The reaction of potassium *tert*-butoxide and 2,6-dibromopyridine, **53**, was carried out in toluene and gave 6-bromo-2-(1,1-dimethylethoxy)pyridine, **58**, in 71 % yield, **Scheme 2.19**-II. The *tert*-butoxide group acts as the protecting group and it can be easily deprotected to the alcohol in the presence of acid.

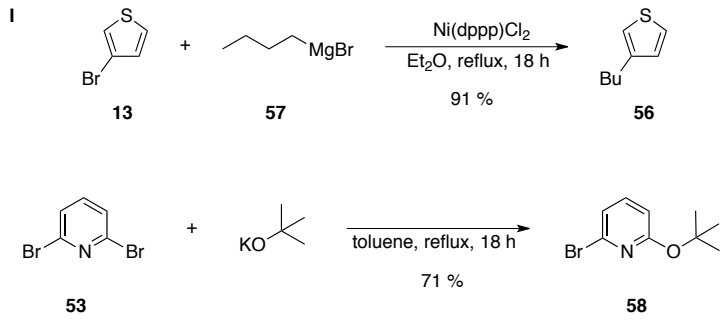

Scheme 2.19: *Syntheis of 3-butylthiophene, **I**. Synthesis of 6-bromo-2-(*tert*-butoxy)pyridine, **58**, **II**.*

The synthesis of the oligomers then starts with a regioselective deprotonation[95] of 3-butylthiophene using lithium tetramethylpiperidide, **59**, as the base; the deprotonation occurs on the α-position of the thiophene that is opposite to the alkyl group, namely the thiophene 5-position, to give intermediate **60** that was then transmetallated, using zinc chloride, to give intermediate **61**, **Scheme 2.20**. This regioselective deprotonation is extremely important to set the regioochemistry of the oligomers, since it assures that only on isomer of the 2-ring building block is formed.

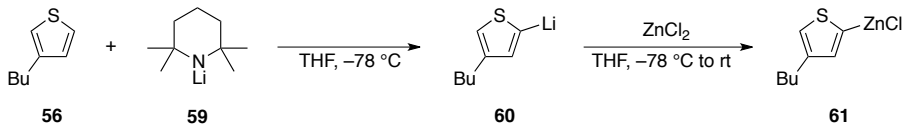

Scheme 2.20: *Regioselective deprotonation of 3-butylthiophene and subsequent zinc transmetallation.*

The first 2-ring building block could be synthesized under Negishi cross-coupling conditions, using intermediate **61** and 6-bromo-2-(*tert*-butoxy)pyridine in the presence of palladium tetrakis to give **26a** in 76 % yield after column chromatography, **Scheme 2.21**. The deprotection was then performed using neat molten pyridine hydrochloride to give **26aOH** in 96 % yield. The second 2-ring building block was prepared by the treatment of **26aOH** with triflic anhydride in the presence of triethylamine to afford **26aOTf** in 90 % yield. The choice of

the triflate group was made because it is highly reactive in the oxidative addition step of cross-coupling reactions.

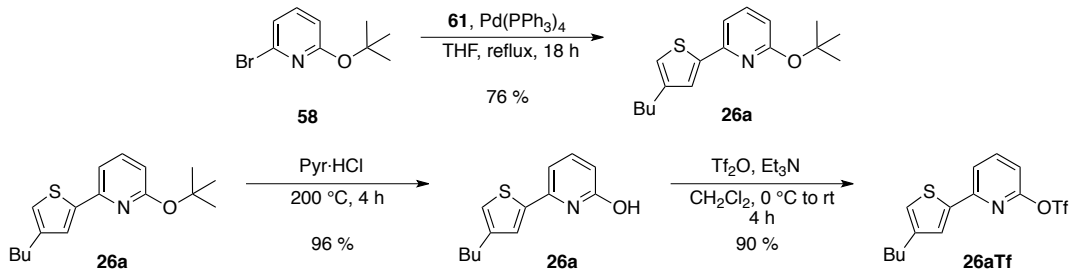

Scheme 2.21: *Synthesis of the* 2,6-series *2-ring building blocks,* ***26a*** *and* ***26aTf****.*

Longer oligomers were then obtained starting with the lithiation of **26a** followed by zinc chloride transmetallation and subsequent Negishi reaction with **26aTf** in the presence of palladium tetrakis to give the 4-ring member of the *2,6-series*, **26b**, in 62 % yield, **Scheme 2.22**. **26b** was then deprotected and converted to the triflate to afford **26bTf** in 85 % yield over the two steps.

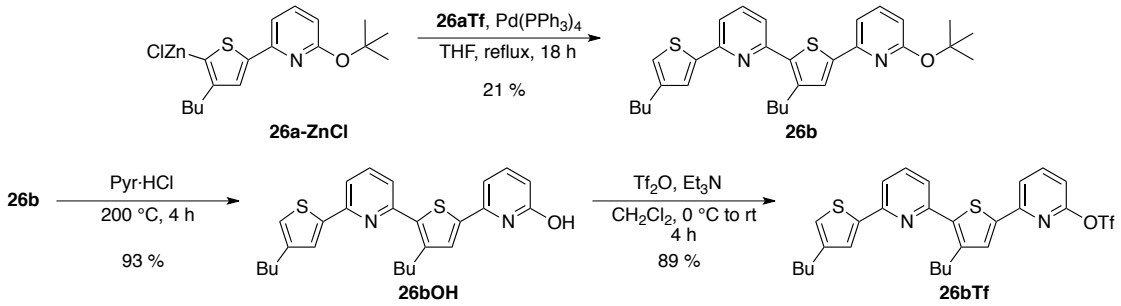

Scheme 2.22: *Synthesis of the 4-ring compound of the* 2,6-series*,* ***26b****, and its subsequent deprotection and triflation.*

The 6-ring component of the *2,6-series* was synthesized by a Negishi cross-coupling reaction between the 2-ring triflate, **26aTf**, and the 4-ring zincate, **26b-ZnCl**; the reaction was performed under standard conditions and **26c** was obtained in 20 % yield, **Scheme 2.23**. To achieve the synthesis of the longer oligomer of the series, possessing 8 heteroaromatic rings, the 4-ring triflate was reacted with 4-ring zincate in the presence of palladium tetrakis catalyst to afford the product, **26d**, in 25 % yield.

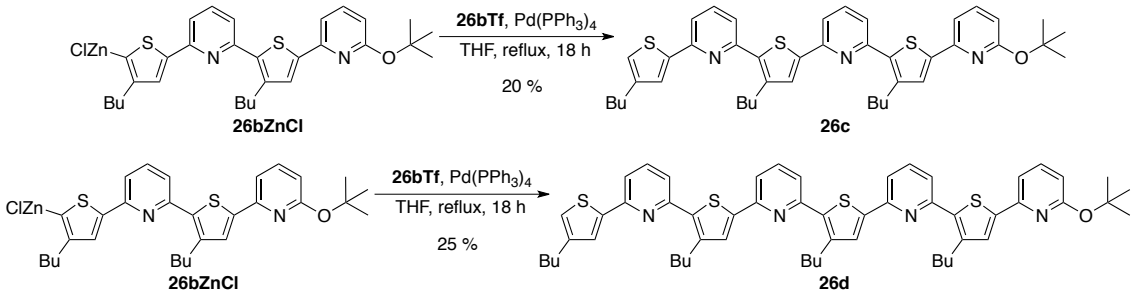

Scheme 2.23: *Synthesis of the 6-ring,* ***26c****, and 8-ring,* ***26d****, members of the* 2,6-series.

2.6 Synthesis of the 2,5-Series

The synthesis of the *2,5-series* is very similar to the one of the *2,6-series* and it explores the same reactivity while it is different on the regiochemistry around the pyridine ring.[96] It started with the preparation of the protected pyridine building block, **62** (5-bromo-2-(1,1-dimethylethoxy)pyridine), via aromatic nucleophilic substitution of the bromo in the 2-position of 2,5-dibromopyridine, **63**, by a *tert*-butoxide group, **Scheme 2.24**. Although it looks like this is a straightforward reaction, yields better than 50-55 % were never achieved and the reaction mixture was always a black slurry; this could be due to formation of pyridynes, since a *meta* halogen is present.[97] Nevertheless, the reaction was feasible and is important to once more highlight the importance of the regioselectivity of this reaction, which is due to the higher reactivity of the 2-position of the pyridine.

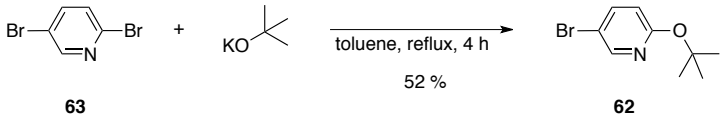

Scheme 2.24: *Syntheis of 5-bromo-2-(*tert*-butoxy)pyridine,* ***62****.*

The synthesis continued with the preparation of the 2-ring building blocks. Employing Negishi cross coupling reaction of **62** with the regioselective zincate of 3-butylthiophene, **61**, in the presence of the IPr N-heterocyclic carbene, **18**, and a palladium source, compound **25a** was obtained in 72 % yield, **Scheme 2.25**. The next step was then removal of the *tert*-butyl group in acidic media to afford **25aOH** and subsequent triflation with triflic anhydride in the presence of triethylamine to give the 2-ring active building block, **25aTf**, in 89 % yield over two steps.

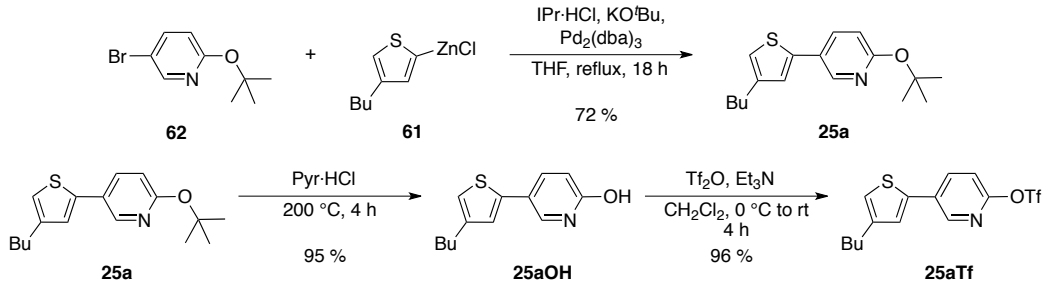

Scheme 2.25: *Synthesis of the* 2,5-series *2-ring building blocks,* ***25a*** *and* ***25aTf****.*

Elongation of the series was accomplished through an iterative pathway that uses the protected version of the oligomers as the organozincate together with the 2-ring triflate, **25aTf**, in a Negishi cross-coupling reaction to afford a 2-ring increase on the length of the oligomer at each iteration, **Scheme 2.26**. Accordingly, the 4-ring member of the series, **25b**, was synthesized by the reaction of **25a** zincade and **25aTf** in the presence of palladium tetrakis in 79 % yield. Lithiation of **25b** followed by transmetallation with zinc chloride and Negishi cross coupling conditions, together with **25aTf** gave **25c** in 76 % yield. The same pathway way applied to afford **25d**, now utilizing the zincate of **25c** and again **25aTf** in the presence of palladium tetrakis to yield **25d** in 25 %.

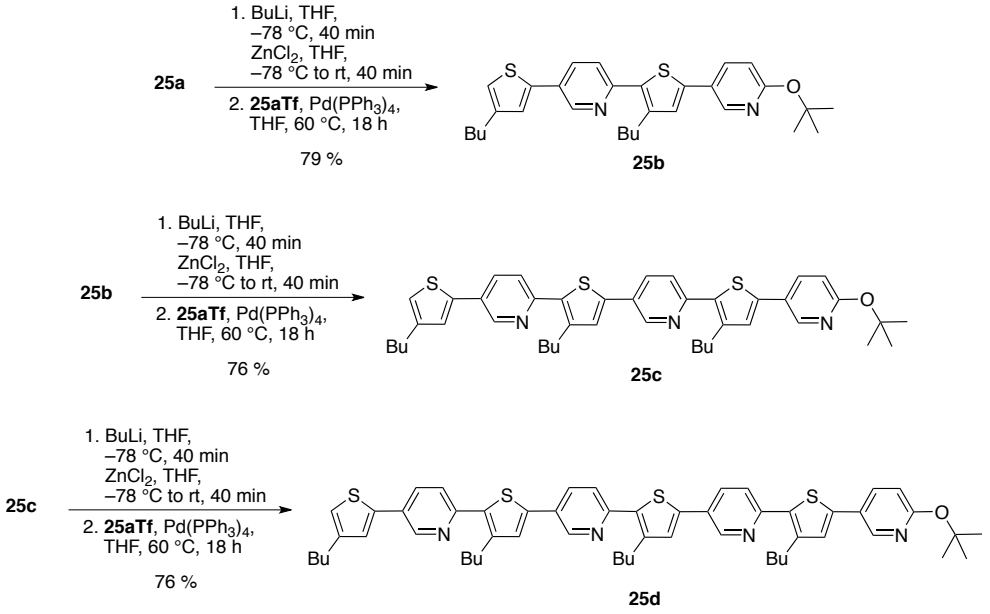

Scheme 2.26: *Synthesis of the 4-ring (****25b****), 6-ring (****25c****) and 8-ring (****25d****) members of the* 2,5-series.

2.7 Synthesis of the Dendrimeric Systems

The synthesis of the dendrimeric systems adopts the same principles and reactivities applied in the synthesis of the oligomers. The dendrimeric structure was constructed through the use of a 2,4,6-tri-substituted pyridine moiety. The chosen starting material was 2,6-dichloro-4-iodopyridine (**64**) because it is of easy access and, more importantly, it possesses a very attractive characteristic to the regioselectivity of the reaction, since the iodo group is more reactive in the oxidative addition step of cross coupling reactions when compared to the chloro substituents.

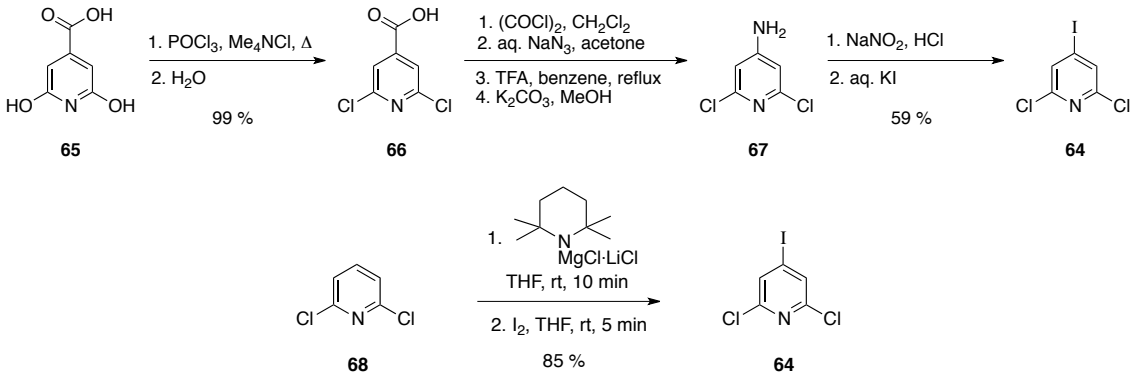

*Scheme 2.27: Preparation of 2,6-dichloro-4-iodopyridine, **64**.*

The fundamental pyridine building block was prepared using two different methods, **Scheme 2.27**; the first starts from inexpensive citrazinic acid, **65**, which was treated with phosphoryl chloride and tetramethylammonium chloride to give **66** in 99 % yield after aqueous workup. Treatment of **66** with oxalyl chloride followed by addition of sodium azide and acid under reflux provided the right conditions for a Curtius rearrangement to occur and 4-amino-2,6-dichloropyridine (**67**) was obtained and utilized in the next step without further purification. It was then treated with sodium nitrite in the presence of acid and subsequent addition of aqueous potassium iodide to give **64** in 59 % yield over two steps. The second method for the preparation of **64** is based on the regioselective deprotonation of the 4-position of 2,6-dichloropyridine (**68**) by a tetramethylpiperidide base followed by quenching with iodine to give the product in 85 % yield in only one step.

2.7.1 Divergent Pathway

The first approach carried out employed the divergent pathway. It started with the synthesis of 2,4,6-tri(thiophen-2-yl)pyridine (**69**) from **64** and **70** under Negishi cross-coupling conditions using N-heterocyclic carbene IPr as the ligand in 43 % yield, **Scheme 2.28**. The next step was the triple lithiation of **69**, which was carried out using 3 equivalents of butyllithium, followed by transmetallation with zinc chloride and Negishi reaction conditions with 3 equivalents of **64** to assumedly give compound **71**. Characterization of the outcome of this reaction was rather difficult due to poor solubility of the isolated product, which was used on the next step without purification, with the hope that the resultant product, **72**, would have better solubility properties. Negishi cross-coupling reaction conditions were then applied; assuming that the crude mixture was primarily composed of **71**, and using **70** as the coupling partner to presumably achieve compound **72**.

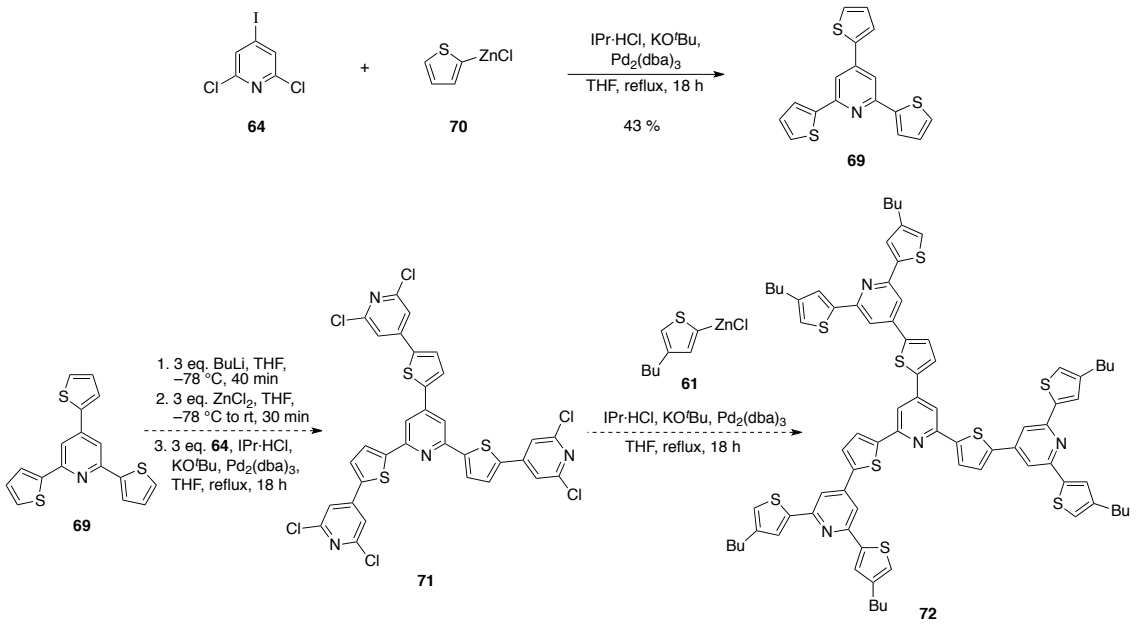

***Scheme 2.28:** Synthesis of the generation zero of the dendrimeric series, **69** and tentative synthesis of the second generation, **72**.*

It was found that the product of the reaction in the tentative formation of **$64** was not the first-generation dendrimer. Mass spectrometry evidence, **Figure 2.6**, shows that the obstacle was the previous step: the formation of **71** did not go to completion but rather stopped at the di-coupling stage and in the tentative synthesis of **71**, the compounds shown as insert in **Figure 2.6** were probably obtained, although no other characterization was performed because of the

poor solubility of the mixture. These observations made it evident that the divergent pathway as proposed would be rather difficult and the convergent pathway was a better choice.

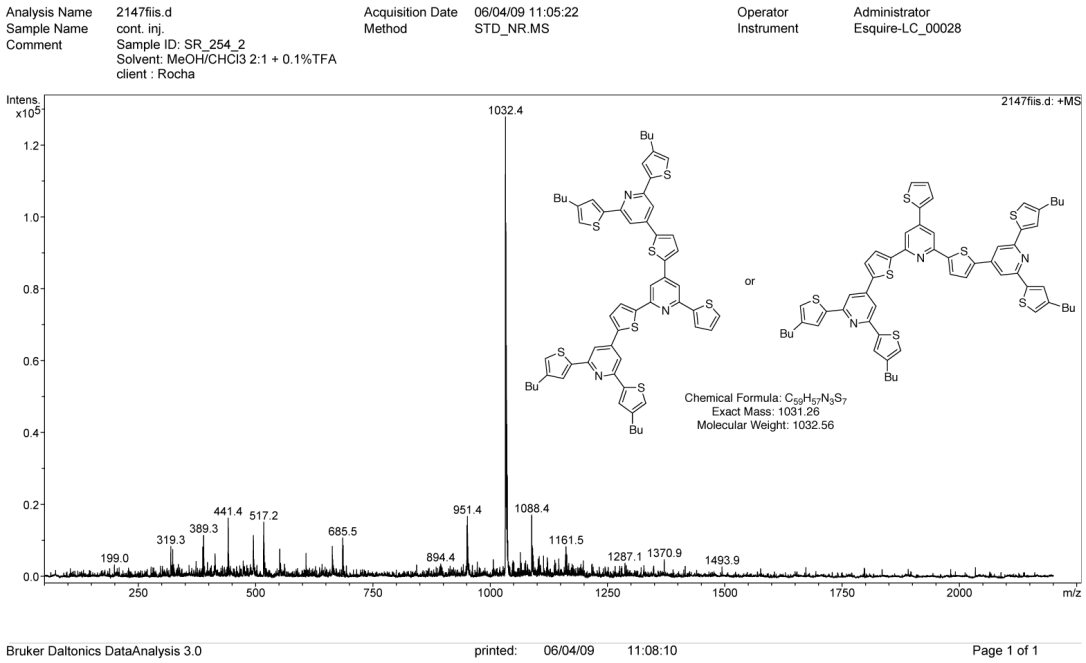

Figure 2.6: *Mass spectrum of the crude reaction mixture of the tentative formation of* ***72****.*

2.7.2 Convergent Pathway

As already discussed, the regioselectivity of the transformations is crucial, and to proceed with the synthesis of the dendrimeric series through the convergent pathway, dendron **73** was designed to have butylthiophene groups in the 2- and 6-positions of the pyridine ring and an unsubstitute thiophene in the 4-position. This was intended to serve as scaffold for a regioselective deprotonation at the alpha-position of the unsusbtituted thiophene applying the same methodology described earlier in **Scheme 2.20**, although it was not clear that this regioselective deprotonation would occur selectively.

Preparation of **73** was accomplished on a stepwise manner, **Scheme 2.29**. Under room temperature Negishi conditions employing palladium tetrakis as the catalyst and thiophene zincate **70**, only the iodo substituent in **64** reacts to form 2,6-dichloro-4-thiophen-2-ylpyridine (**74**) in 94 % yield. This product can also be submitted to Negishi cross coupling conditions, only this time employing butylthiophene zincate **61** with IPr and palladium as the catalyst system under reflux for 18 hours to give dendron **73** in 93 % yield.

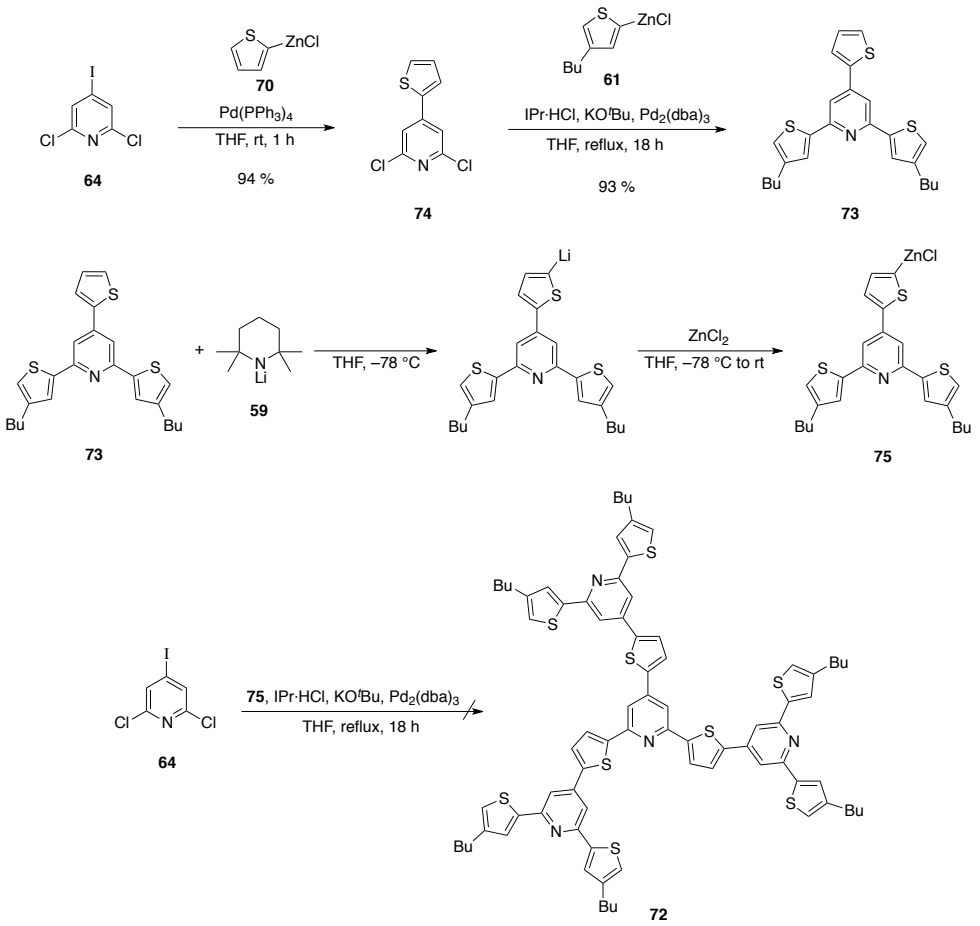

Scheme 2.29: *Synthesis of dendron* ***73****, regioselective deprotonation of* ***73*** *and tentative formation of first-generation dendrimer* ***72****.*

Attempted synthesis of the first-generation dendrimer, **72**, was performed by Negishi reaction of the regioselective zincade **75** and tri-halopyridine **64**. The outcome of the reaction was a mixture that was extremely hard to characterize and purify as a consequence of its solubility properties. With the hypothesis that the butyl side chains were insufficient to assist with the solubility properties, the use of octyl side chains was proposed.

3-Octylthiophene was prepared using the same conditions applied in the preparation of 3-butylthiophene. The synthesis of the octyl-version of the dendron was performed using Negishi cross-coupling conditions in the presence of IPr ligand, palladium and zincate **76** and gave the product **77** in 87 % yield, **Scheme 2.30**. This dendron could then be regioselective lithiated and transmetallated with zinc chloride to give intermediate **78**.

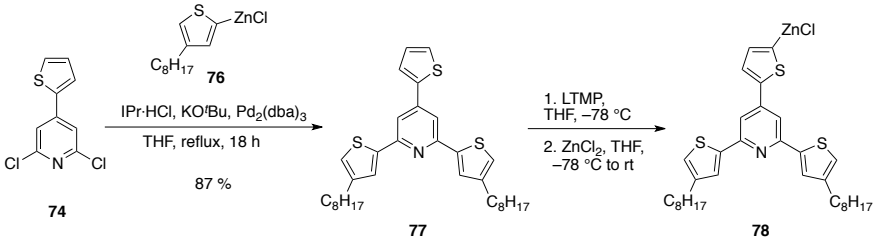

Scheme 2.30: *Sythesis of octyl-dendron* ***77*** *and its regioselective activation as the zincade* ***78****.*

The use 3 equivalents of **78** and one equivalent of **64** under Negishi cross-coupling conditions were applied with the intention of synthesizing dendrimer **79**. Many attempts of this reaction always resulted in a mixture that was quite challenging to purify, which led us to follow a stepwise coupling. Intermediate **80** was prepared by the regioselective mono-coupling of **78** with **64** in 76 % yield after purification, further reaction with **78** afforded the first-generation octyl dendrimer **79** in 53 % yield, **Scheme 2.31**. It must be highlighted that the purification remained challenging and was done by several consecutive column chromatography processes.

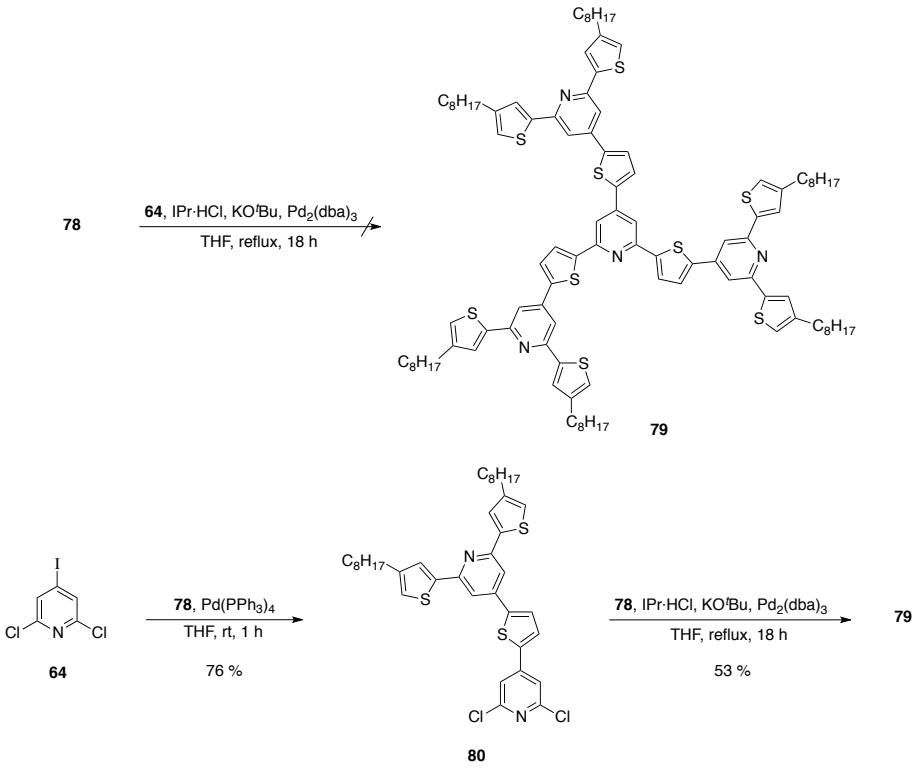

Scheme 2.31: *Attempted direct synthesis of first geration dendrimer* ***79*** *and accomplished stepwise synthesis through intermediate* ***80****.*

The next step was the preparation of the second-generation dendrimer. It requires the synthesis of the corresponding first-generation dendron **81**, which could be accomplished by the coupling of **74** and **78** under Negishi cross-coupling conditions to afford the product in 40 % yield, **Scheme 2.32**.

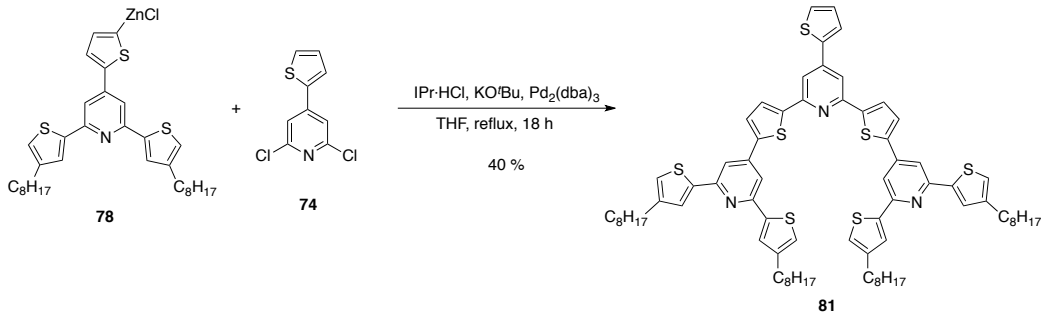

Scheme 2.32: *Syntheis of first generation dendron, **81**.*

Applying the stepwise route towards the preparation of higher generation dendrimers, mono-coupling of **81** and **64** was achieved through the regioselective lithiation of **81** followed by transmetallation with zinc chloride and Negishi cross-coupling conditions in the presence of palladium tetrakis over 20 hours to afford **82** in 45 % yield, **Scheme 2.33**.

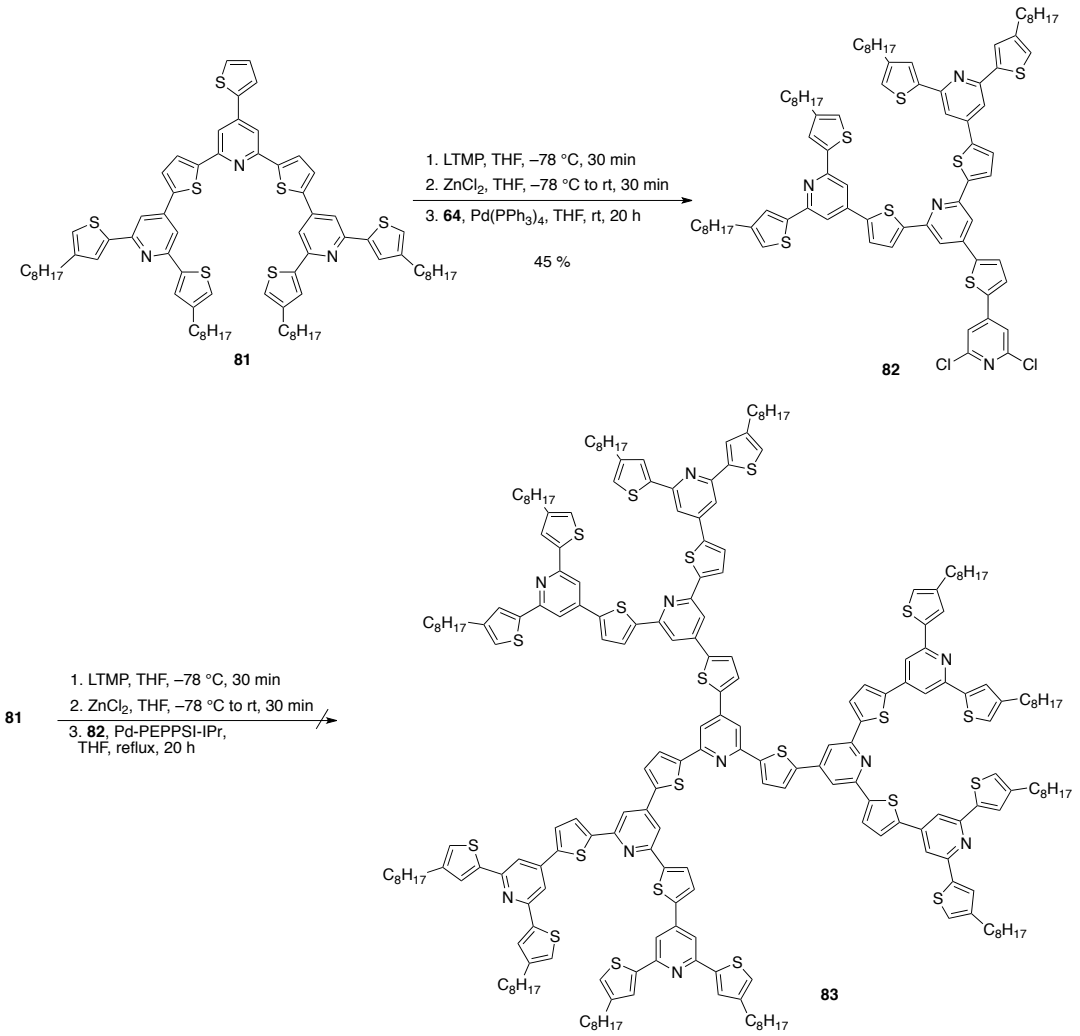

Scheme 2.33: *Attempted stepwise synthesis of second-generation dendrimer* ***83*** *through the formation of intermediate* ***82****.*

The synthesis of the third-generation dendrimer **83** was attempted by the coupling of **82** and **81** zincate in the presence of the catalyst precursor Pd-PEPPSI-IPr. It was possible to observe the desired product by MALDI mass spectrometry, **Figure 2.7**, but many purification attempts failed to deliver clean product. One of the main reasons for the difficulty in purification seems to be due to aggregation, since it is possible to observe by thin layer chromatography that the R_f of what appears to be the product in the reaction mixture is extremely concentration dependent.

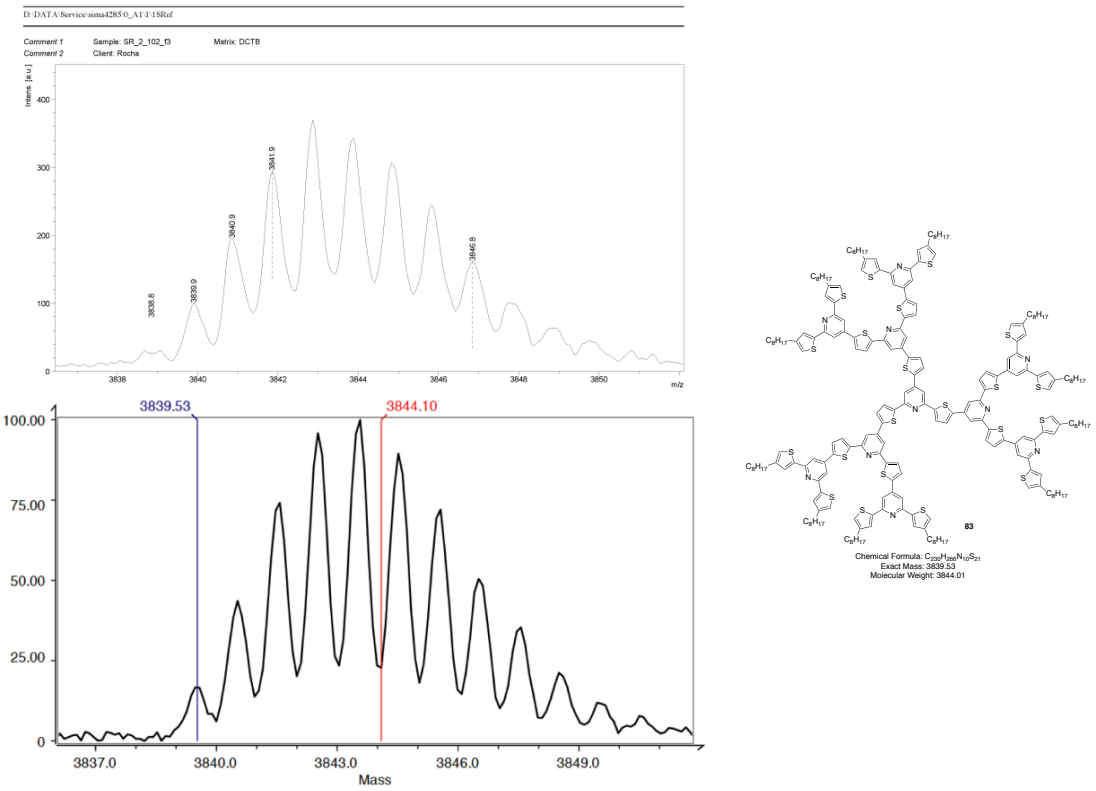

Figure 2.7: *Zoom of the measured, top, and calculated, bottom, mass spectra for the reaction mixture of the formation of* ***83****.* [vii]

2.8 Mixed System

A molecule that comprises a 2,5-pyridine ring bonded to two zero-generation dendrons is what will be designated by mixed system (**84**), since it contains structural features from the *2,5-series*, the *2,6-series* and the dendrimeric system. The synthesis of **84** was straightforward from 2,5-dibromopyridine and **71** under Negishi cross coupling conditions to give the desired product in 61 % yield, **Scheme 2.34**.

[vii] Other compounds were also observed in the mass spectrum, but only a zoom of the mass corresponding to the product is shown.

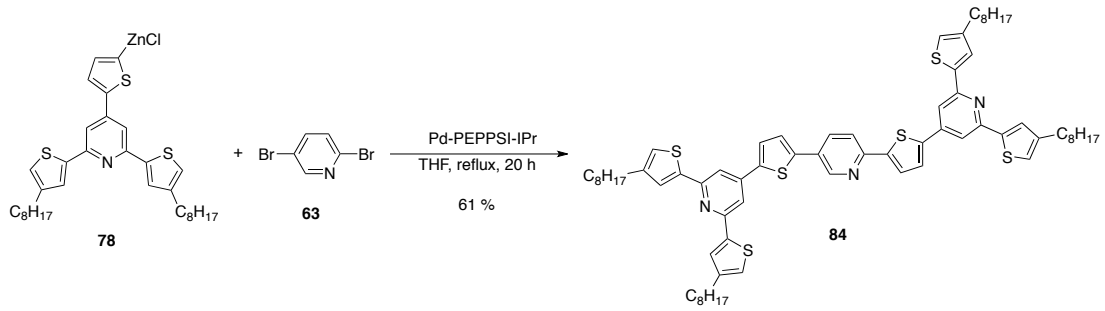

Scheme 2.34: *Synthesis of **84**.*

CHAPTER 3

3 PHOTOPHYSICAL PROPERTIES

Organic chromophores are extremely important for a variety of optical and optoelectronic applications, hence the study and characterization of the photophysical properties of these species is of great interest. In particular, the use of conjugated polymers and oligomers containing D–A alternating units has been shown to be of significant importance in many areas, such as heterojuction solar cells, organic field effect transistors, organic light emitting diodes among others; where the photophysical characterization of the materials is crucial for the device design and fabrication. To better understand how structural modifications lead to changes in the absorption and emission behavior, a systematic structure-property relationship photophysical study of the alternating pyridine–thiophene oligomers and dendrimers previously introduced was conducted and will be presented in this chapter, as well as some examples of similar systems.

3.1 Photophysical Processes

A photophysical process is defined as the photo-excitation and the following events that lead from one to another electronic state of a molecular entity through radiative and nonradiative transitions, without chemical changes.[98] The photophysical processes can be summarized in the Jablonski diagram, **Figure 3.1**, which depicts, in a comprehensible way, the main events that occur. Upon absorption of a photon, one electron of the molecule is promoted from the singlet ground state, S_0,[viii] to a singlet excited state. The molecule is then said to be in the excited state and many processes are important for the deactivation of the excited state; the first one in the internal conversion (IC), which is a nonradiative decay from higher to lower vibrational levels in states of same multiplicity ($S_2 \rightsquigarrow S_1$; $S_1 \rightsquigarrow S_0$), this process is very fast and occurs on the order of 10^{-12} s.[99]

[viii] Triplet ground states also exist, as in molecular oxygen, but they are not common in organic molecules and will not be considered for the purpose of this thesis.

Intersystem crossing is another path for the deactivation of the excited state; it is also a nonradiative transition but now occuring between states of different multiplicities ($S_1 \rightsquigarrow T_1$; $T_1 \rightsquigarrow S_0$), and it is a spin forbidden process. The term spin forbidden indicates a lower quantum mechanical probability, but this can be relaxed by spin-orbit coupling, which occurs on the presence of heavy atoms and is not common in the most commonly studied organic fluorophores.

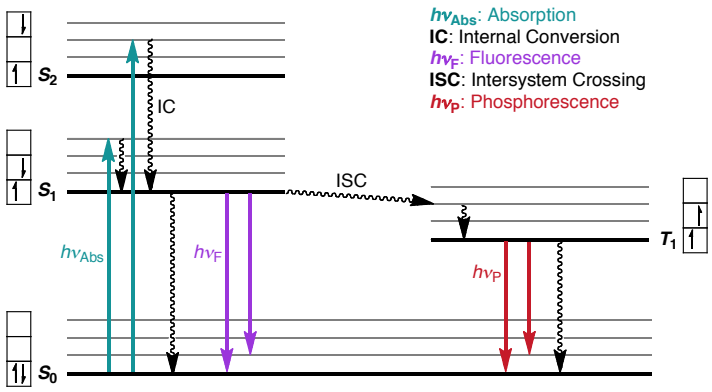

Figure 3.1: *Jablonski diagram. Squiggly arrows indicate nonradiative processes and normal arrows indicate radiative processes.*

The rate of the nonradiative processes is influenced by two main factors: (*a*) the energy separation; the larger the energy gap the slower the process rate ($k(S_2 \rightsquigarrow S_1) > k(S_1 \rightsquigarrow S_0)$) and (*b*) the conservation of spin, transitions between states of different multiplicities are forbidden and consequently have a lower rate ($k(S_2 \rightsquigarrow S_1) > k(S_1 \rightsquigarrow T_1)$). Typical rate constants for the nonradiative processes of organic molecules are:

$$k(S_2 \rightsquigarrow S_1) = 10^{11}–10^{14}\ s^{-1}$$

$$k(S_1 \rightsquigarrow S_0) = 10^{5}–10^{8}\ s^{-1}$$

$$k(S_1 \rightsquigarrow T_1) = 10^{7}–10^{8}\ s^{-1}$$

$$k(T_1 \rightsquigarrow S_0) = 10^{-1}–10^{4}\ s^{-1}$$

Fluorescence and phosphorescence are the names given to the radiative processes that occur for the deactivation of the excited state with the concomitant emission of a photon. Fluorescence is a spin allowed process in which the decay from the lowest singlet state to the singlet ground state is accompanied by the emission of a photon ($S_1 \longrightarrow S_0 + h\nu_F$). Phosphorescence is a spin forbidden transition from the lowest triplet state to the singlet ground state with the emission of a photon ($T_1 \longrightarrow S_0 + h\nu_P$). Since the phosphorescence phenomena is

derived from a spin forbidden transition, its rate, when compared to fluorescence, a spin allowed transition, is much lower. Typical rate constants for the two processes are:

$$k_P = 10^{-1}–10^{4}\ s^{-1}$$

$$k_F = 10^{7}–10^{9}\ s^{-1}$$

When the rate constants for radiative and nonraditive processes are compared, it is evident that the nonradiative processes occur much faster. With this observation, Kasha postulated that always the lowest excited level of a multiplicity (S_1 or T_1) is the one involved in the emissive transition; this statement is also known as Kasha's rule.[100] This means that even if the molecule is excited to higher electronic states (such as S_2, S_3, …) it would rapidly decay, through internal conversion, to the lowest vibrational level of S_1 state and undergo the radiative transition from there.[99]

The efficiency of a radiative process is measured by its quantum yield (Φ), which is defined as the number of emitted by that process divided by the number of photons absorbed by the molecule:

$$\Phi = \frac{\text{number of photons emitted}}{\text{number of photons absorbed}}$$

The fluorescence quantum yield can also be written in terms of the rates of all the processes, radiative and nonradiative, that the molecule is subjected to upon photo-excitation:

$$\Phi_F = \frac{k_F}{k_{IC} + k_{ISC} + k_F} = k_F \tau_F$$

$$\tau_F = \frac{1}{k_{IC} + k_{ISC} + k_F} \quad ,$$

where k's are the rate constants, F: fluorescence, IC: internal conversion, ISC: intersystem crossing; and τ_F is the fluorescence lifetime. The total quantum yield of the system is the sum of the quantum yield for all the processes, radiative (Φ_F and Φ_P) and nonradiative ($\Phi_{IC} + \Phi_{ISC} = \Phi_{NR}$), and it is, by definition, equal to 1.

$$\Phi_T = \Phi_F + \Phi_P + \Phi_{NR} = 1$$

Another important concept in the photophysical processes discussion is the Franck–Condon principle which states: "*Electronic transitions are so fast (10^{-15} s) in comparison to nuclear motion (10^{-13} s) that immediately after the transition, the nuclei have nearly the same relative position as they did just before the transition.*"[101] This is what is commonly called vertical transition, where upon the photo-excitation, the nuclear coordinates are constant and the system is brought to a higher vibrational level of the excited state.

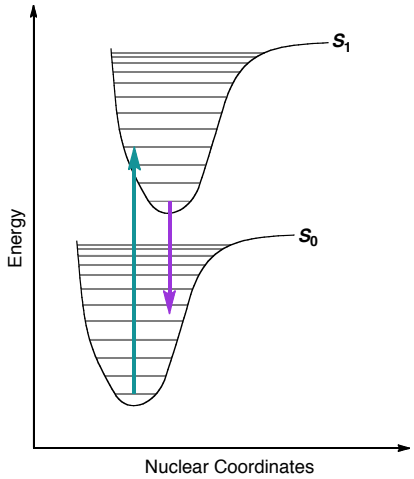

Figure 3.2: *Illustration of the Franck–Condon principle. The potential energy curves of the singlet ground state,* S_0*, and singlet excited state,* S_1*, are depicted as well as the radiative processes absorption, blue arrow, and emission, violet arrow.*

In π-conjugated chromophores containing heteroatoms, the difference in the dipole moment of the ground state and the lowest energy excited singlet state is very pronounced, that is the case because they exhibit internal charge transfer (ICT).[102] If we assume that a donor and an acceptor moiety are present, and that they have poor interaction in the ground state; upon photo-excitation, the system is brought to a non-polar Franck–Condon locally excited state (LE), which thermally equilibrates to the emissive charge transfer state (CT), **Figure 3.3**. The photo-excitation can occur either on the donor or the acceptor LE state, but both generate the same CT state.

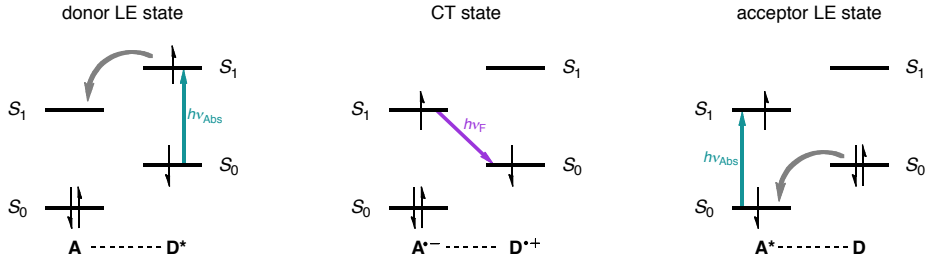

Figure 3.3: *Schematic representation of the locally excited states of non-interacting donor and acceptor and the corresponding charge transfer state.*

On the other hand, if donor and acceptor are conjugated in the ground state, the photo-excitation can occur directly into the CT state, but full separation of charges cannot be attained. If the D and A portions are connected through a single bond and are in a twisted conformation, a higher degree of charge separation can be observed, and the excited state is called twisted

intramolecular charge transfer state (TICT).[103] The most discussed example is 4-(dimethylamino)benzonitrile, where the dimethylamino group is the donor and the benzonitrile is the acceptor. This compound shows dual fluorescence through two fluorescence bands, and their relative intensity is strongly dependent on the solvent polarity. The lower wavelength band comes from the direct decay of the locally excited state, $h\nu_{F(LE)}$, and is the only one observed in apolar solvents. With increasing solvent polarity, the second fluorescence band, at longer wavelength, appears, and its relative intensity also increases. This longer wavelength emission, $h\nu_{F(CT)}$, comes from the TICT state, where the amino group is twisted by a 90° angle relative to the plane of the benzene ring, therefore observing a charge separation between the donor and the acceptor; and due to its very polar character, this emission is exclusively observed in polar media. **Figure 3.4** shows a representation of the TICT state for 4-(dimethylamino)benzonitrile as well as the relative energies of the LE and CT states.

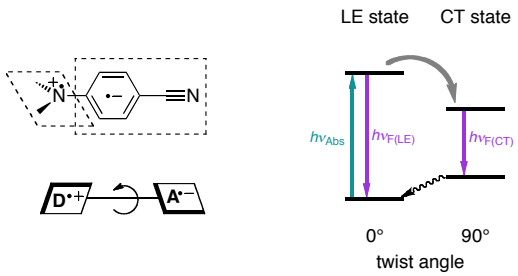

Figure 3.4: *Representation of the TICT state through the rotation of the nitrogen- aromatic carbon single bond and the corresponding relative energy levels for the non-twisted and twisted states.*

In cases where the electronic excited state has a bigger dipole moment compared to the ground state, the effects of solvent polarity are more visible in the emission wavelength, and practically no change is observed in the absorption. This is the case because prior to photo-excitation, the dipole of the solvent molecules are thermally equilibrated around the chromophore; when the excitation occurs, the system goes to an excited Franck–Condon state, which is not yet thermally equilibrated with the surrounding solvent molecules, and therefore has the same energy in polar and apolar media, the observed effect is that the chromophore has nearly the same absorption in both polar and apolar solvents, **Figure 3.5**-A. Once the excited state is thermally equilibrated, the emission can occur. In the case of polar solvents, the CT excited state is stabilized by the dipole of the solvent molecules and the Franck–Condon ground state, reached the system after emission, is destabilized; as a consequence, the more polar the media, the longer the wavelengths observed, **Figure 3.5**-B, or in other words, a red shift is observed. Furthermore, with increasing media polarity, the CT state can be deactivated through

coupling with the solvent molecules. During the thermal equilibration process, the solvent dipoles are reoriented around the CT excited state, which contributes to the nonradiative decay of the emissive state. As a consequence, both the lifetime and the quantum yield are lowered in polar media.

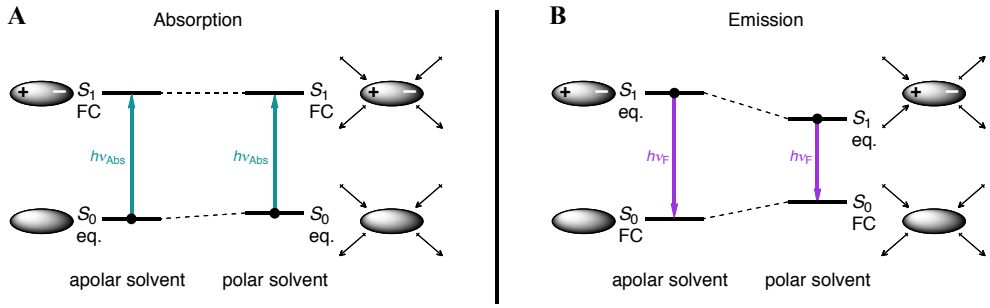

Figure 3.5: *Schematic representation of the solvent effect in the absorption, **A**, and emission, **B**, of chromophores exhibiting a CT polar excited state. FC denotes the Franck–Condon, not thermally equilibrated, state; eq. denotes thermally equilibrated states.*

If the ground state is more polar when compared to the excited state, a stabilization of the ground state occurs with increasing solvent polarity, therefore, a blue shift in the absorption is observed, this is called negative solvatochromic effect, and many dyes exhibiting this effect have been studied. A method of quantifying relative solvent polarities is through the study of such dyes and many solvent polarity scales based on this phenomena have been reported,[104] one of the most commom ones being the $E_T(30)$, where a betaine dye was used as the probe for solvent polarity.[105]

3.2 Properties of Selected Oligomers

Oligothiophenes, together with modified oligothiophenes, are among the most studied class of π-conjugated oligomers. This is the case because there are many well-known methods to modify thiophene units, as well as many methods to promote thiophene-thiophene bond formation. The first studies of chain length and properties correlation was reported for oligothiophenes and it allowed extrapolations and the prediction of the properties in polymeric systems.

The oligothiophene family depicted in **Figure 3.6** was reported in 1992 by Bäuerle,[41] one of the most active researchers in the area of olithiophenes and its derivatives and applications. The systematic study of the family of compounds shown demonstrated that it was possible to correlate the photophysical properties with the chain length for α-oligothiophenes

and use this as an instrument to estimate maximum conjugation length in a polymer chain. A linear relationship between the absorption energy, in eV, and the inverse chain length is observed when conjugation of the units is present; if conjugation is disrupted, the linear relationship is not observed anymore and the chain length where this occurs is said to be the maximum effective conjugation length of that particular system; in other words, the maximum effective conjugation length is calculated as the saturation point of the red shift in the absorption spectra. The maximum effective conjugation length for α-oligothiophenes was believed to be 11 units,[106] but subsequent studies increased the estimated number to be 20 units.[107]

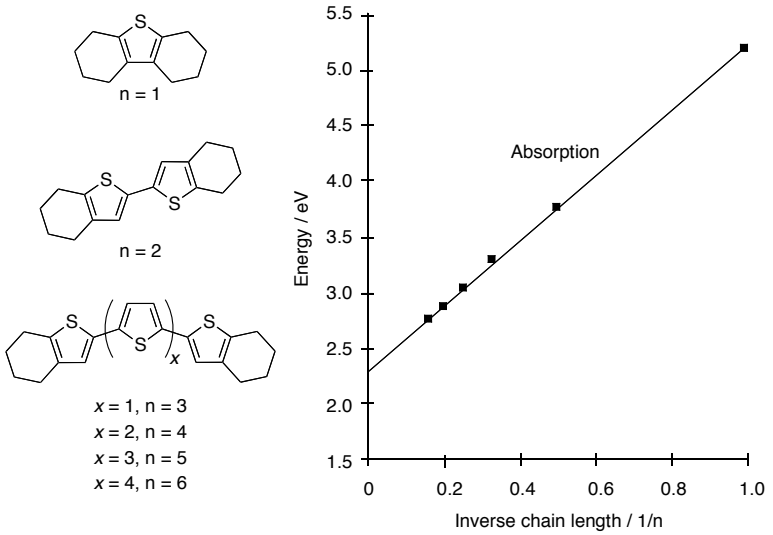

Figure 3.6: *Linear relationship between the absorption maximum and the inverse chain length for the oligothiophene family depicted. Adapted from reference 41.*

Although there are many reports of studies of oligothiophes or thiophene-containing oligomers, not many systematic studies have been shown for oligomers containing both pyridine and thiophene groups. One of the few reports comes from Fukumoto *et al.*, where they describe the synthesis of pyridine and thiophene co-oligomeres (shown in **Scheme 2.11**) and report photophysical data, **Table 3.1**, which is of interest in the context of the oligomers reported in this dissertation. Two series of co-oligomers were studied and they are composed of oligomers containing 4-, 5- and 6-rings; the first series, **a**, possesses a central α-oligothiophene end-capped by pyridine units, and the second, **b**, can be considered a sort of alternating series.

It is interesting to note that for the same oligomer length, series **a** observes longer absorption and emission wavelengths when compared to series **b**; the authors explain this observation arguing that a CT state is present and occur from the central thiophene moiety to

the peripheral pyridine rings in series **a**, while this is not possible in series **b**. Although this explanation is plausible, one evidence that does not corroborate with it are the Stokes shift values, **Table 3.1**, since they are very similar for oligomers of the same length in the different series and CT states should observe higher Stokes shift when the same solvent system is considered for similar molecules. Furthermore, it is known that alternating donor–acceptor (D–A) polymers exhibit excited states with charge transfer character and some have energy transitions as low as 1.4 eV.[108] Alternatively, a hypothesis to explain the difference between the two series is the degree of conjugation; series **a** seems to have a higher degree of conjugation across the backbone than series **b**, which leads to a red shift in both absorption and emission; this is supported by the fact that the central α-oligothiophene unit in series **a**, which is comprised of 5-membered rings are connected to each other and leads to less steric interactions than series **b**, where the bonds are between 5- and 6-membered heterocycles.

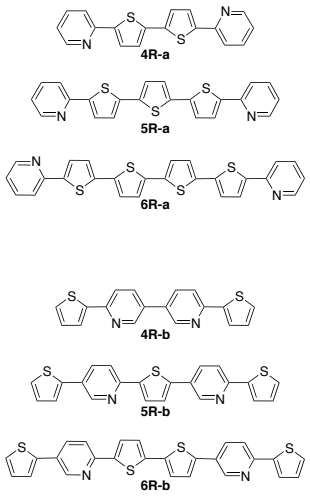

Table 3.1: *Photophysical data reported by Fukumoto* et al. *for the series of oligomers represented on the left.*[65]

	absorption / nm		emission / nm (Φ, quantum yield)		Stokes shift / cm^{-1}	
	CH_3Cl	HCOOH	CH_3Cl	HCOOH	CH_3Cl	HCOOH
4R-a	390	414	435, 462 (0.17)	478 (0.21)	2652	3234
5R-a	418	451	476, 505 (0.21)	563 (0.19)	2915	4411
6R-a	435	473	503, 537 (0.35)	636 (0.10)	3108	5418
4R-b	345	379	388, 409 (0.71)	431 (0.43)	3212	3183
5R-b	384	410	432, 459 (0.33)	488 (0.28)	2894	3898
6R-b	408	439	470, 501 (0.37)	596 (0.07)	3233	6001

Moreover, a plot of the absorption energy versus the inverse of the total number of aromatic units shows a good linear correlation, **Figure 3.7**. It is interesting to notice that the slope obtained for the two series is quite different, being steeper in the case of series **b**, which means this series is predicted to have a lower absorption energy, or longer absorption wavelength, than series **a** already at an oligomer composed of 10 aromatic units. This observation makes the study of alternating pyridine–thiophene oligomers quite appealing.

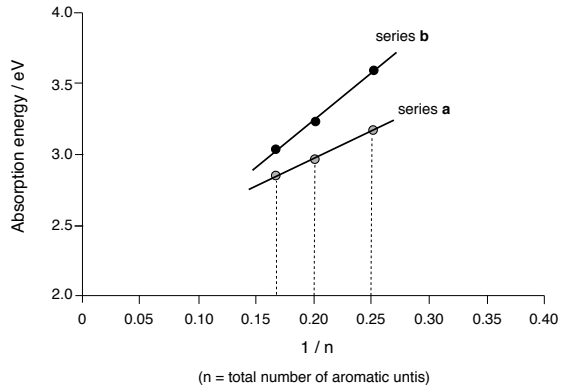

***Figure 3.7**: Plot of absorption energy versus 1/n, where n is the total number of aromatic units, for series **a** and **b**. Adapted from reference 65.*

Another significant observation, also reported in **Table 3.1**, is the characterization of the two series in formic acid, which leads to the protonation of the pyridine units; and where a red shift is observed in both the absorption and emission properties accompanied by a decrease in the quantum yield. This modulation of the optical properties by coordination on the nitrogen atom of oligomers containing N-heterocycles has attracted some attention in the past years and will be discussed further, an example for pyridine-containing polymers where the alkylation of the pyridine ring leads to the formation of a pyridinium ion and results in significant changes in the properties was already discussed in Chapter 1, **Table 1.3**.

In 2009, Bazan and coworkers reported interesting optical properties of a benzo-2,1,3-thiadiazole and thiophene co-oligomer (**BT**). The nitrogen-containing heterocycle present in the oligomer is capable of coordinating to Lewis acids, and it is very interesting to observe that the absorption properties of the complex depend on the strength of the different Lewis acids.

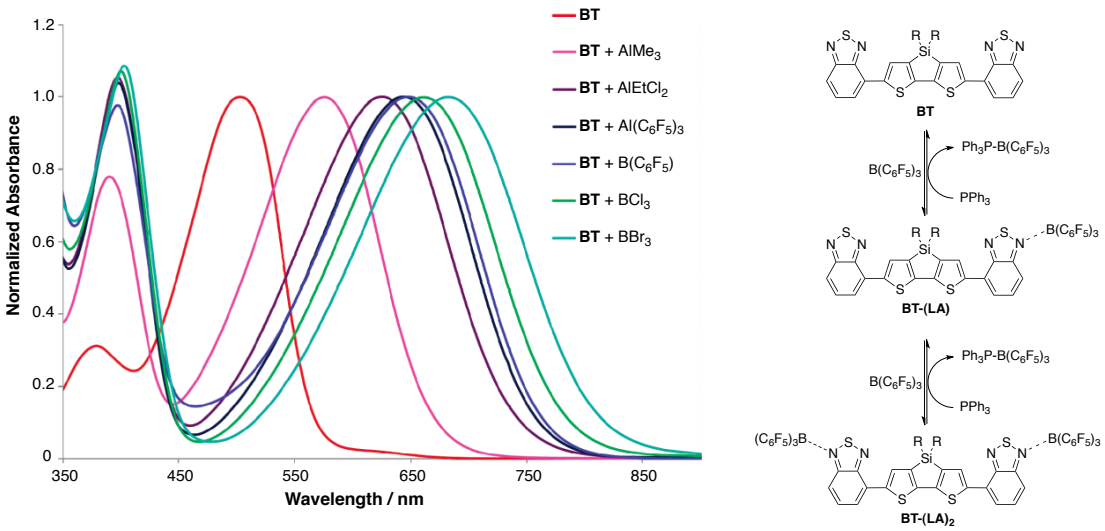

Figure 3.8: *Normalized absorption spectra of* ***BT*** *in the presence of 2 equivalents of different Lewis acids; scheme of the equilibrium between* ***BT*** *and* $B(C_6F_5)_3$*, the coordination can be disrupted by a better Lewis base, in this example* PPh_3*.*

In **Figure 3.8** it is possible to see that the coordination with a range of Lewis acids causes a red shift in the absorption that leads to a broad coverage of the visible spectra. Analyzing the spectrum obtained for the strongest Lewis acid reported, BBr_3, it is possible to see the most pronounced red shift, of 178 nm. From the plot it seems reasonable to affirm that the stronger the Lewis acid, the larger the red shift. Furthermore, the authors reported the isolation of complex **BT-(LA)$_2$** after the treatment of **BT** with 2 equivalents of $B(C_6F_5)_3$. On the other hand, complex **BT-(LA)** was not isolated, but through NMR experiments of 1:1 mixtures of **BT** and $B(C_6F_5)_3$, the authors were able to show that the coordination of the Lewis acid is statistical, since at –30 °C a mixture of 1:2:1 between **BT**, **BT-(LA)** and **BT-(LA)$_2$** was observed. Additionally, the coordination between the oligomer and the Lewis acid can be disrupted by the addition of a better Lewis base, like triphenylphosphine (PPh_3).

3.3 Alternating Pyridine–Thiophene Oligomers

In the next sections, a discussion regarding the photophysical properties found for the series of alternating pyridine–thiophene oligomers that are the theme of this work will be presented.

3.3.1 2,6-Series

The first series investigated was the *2,6-series*; and the absorbance spectra of the compounds belonging to this series (**26a**, **26b**, **26c** and **26d**, **Figure 3.9**) are shown in **Figure 3.10**. The spectra are of ~10^{-6} M solutions in acetonitrile and a red shift trend, although not very pronounced, can be observed with increasing oligomer length. The largest absorption maxima wavelength difference, of 48 nm, was observed between **26a** and **26d**, but a tailing off to 2 nm difference between the two longest oligomers, **26c** and **26d**, is an indication that the maximum effective conjugation length is not far from the four repeating pyridine–thiophene units present in **26d**.

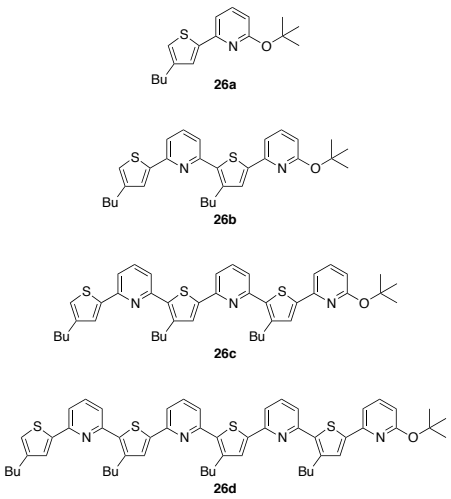

Figure 3.9: *Compounds belonging to the* 2,6-series.

In addition, the spectra were recorded in the presence of excess of trifluoroacetic acid (TFA) and when the neutral and protonated species absorption properties are compared, the protonated versions exhibit longer wavelength absorption for the same oligomer length. This could be an indication of a higher degree of conjugation in the protonated state, since the protonated pyridine ring has a more electron poor character, which is in agreement with a higher D–A character. It is interesting to observe that the change in the 8-ring compound, **26d**,

is less pronounced compared to the rest of the series, which suggests that steric effects might play an important role in longer oligomers when the pyridine units are protonated and have substituents that are *meta* relative to each other.

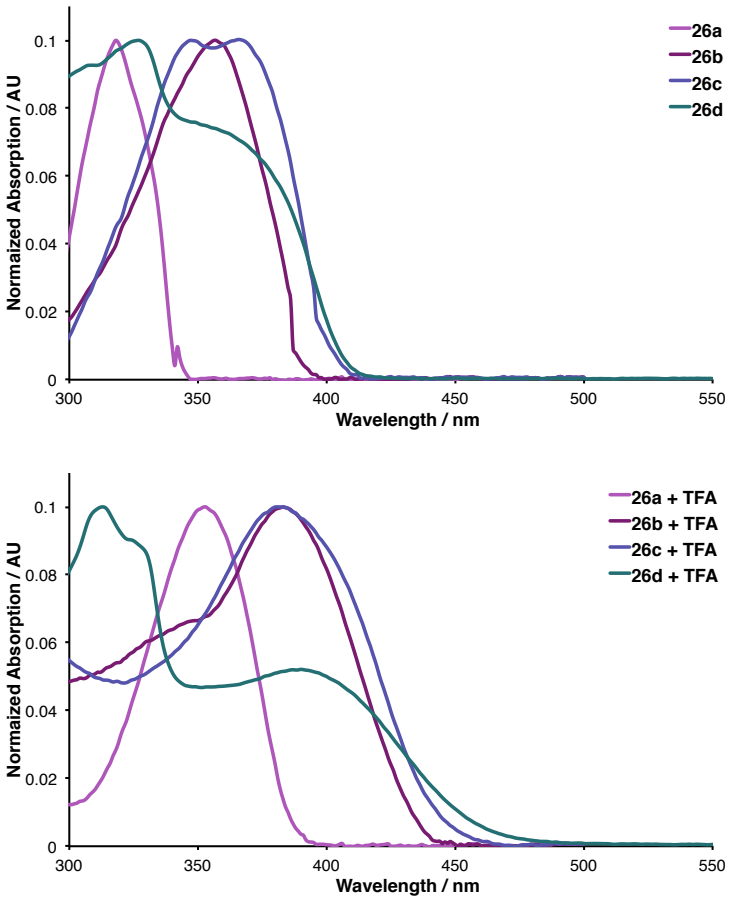

Figure 3.10: *Normalized absorption spectra of* ***26a-d****, top; and after the addition of excess of TFA, bottom. Solutions in acetonitrile at ~10^{-6} M.*

Similarly, the study of the emission properties shows a red shift with increasing oligomer length and, like in the absorption maxima, the largest difference is observed in the beginning of the series, 50 nm between **26a** and **26b**, and the effect tails off to 4 nm difference among the two longer oligomers, **26c** and **26d**. As in the absorption spectra, the protonated versions of the oligomers exhibit longer wavelength emission when compared to the neutral species, which is again an indication of a higher degree of conjugation or of a stronger character of a twisted charge transfer excited state.

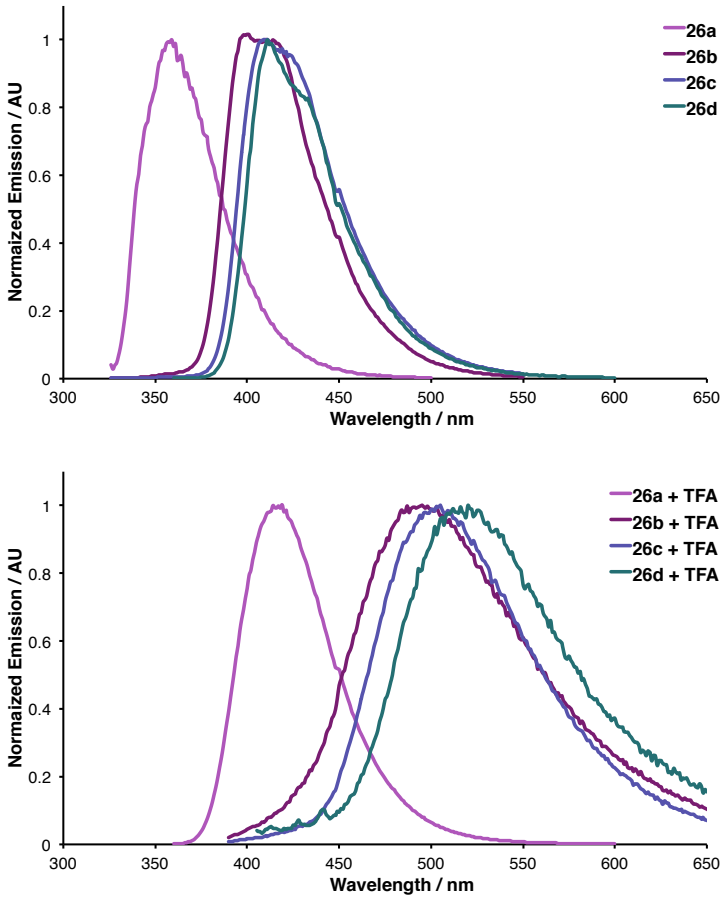

Figure 3.11: *Normalized emission spectra of the* 2,6-series *compounds before (top) and after the addition of excess of TFA (bottom); in acetonitrile at ~10^{-6} M concentration.*

3.3.2 2,5-Series

Analyzing the data obtained for the *2,5-series* (compounds **25a**, **25b**, **25c** and **25d**, represented in **Figure 3.13**), the same trend as observed in the *2,6-series*, namely, a red shift with oligomer length increase is evident. In the absorption spectra, **Figure 3.13**, the bathochromic shift is very pronounced with oligomer length and even when the two longest oligomers are compared, a difference of 16 nm is found, in contrast to the *2,6-series*, where the difference in the absorption maxima is of only 2 nm. Regarding the absorption properties of the protonated species in the presence of excess of TFA, again a red shift in the absorption spectra is observed when compared to the neutral counterparts. In contrast to the *2,6-series*, the protonated version of the longer oligomer of the *2,5-series*, compound **25d**, shows the same behavior as the other members of the series; in this case, the substituents steric effects seem to be much less pronounced, since they are *para* relative to each other in the pyridine ring.

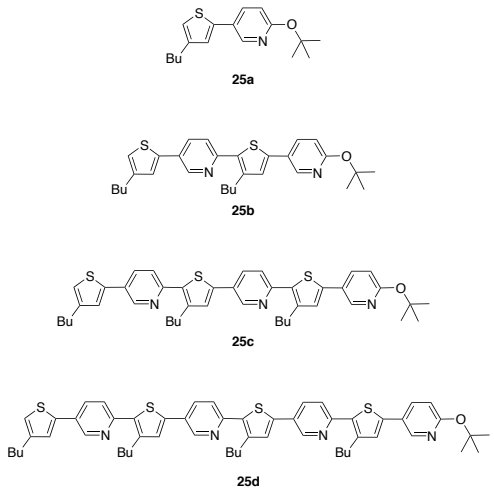

Figure 3.12: *Compounds belonging to the* 2,5-series.

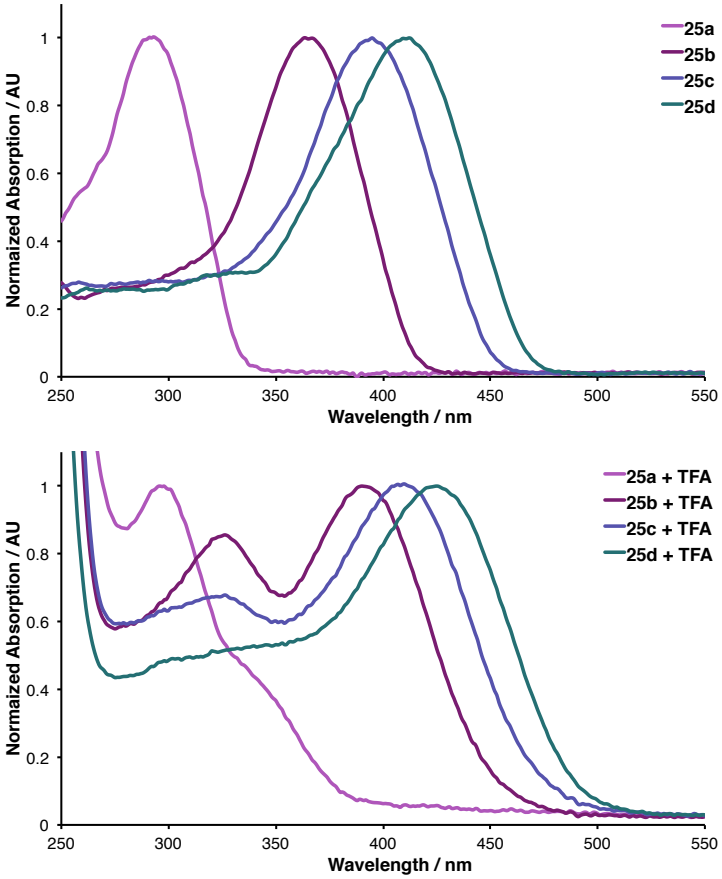

Figure 3.13: *Normalized absorption spectra of oligomers* ***25a-d****, top; and after the addition of excess of TFA, bottom. Solutions in acetonitrile at ~10*$^{-6}$ *M.*

In a similar fashion, the emission spectra of the *2,5-series* exhibit a red shift with increasing oligomer length, **Figure 3.14**, indicating that the maximum conjugation length has

not been reached yet. When the oligomers are protonated with excess of TFA, again a red shift is seen when compared to the neutral species. It is interesting to note that the emission is of quite low energy for the longest oligomer in the protonated state, its maximum being at 564 nm and tailing off up to 700 nm.

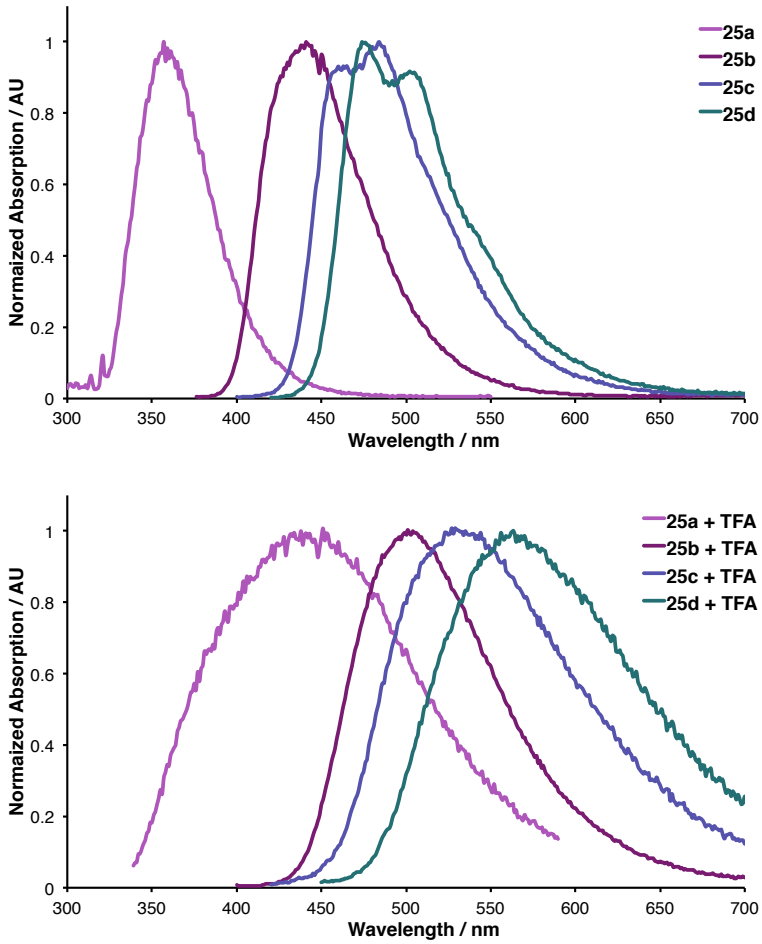

Figure 3.14: *Normalized emission spectra of the* 2,5-series *compounds before (top) and after the addition of excess of TFA (bottom); in acetonitrile at ~10^{-6} M concentration.*

3.3.3 Discussion

A summary of the data found for the oligomers in both series is shown in **Table 3.2**. As expected from the discussion in Chapter 1, the *2,5-series* oligomers exhibit absorption and emission maxima that are at longer wavelength when compared to oligomers of the same size from the *2,6-series*. The same tendency is observed in the experimental optical bandgap (E_g, calculated from the absorption onset), which represents a direct estimation of the HOMO/LUMO gap and where a decrease in its value is expected with a higher degree of conjugation between the units.

One exception is observed for the shortest oligomers, since **26a** has a longer absorption wavelength (320 nm) than **25a** (290 nm); this observation can be attributed to the regiochemistry around the pyridine ring, since in the case of **26b** the thiophene substituent is *orto* relative to the pyridine nitrogen atom, while for **25a** it is in the *meta* position. It is interesting that the wavelength for the emission maxima is the same for both **26a** and **25a** (360 nm), which leads to a much larger Stokes shift in the case of **25a**; this can be rationalized by a bigger difference between the ground and excited state geometries in the case on **25a**, which can be an indication that a higher charge transfer character is present in the case of the latter.

Table 3.2: *Summary of the photophysical properties of the two series of compounds studied,* 2,6-series *and* 2,5-series *in the absence (neutral) and presence of excess of TFA (prot.). All the measurements were performed using ~10^{-6} M solutions in acetonitrile. The quantum yield is reported for the neutral species relative to a standard, either PPO (**Φ** = 0.94, in cyclohexane) or DPA (**Φ** = 1, in cyclohexane).*

		2,6-series				*2,5-series*			
		26a	**26b**	**26c**	**26d**	**25a**	**25b**	**25c**	**25d**
λ_{max} (abs) / nm	neutral	320	355	368	370	290	363	394	410
	prot.[a)]	*351*	*383*	*386*	*395*	*295, 340[b)]*	*390*	*407*	*424*
λ_{max} (em) / nm	neutral	360	410	415	422	360	438	473	488
	prot.[a)]	*415*	*494*	*503*	*520*	*441*	*500*	*530*	*564*
E_g^{opt} [c)] / eV	neutral	3.56	3.11	3.02	2.99	3.69	2.95	2.72	2.63
	prot.[a)]	*3.14*	*2.80*	*2.67*	*2.57*	*3.25*	*2.63*	*2.52*	*2.46*
Stokes shift / cm^{-1}	neutral	3472	3779	3078	3330	6705	4717	4239	3898
	prot.[a)]	*4394*	*5867*	*6026*	*6086*	*6736*	*5641*	*5702*	*5854*
Φ	neutral	0.05	0.60	0.69	0.74	0.10	0.38	0.74	0.76

a) protonated species after the addition of excess of TFA; b) shoulder, considered for the calculation of the Stokes shift; c) calculated from the absorption onset.

It is interesting to note that for both series the Stokes shift magnitude decreases with increasing oligomer length, which shows that a larger difference in the geometries of the excited and ground states is favored in shorter oligomers, indicating that shorter oligomers observe a higher degree of charge transfer excited state character. In general, the Stokes shift observed for the oligomers in the *2,5-series* is larger compared to the *2,6-series*, indicating that a charge transfer excited state character is favored in the former, which is another evidence that a higher degree of conjugation is present in the *2,5-series*.

When the protonated species are considered, a red shift in both emission and absorption is observed for all oligomers.[ix] The reasoning behind this effect was already pointed out in previous examples, but it essentially consists of the fact that the pyridine units become more electron deficient when protonated (or coordinated to Lewis acids) and an increased conjugation can be expected. This leads the absorption maximum to shift in all the cases studied which is reflected on a smaller optical bandgap, as low as 2.56 eV (485 nm) in the case of the protonated **25d**.

Although quantum yields for the protonated species were not determined, it was visible that the emission efficiency decreases. This decrease in the quantum yield reflects a higher efficiency of the internal conversion process. Two possible explanations for this observation were considered; the first has to do with the equilibrium between the protonated *versus* non-protonated species and the presence of the counter ion, which could lead to thermal and collision promoted radiationless decay. The second possible explanation has to do with the energy-gap law,[109] which takes into consideration the energy difference between the ground (S_0) and excited (S_1) states, it asserts that the non-radiative decay rate of an excited state increases exponentially as the energy gap decreases; this is a plausible explanation in this case, since the absorption is at lower energy for the protonated series.

Also noteworthy is the quantum yield, which increases with oligomer length and is quite high for the longest oligomers, reaching 0.69 and 0.74 for **26c** and **26d**, and 0.74 and 0.76 for **25c** and **25d**.

[ix] The emission response to added TFA is instantaneous. However, ^{1}H-NMR studies show conversion of protonated oligomers to the corresponding pyridols (via loss of the *tert*-butyl group) over the course of several hours.

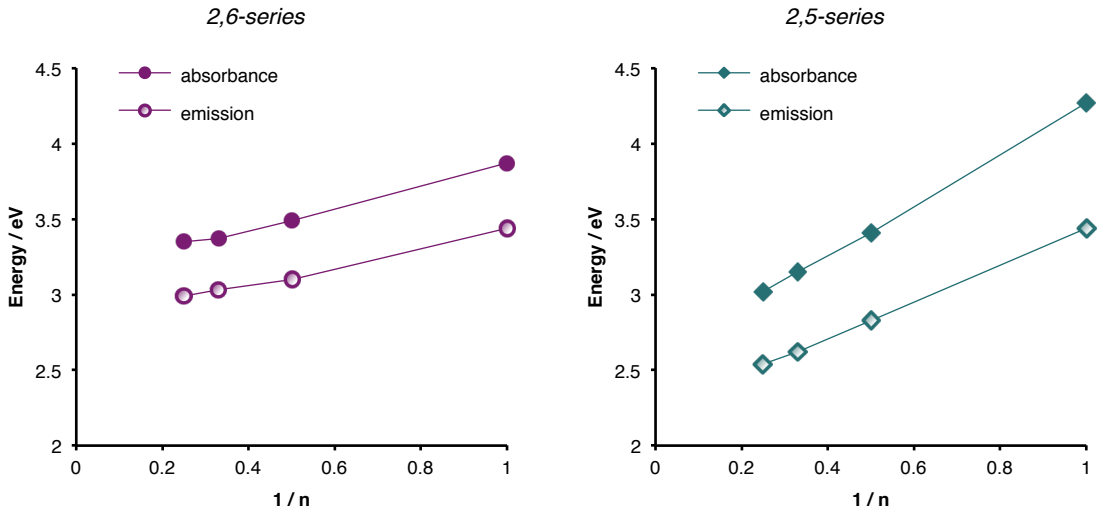

Figure 3.15: *Plot of energy versus the inverse chain length for the two series studied, where* n *is the number of pyridine–thiophene repeating units. The maximum wavelength of absorption and emission was used for the plot. The values are merely connected by lines; linear regression details are given in the experimental section, Chapter 6.*

As discussed earlier, being able to carry out property-structure relationships is of great interest and a plot of the absorption and emission energies *vs.* the inverse chain length of the oligomers is shown in **Figure 3.15**. One difference between the two series that was already mentioned, but now can be graphically visualized, is that the *2,5-series* has lower absorption and emission energies (more red-shifted) for the same oligomer length than the *2,6-series*. Another difference is the extent of the conjugation, and although a very good linear relationship was found for all the correlations,[x] a careful observation of the *2,6-series* plot in **Figure 3.15**, where the values are connect by lines, suggests that the maximum conjugation length in that series is very close to the largest oligomer reported here. The same is not the case for the *2,5-series*, and the maximum conjugation length in this case is estimated to be of at least around the double of units of the longest oligomer examined here, namely 16 heterocyclic units.

Utilizing the linear regression[x] to predict the absorption energy of a polymer with infinite chain length and idealized conjugation (1/n = 0) we find 3.15 eV (394 nm) and 2.60 eV (477 nm) for the *2,6-series* and *2,5-series*, respectively, applying the same for the emission energy gives 2.82 eV (440 nm) and 2.23 eV (555 nm). The estimated absorption energy for a *2,5-series* polymer is smaller than the one observed for a poly 3-hexylthiophene (**P3HT**) solution: 2.77 eV (447 nm).[110]

[x] The value for the R^2 in the linear regressions were found to be 0.98 and 0.99 for the *2,6-series* absorption and emission, respectively, and 0.99 for both series in the *2,5-series*. Details are given in the experimental session, Chapter 6.

Although the value predicted for the *2,5-series* polymer is not very far from the one found for **P3HT**, the two systems are very distinct in the sense that general unsubstituted oligothiophenes are not good fluorophores, sexithiophene has a quantum yield of 32 %,[111] while the 6-ring member of the *2,5-series*, **25c**, observes a quantum yield of 74 %, more than the double of the thiophene-only counterpart.

3.4 Dendrimeric Systems

The characterization of the molecules belonging to the dendrimeric series will be presented in two parts, first the generation zero and generation one dendrimers will be presented, followed by the mixed system and other molecules members of this general dendrimer classification.

3.4.1 Dendrimers: G0 and G1

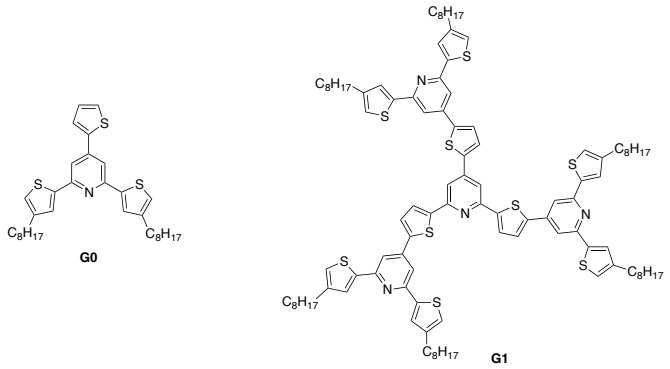

Figure 3.16: *Structures of generation zero,* ***G0****, and generation one,* ***G1****, of the dendrimeric series.*

Dendrimers **G0** and **G1**, **Figure 3.16**, had their photophysical properties determined on the same way as the oligomer series. The normalized absorption spectra of the nominal compounds in the absence and in presence of TFA are shown in **Figure 3.17**. The absorption maximum for both species is the same: 355 nm. Although it seems reasonable to expect a longer wavelength absorption for **G1**, because of the higher number conjugated heterocycles present in the structure, the observation that both species have very similar absorption maxima wavelengths indicates that the heterocycles might not be in conjugation, which could be due to the 2,4,6-trisubstitution pattern and the mismatch resonance conjugation or due to steric clashing of the three thiophene rings around a pyridine moiety. It is interesting to note that the

tailing off of the absorption for **G1** covers longer wavelengths, extending the absorption to 430 nm (2.88 eV) in contrast to 389 nm (3.19 eV) for **G0**.

Similarly to the oligomer series, protonation of the pyridine rings also leads to a red shift in the absorption of 57 nm for **G0** and 67 nm for **G1**, when compared to the neutral counterparts. The absorption maxima is once more very similar for **G0** and **G1** (412 and 422 nm, respectively), **Figure 3.17**, but again a longer tailoring towards lower energy is observed for the latter, leading to an absorption onset of 2.56 eV (485 nm) for **G1** compared to 2.68 eV (462 nm) for **G0**.

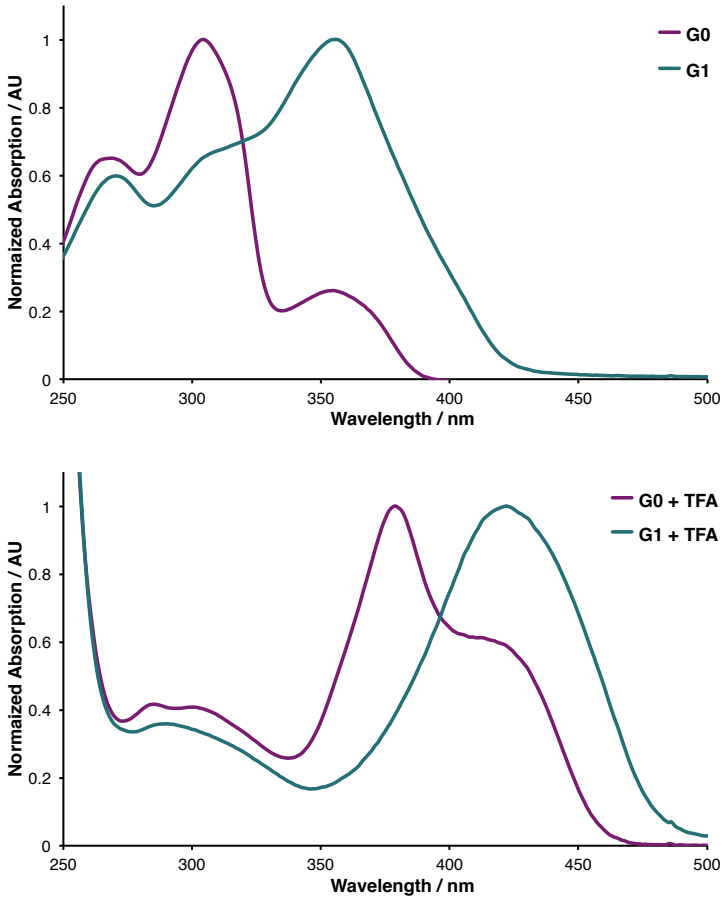

Figure 3.17: *Normalized absorption spectra of dendrimers **G0** and **G1**, top; and after the addition of excess of TFA, bottom; ~10^{-6} M solutions in dichloromethane.*

Although the absorption properties for the neutral version of these two species seem to be very similar in the normalized spectra, their extinction coefficients are very different; **Figure 3.18** shows the spectra where this difference is depicted. The value of the extinction coefficient for **G1** (ε_{355} = 141000 M^{-1} cm-^{1}) is approximately 15 times bigger than the one for **G0** (ε_{355} = 9500 M^{-1} cm^{-1}), at the absorption maximum.

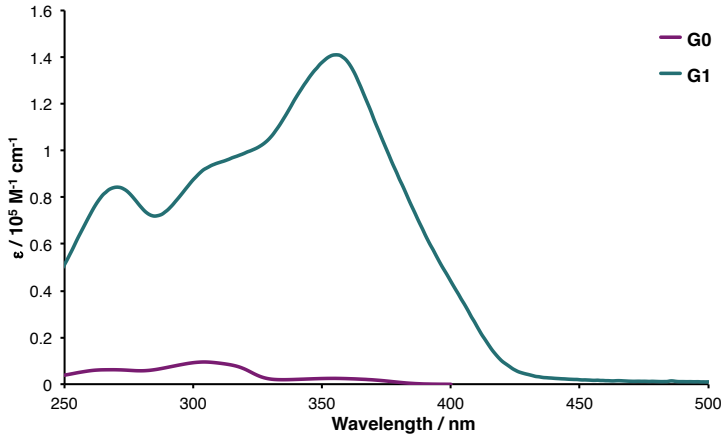

Figure 3.18: *Absorption spectra for **G0** and **G1** where the extinction coefficient is depicted, ~10^{-6} M solutions in dichloromethane.*

The emission properties of **G0** and **G1** are shown in **Figure 3.19**. The emission wavelength for **G1** is at longer wavelengths when compared to **G0**, 435 *versus* 400 nm, a difference of 35 nm. Protonation of the species leads to a red shift, and the observed emission maxima is changed to 480 and 495 nm, respectively for **G0** and **G1**, a difference of 80 and 60 nm from the neutral counterparts. It is noteworthy that the change observed with protonation is more pronounced in the case of the smaller dendrimer.

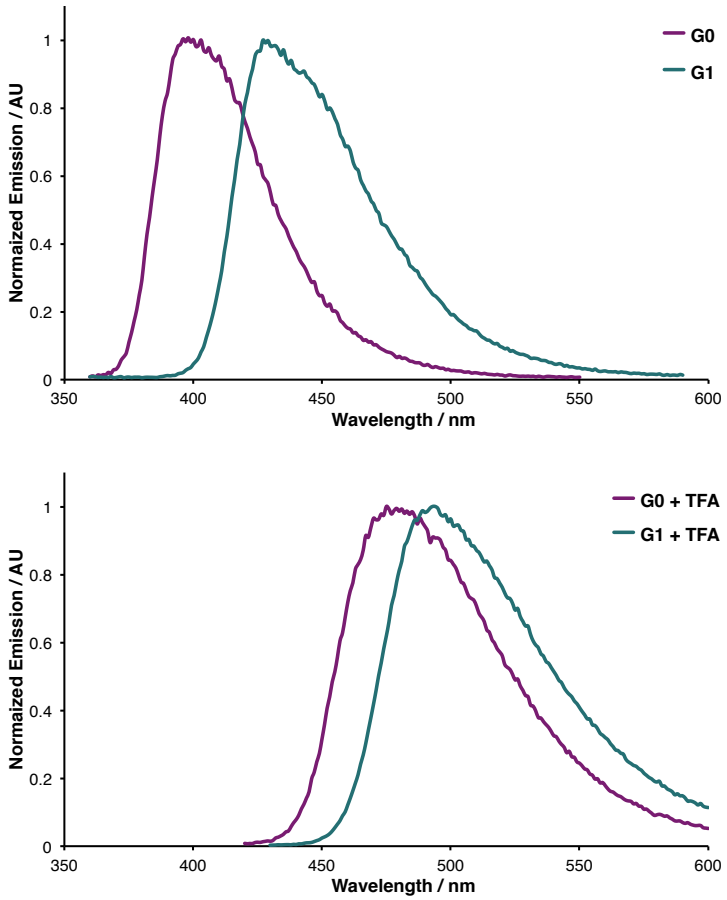

Figure 3.19: *Normalized emission spectra of dendrimers **G0** and **G1**, top; and after the addition of excess of TFA, bottom; ~10^{-6} M solutions in dichloromethane.*

A summary of the properties observed for **G0** and **G1** is shown in **Table 3.3**. A striking difference between the two neutral species is the value of the Stokes shift, 3169 and 5180 cm^{-1} for **G0** and **G1**, respectively. Since the absorption maxima of the two compounds is the same, the difference in the Stokes shift values must arise from differences in the excited states, and we can postulate that **G1** observes a greater geometry change between the ground and excited states than **G0**. It is interesting that the same is not the case for the protonated versions or is present to a much lower extent, since the Stoke shift values are very similar for both species. A rationalization for this observation is the fact that the protonation of a 2,6-diarylsubstituted-pyridine moiety causes a big change in ground state geometry, because of steric interactions, and which in turn reduces the space available for big geometry changes to occur even in the excited state.

Table 3.3: *Summary of the photophysical properties for dendrimers **G0** and **G1** in the absence (neutral) and presence of excess of TFA (prot.). All the measurements were performed using ~10^{-6} M solutions in dichloromethane. The quantum yield is reported for the neutral species relative to standards PPO (**Φ** = 0.94, in cyclohexane) and DPA (**Φ** = 1, in cyclohexane).*

		G0	**G1**
λ_{max} (abs) / nm	neutral	355, 305, 268	355, 310, 270
	prot.[a)]	*412, 379*	*422, 390*
λ_{max} (em) / nm	neutral	400	435
	prot.[a)]	*480*	*495*
E_g^{opt}[b)] **/ eV**	neutral	3.19	2.88
	prot.[a)]	*2.68*	*2.56*
Stokes shift / cm^{-1}	neutral	3169	5180
	prot.[a)]	*3439*	*3495*
Φ	neutral	0.15	0.22

a) protonated species after the addition of excess of TFA; b) calculated from the absorption onset.

Analyzing the values reported for the bandgaps and comparing to the ones observed for the oligomer series, it is found that in the case of **G0**, the value is comparable to the one found for the 4-ring member of the *2,6-series*, **26b**, 3.19 and 3.11 eV, respectively; interestingly, the value for the protonated version of **G0** is lower the one for **26b**, being more similar to the one found for **26c**, a longer oligomer of the same series; 2.68, 2.80 and 2.67 eV are the bandgap values for **G0**, **26b** and **26c**, respectively. When the bandgap value for **G1** is taken into account, 2.90 eV, it is found that again it is comparable to a 4-ring oligomer, but this time to the one belonging to the *2,5-series*, **25b**, with a value of 2.95 eV; again the value for the protonated version is related to a longer oligomer of the family, compound **25c** in this case, and the observed values are 2.56, 2.63 and 2.52 eV, respectively for the protonated analogues of **G1**, **25b** and **25c**.

The quantum yields are reported for the neutral species, and although **G1** has a higher quantum yield than **G0**, 0.22 *versus* 0.15, the difference is not drastic, especially if we consider that **G1** has a much larger molar absorptivity than **G0**. It is also interesting that the dendrimers have lower quantum yields than the ones observed for the oligomers in either series (with the exception of the 2-ring members).

3.4.2 Dendrimers: Additional Series

The additional series of compounds studied is comprised of dendrons and substituted dendrons that were prepared for different reasons: as intermediate during the attempted synthesis of higher order dendrimers, the case of **G1-dendron**; obtained as side product, case of **G0-G0**; designed to merge the two series of oligomers and the dendrimeric system, **G0-py-G0**; and finaly, **G0-bipy**, which was designed to have a bipyridyl moiety and is a potential ligand for transition metal complexes. The structures of all the members of this series can be seen in **Figure 3.20**.

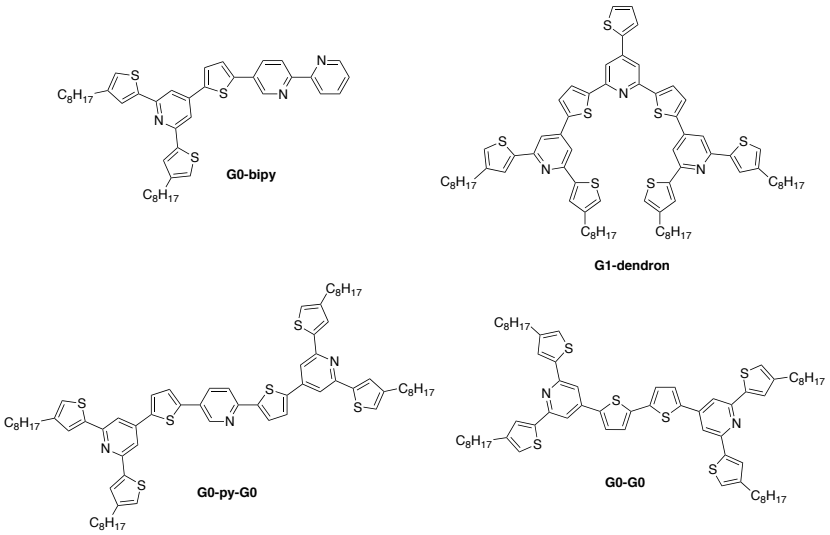

Figure 3.20: *Structures of the members of the dendrimeric additional series.*

The absorption spectra for this additional series of dendrimers can be seen in **Figure 3.21**, and like for the other series, the compounds were characterized in their neutral and protonated forms. In this series, **G0-py-G0** is the compound that shows the longest absorption wavelength with the absorption maxima at 390 nm, followed closely by **G0-G0** at 380 nm; in comparison, the other two compounds have absorption maxima shifted to the blue, **G1-dendron** at 373 nm and **G0-bipy** at 360 nm. Like in all the cases discussed so far, the absorption spectra for all the compounds exhibit a red shift when the species are protonated, and the most substantial change is encountered for **G0-G0**, which exhibits a 90 nm change in the absorption maxima, from 380 nm for the neutral to 470 nm for the protonated species, it is also interesting that the absorption in this case is quite broad and is extended to 540 nm.

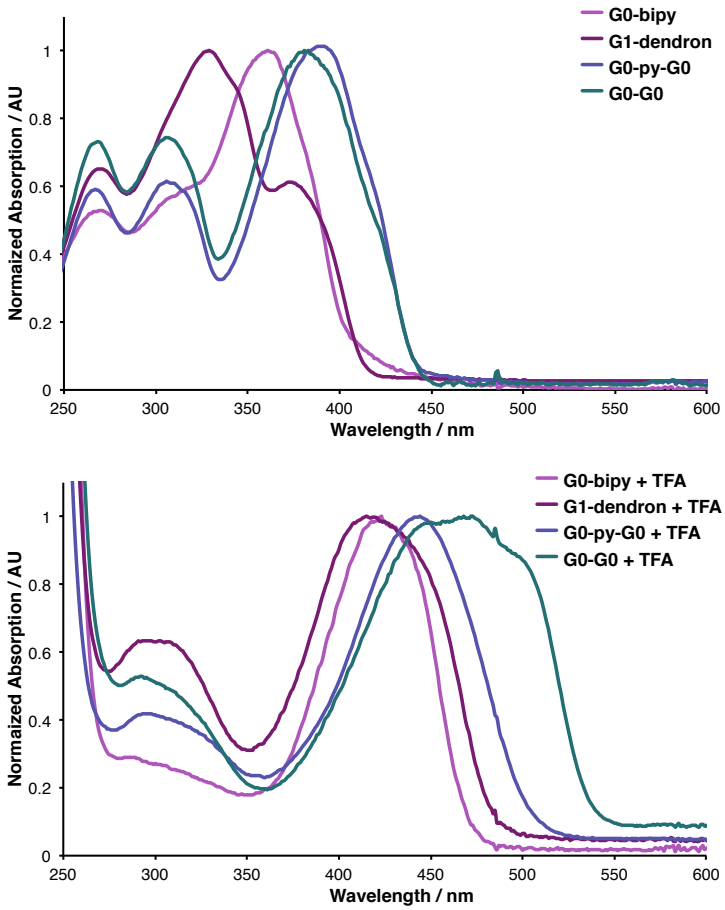

Figure 3.21: *Absorption spectra for the dendrimeric compounds* ***G0-bipy****,* ***G1-dendron****,* ***G0-py-G0*** *and* ***G0-G0*** *in the absence, top, and presence of excess of TFA; ~10^{-6} M solutions in dichloromethane.*

The emission spectra for this series is shown in **Figure 3.22**, and compounds **G0-G0** and **G0-py-G0** have very similar spectra and their emission is more red shifted, at 445 and 443 nm respectively, when compared to the other two members of the series, exhibiting emission maxima at 424 and 418 nm, respectively for **G0-bipy** and **G1-dendron**. Again the emission exhibits a red shift with protonation and once more **G0-G0** and **G0-py-G0** display similar spectra, the first observing a 95 nm red shift, with emission maximum at 540 nm, and the second an 87 nm shift, leading to an emission maximum at 530 nm. **G0-bipy** and **G1-dendron** show comparable red shifts in magnitude upon protonation, of 74 and 78 nm respectively, which results in emission absorption maxima at 498 and 496 nm.

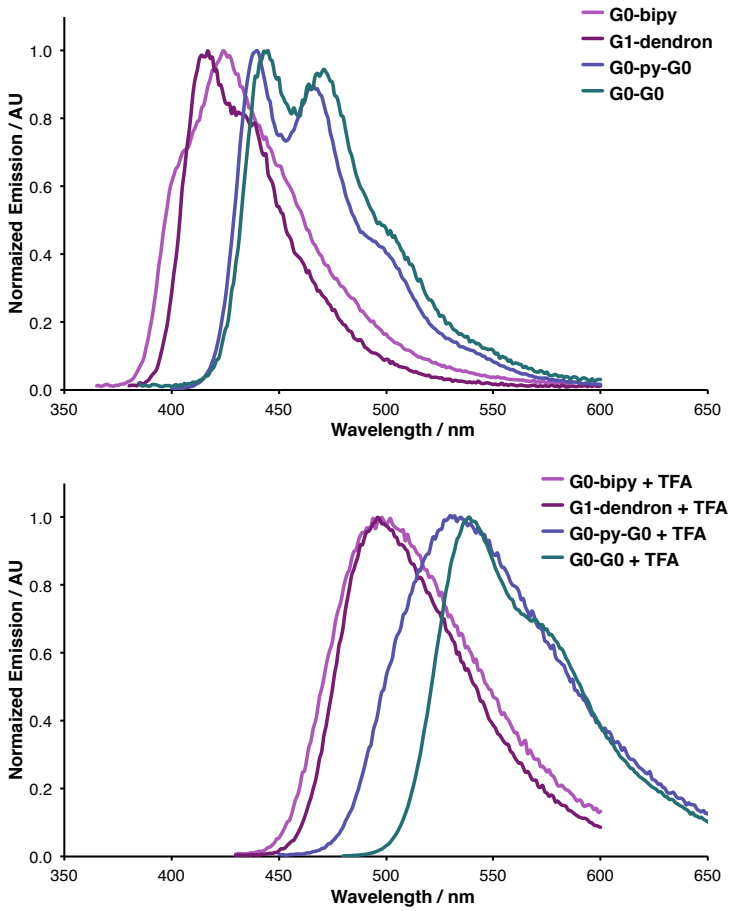

Figure 3.22: *Emission spectra for the dendrimeric compounds* ***G0-bipy***, ***G1-dendron***, ***G0-py-G0*** *and* ***G0-G0*** *in the absence, top, and presence of excess of TFA; ~10^{-6} M solutions in dichloromethane.*

All the data found for the additional dendrimeric series is summarized in **Table 3.4**. It is noticeable that all the members of the series exhibit three absorption maxima in their neutral form, while the protonated versions display two maxima. The emission maxima of the neutral species ranges from 400 to 445 nm, the protonated species emit over a larger range of wavelengths, ranging from 480 to 540 nm.

It is interesting to note that the Stokes shift decreases with increasing molecular size for the additional dendrimer series molecules in the neutral form, which does not correlate to the dendrimers **G0** and **G1**, since **G1** is the largest molecule and observes the largest Stokes shift. Regarding the Stokes shift for the protonated species, all of them seem to be in the same range, **G0-G0** being an exception.

Table 3.4: *Summary of the photophysical properties for the dendrimeric compounds in the absence (neutral) and presence of excess of TFA (prot.). All the measurements were performed using ~10^{-6} M solutions in dichloromethane. The quantum yield is reported for the neutral species relative to standards PPO (**Φ** = 0.94, in cyclohexane) and DPA (**Φ** = 1, in cyclohexane).*

		G0	**G0-bipy**	**G0-G0**	**G0-py-G0**	**G1-dendron**	**G1**
λ_{max}(abs) / nm	neutral	355 305, 268	360 305, 268	380 305, 268	390 308, 268	373 329, 270	355 310, 270
	prot.[a)]	*412* *379*	*422* *280*	*470* *293*	*442* *294*	*420* *300*	*422* *390*
λ_{max} (em) / nm	neutral	400	424	445	443	418	435
	prot.[a)]	*480*	*498*	*540*	*530*	*496*	*495*
E_g^{opt}[b)]**/ eV**	neutral	3.19	2.97	2.79	2.80	2.98	2.88
	prot.[a)]	*2.68*	*2.60*	*2.29*	*2.41*	*2.55*	*2.56*
Stokes shift /cm^{-1}	neutral	3169	4193	3844	3068	2886	5180
	prot.[a)]	*3439*	*3616*	*2758*	*3757*	*3648*	*3495*
Φ	neutral	0.15	0.14	0.17	0.57	0.24	0.22

a) protonated species after the addition of excess of TFA; b) calculated from the absorption onset.

With respect to the quantum yields, we can classify the compounds in three groups; **G0**, **G0-bipy** and **G0-G0** are the first group, they are the smallest molecules of the whole dendrimeric series and also they exhibit the lowest quantum yields, 0.15, 0.14 and 0.17, respectively. The two largest molecules of the set, **G1-dendron** and **G1**, constitute the second group and they have quantum yields that are a bit higher than the observed for the first group, 0.24 and 0.22, respectively. In this sense, **G0-py-G0** is the exception, since it exhibits a quantum yield of 0.57, more than two times higher than the highest value observed for the rest of the series.

In fact, it is quite interesting that the neutral versions of **G0-py-G0** and **G0-G0** have extremely similar absorption and emission spectra, but very different quantum yield values, with **G0-py-G0** observing a quantum yield 3.35 times higher. This observation, together with the fact that **G0-G0** is an exception with a much lower Stokes shift for the protonated version, leads us to speculate that the α-thiophene–thiophene bond has a big influence in the photophysical properties of this molecule, since **G0-G0** is the only molecule to have this structural feature and in the view of the fact that α-oligothiophenes are not good emitters. Another possibility is that the 2,5-pyridine linking moiety present in **G0-py-G0** considerably affects the system.

3.5 Conclusion

In summary, two series of oligomers and two series of dendrimers had their photophysical properties described in this chapter. It is interesting to note that in the oligomeric series, increasing length leads to a red shift in both the absorption and emission properties, while in the dendrimeric series, the 2,4,6-trisubstitution around the pyridine branching units is likely to affect the extension of conjugation that can be observed, leading to a much less pronounced red shift with increasing number of conjugated heterocycles. A discussion and for the additional dendrimer series properties has been presented, although it is not entirely clear which structural differences induce the range of observations shown. A common feature across all the compounds presented is the observation of a red shift with protonation, which can be envisioned as a potential method, together with alkylation or Lewis acid coordination, to manipulate the optical and electronic properties of the compounds.

CHAPTER 4

4 ADDITIONAL PROPERTIES

This chapter focuses on the discussion of additional properties found for the compounds that are the theme of this work. These include cyclic voltammetry characterization of the oligomeric series and the consequent frontier molecular orbital energy levels that can be derived. In addition, two oligomers belonging to the *2,6-series* had their acid titration characterized by ^{1}H-NMR spectroscopy, which shows a clear change with increasing number of equivalents of acid.

Additionally, during the purification process of the compounds belonging to the dendrimeric series, it was evident that some sort of aggregation was taking place in solution, which led us to perform concentration-dependent photophysical as well as ^{1}H-NMR characterization of **G1**.

4.1 Cyclic Voltammetry of the Oligomeric Series

The use of conjugated materials in organic photovoltaics and electronic devices has been an intense subject of investigation in the last decades.[112] An important aspect of the materials in the device operation is the junction between the donor (*p*-type material) and the acceptor (*n*-type) layers, and the frontier orbital energies of the individual components have been shown to be associated to the device performance. Therefore, determining the individual HOMO and LUMO energy levels for materials that might be applied in organic photovoltaic devices is of great importance.

One of the most common methods used in the determination of the frontier orbitals energy levels is cyclic voltammetry (CV). This technique is based on the application of linearly ramped potential over time to a working electrode (normally platinum or glassy carbon). The current changes when a reduction or oxidation process takes place, and plotting this current against the potential gives the typical cyclic voltammograms. In this fashion, oxidation and reduction potentials can be determined, and they are associated, respectively, to the ionization energy (IE) and the electronic affinity (EA) of the species; which in turn can be correlated to

the HOMO and LUMO energy levels. This correlation assumes that a linear relationship between the IE and EA with regard to the respective orbital energy levels is present.[113]

Since many of the organic compounds cannot have their CV measured in aqueous media, the use of organic solvents is crucial. In these cases, the IUPAC recommendation is to measure the electrode potential against the ferrocenium/ferrocene (Fc^+/Fc) redox couple, which can be translated into standard or absolute potentials. This conversion is one of the complications when using CV to determine the HOMO and LUMO energy levels, since it makes the correlation between the measured data and the vacuum scale. Many assumptions have to be made and the literature has a vast number of inconsistent redox values for standard electrode potentials, making it difficult to compare the data already reported; a review and discussion on this topic has been recently published by Bazan and coworkers.[114]

Assuming the value of –4.46 eV is equivalent to 0.0 V *vs.* the normal hydrogen electrode (NHE),[114] and taking into consideration that the Fc^+/Fc redox couple potential has a value of 0.53 V *vs.* SCE (standard calomel electrode) in THF,[115] we can approximate the formal potential of Fc^+/Fc to be -5.23 eV in THF, since the difference between SCE and NHE should also be considered and it has a value of 0.24 V. Therefore, the energy levels can be written as shown in Equations 21 and 22.

$$E_{HOMO} = -(E_{[onset,\ oxidation\ vs.\ Fc^+/Fc]} + 5.23)\ (eV) \quad (21)$$

$$E_{LUMO} = -(E_{[onset,\ reduction\ vs.\ Fc^+/Fc]} + 5.23)\ (eV) \quad (22)$$

When both oxidation and reduction are observed, the formulas shown above can be applied to directly give the frontier orbitals energy levels. In the case where only the oxidation or the reduction are observed, the energy of one of the orbitals can be directly determined and, together with the optical band gap, can be used to estimate the energy level of the other orbital.

4.1.1 Cyclic Voltammograms

The cyclic voltammograms obtained for the *2,6-series* and the *2,5-series* are displayed in **Figure 4.1** and **Figure 4.2**, respectively. Only the reductive portions of the voltammograms are shown, since the oxidation of the nominal compounds could not be observed with the conditions used during the measurements.

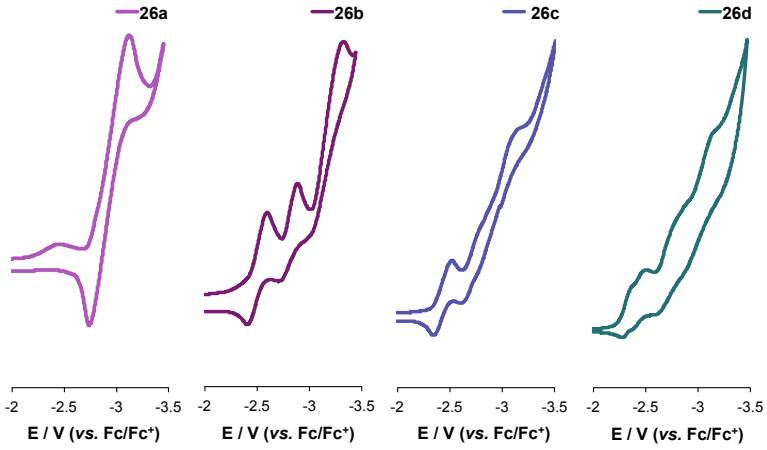

Figure 4.1: *Reductive portion of the cyclic voltammograms for the* 2,6-series. *(1 mM in THF, 0.1 M Bu_4NClO_4, scan rate 50 mV s^{-1}, glassy carbon working electrode, Pt wire counter electrode, Ag/AgCl reference electrode, ferrocene (Fc) internal reference.).*

An interesting aspect of the cyclic voltammograms found for both series is that the first reduction potential value increases with increasing oligomer length. In this regard, the *2,5-series* oligomers show lower reduction potential when compared to oligomers of the same length belonging to the *2,6-series*.

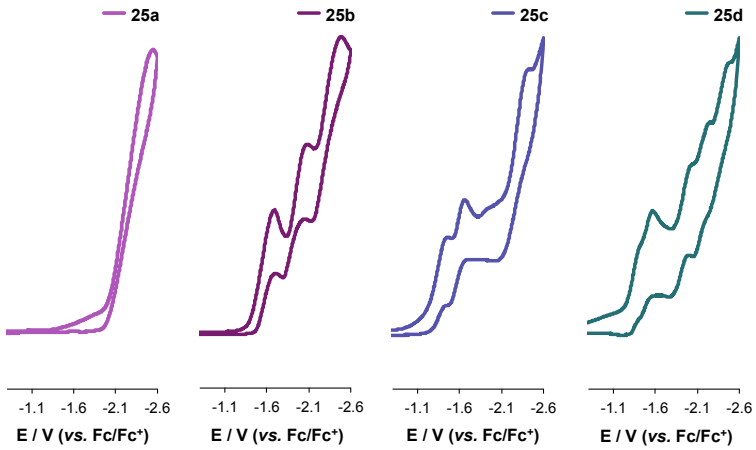

Figure 4.2: *Reductive portion of the cyclic voltammograms for the* 2,5-series. *(1 mM in THF, 0.1 M Bu_4NClO_4, scan rate 50 mV s^{-1}, glassy carbon working electrode, Pt wire counter electrode, Ag/AgCl reference electrode, ferrocene (Fc) internal reference.).*

Furthermore, the number of reduction waves observed also increases with oligomer length; in both series the 2-ring oligomers (**26a** and **25a**) observe one reduction wave and the 4-ring oligomers (**26b** and **25b**) show three reduction waves. It is curious that the 6-ring oligomers seem to be an exception in both series; the voltammogram of **26c** indicates that a three wave

reduction process occur, although this cannot be assured due to the low resolution of the waves; in the case of **25c**, a three wave reduction process is clearly visible, the peculiar aspect is the interval between the two first waves and the third one. The trend of increasing number of reduction waves with oligomer length continues, and the 8-ring oligomer **26d** displays four reduction waves while **25d** exhibits five reduction waves, again in the case of the oligomer belonging to the *2,6-series* (**26d**) a lower resolution of the waves is observed and in the case of **25d** again the first two waves are close together and an interval is observed between them and the following three waves.

The five-wave reduction observed in the case of **25d** is somewhat a rare phenomenon in the field of oligothiophenes, since in most of the cases their oxidation can be observed but not the reduction.[65,66,116] Some exceptions are oligothiophenes end-capped with fluoro-aryl moieties and pyrimidine–thiophene conjugated oligomers, which observe two-wave reduction process.[64,117,118]

4.1.2 Frontier Orbitals Energy Levels and Discussion

Through cyclic voltammetry and optical spectroscopy, the energy levels found for the frontier molecular orbitals of the series of oligomers are given in **Table 4.1**. The values for the LUMO levels were calculated directly from the reduction waves, as discussed above. The HOMO levels were derived from the optical band gap and the corresponding LUMO levels.

Table 4.1: *Frontier orbitals energy levels for the oligomers of the* 2,6-series *and* 2,5-series.

	2,6-series				*2,5-series*			
	26a	**26b**	**26c**	**26d**	**25a**	**25b**	**25c**	**25d**
$E_{onset\ red\ vs.\ Fc/Fc^+}$ [a] / V	-2.75	-2.42	-2.31	-2.20	-2.11	-1.38	-1.19	-1.10
LUMO [b] / eV	-2.48	-2.81	-2.92	-3.03	-3.12	-3.85	-4.04	-4.13
HOMO [c] / eV	-6.04	-5.92	-5.94	-6.02	-6.81	-6.80	-6.76	-6.76
E_g^{opt} [c] / eV	3.56	3.11	3.02	2.99	3.69	2.95	2.72	2.63

a) From the voltammograms shown in **Figure 4.1** *and* **Figure 4.2**, *solutions in THF. b) Derived from the* $E_{onset\ red\ vs.\ Fc/Fc^+}$ *and Equation 22. c)* $E_{HOMO} = E_{LUMO} - E_g^{opt}$. *d) Optical band gap for solutions in acetonitrile.*

In **Figure 4.3**, a graphic representation of the frontier orbitals energy levels is shown. It is interesting to observe that the LUMO levels for both series observe changes with oligomer length, the longer the oligomer, the lower the LUMO energy. This does not happen for the HOMO levels, as in each series they lie at approximately the same energy level. It is also noticeable that the *2,5-series* oligomers have lower energy values associated with the orbitals of oligomers of same length in the *2,6-series*; this corroborates the hypothesis that the *2,5-series* oligomers experience a higher degree of conjugation.

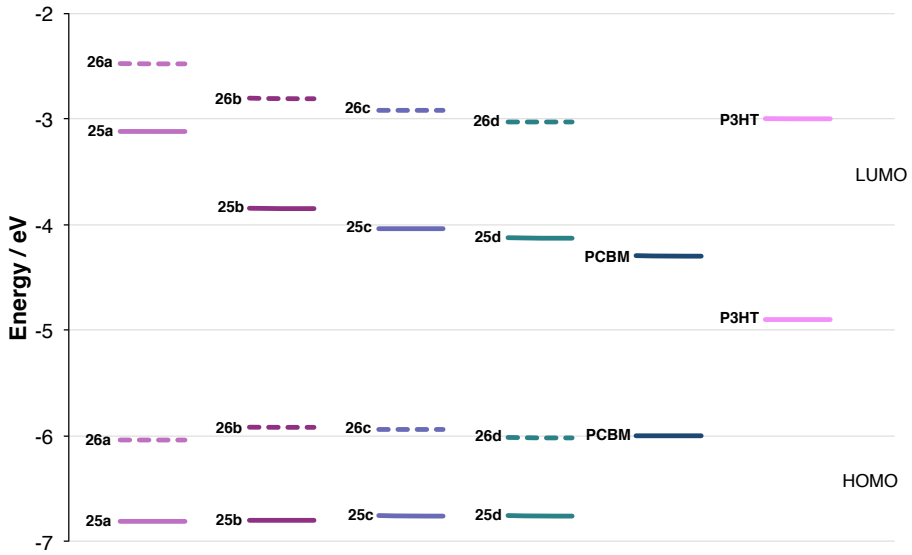

Figure 4.3: *Frontier orbitals energy levels of the oligomer series, LUMO derived from the reduction wave of cyclic voltammetry and HOMO derived from the band gap and LUMO level. Levels for* ***PCBM*** *and* ***P3HT*** *are literature values.*

The energy levels for two of the most commonly used materials in organic photovoltaics are also shown in **Figure 4.3**. Fullerene derivatives have been proven to be one of the most efficient materials as the acceptor layer in organic solar cells, with **PCBM** (phenyl-C61-butyric acid methyl ester), a C61-fullerene derivative, as one of the most frequently used. It is interesting to note that the LUMO levels of **PCBM** and **25d** are very similar, −4.3 eV and −4.13 eV respectively. This observation makes **25d** a good candidate to be used as the acceptor layer in organic photovoltaics.

On the other hand, the orbital energy levels of the oligomer series are very distinct from the ones of **P3HT** (poly(3-hexylthiophene)), for both oligomer series the HOMO lies at much lower energy levels when compared to **P3HT**, while the LUMO of the *2,6-series* has comparable energy levels to **P3HT**. This observation indicates that the introduction of a

pyridine ring, in an alternating manner, in the oligothiophene backbone leads to higher degree of conjugation and stabilization of the system.

4.2 Acid Titration

Following the discussion presented in Chapter 3 for the photophysical properties of the oligomers in their protonated form, two model compounds were prepared and had their protonation charaterized by ^{1}H-NMR through a titration with TFA. Compounds **26e** and **26f** were designed to not have the *tert*-butoxy group, since the loss of the *tert*-butyl group occurs over the course of hours in the presence of acid. Only oligomers belonging to the *2,6-series* were characterized by acid titration and a similar effect is expected from *2,5-series* analogs.

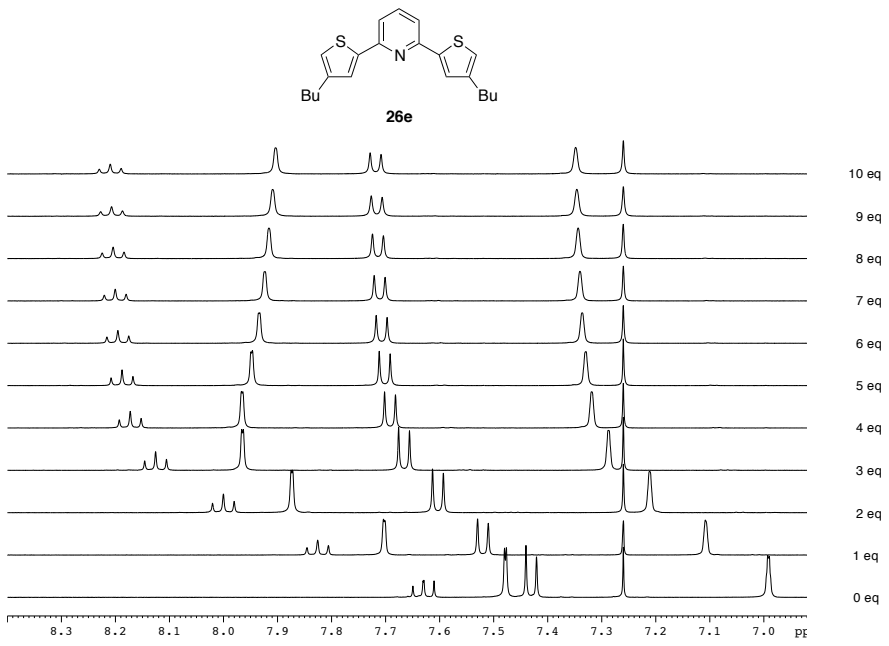

Figure 4.4: *Acid titration of* ***26e*** *using TFA, number of equivalents of added TFA on the right. ^{1}H-NMR in $CDCl_3$, at 300 K, 400 MHz.*

The NMR chemical shift values are a reflection of the electronic shielding around the nucleus, and the more shielded a nucleus (higher electronic density), the lower the chemical shift measured; the deshielding of a nucleus yields higher chemical shifts. In the series of oligomers presented in this work, the protonation of the pyridine is expected to lower the electronic density of the pyridine ring and therefore afford higher chemical shifts (downfield shifted compared to the neutral versio) in an NMR experiment.

The ^{1}H-NMR spectra corresponding to the acid titration of **26e** are shown in **Figure 4.4**, and a clear downfield shift in all of the proton signals can be observed with increasing acid content. In particular, the triplet corresponding to the pyridine 4-position is a good indicator of the electronic density of the pyridine ring, as it is in the *para*-position relative to the positive charge present in the nitrogen atom upon protonation. For the neutral form of the **26e**, the chemical shift of the proton in the 4-position of the pyridine has a value of 7.63 ppm that changes to 8.20 ppm, a difference of 0.57 ppm in the chemical shift between the neutral and protonated forms. From the titration spectra, we can conclude that 6 equivalents of TFA are sufficient to protonate **26e**, and after that, the small changes observed in the spectra are most likely due to environmental modifications due to the high polarity of TFA.

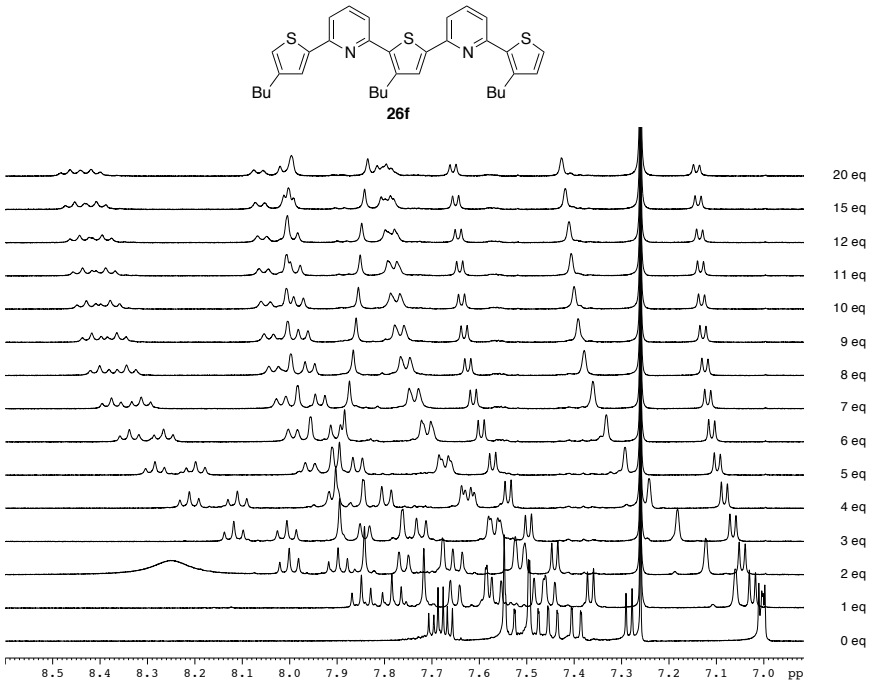

***Figure 4.5:** Acid titration of **26f** using TFA, number of equivalents of added TFA on the right. ^{1}H-NMR in $CDCl_3$, at 300 K, 400 MHz.*

In the case of **26f**, two non-equivalent pyridine rings are present, and the signal for the protons on the 4-position of the pyridines is very similar in the neutral version, appearing as a multiplet between 7.65–7.71 ppm. The addition of TFA induces a differentiation of the two protons, and two triplets are visible already after the addition of 1eq. of TFA, this indicates that the pK_a of the two pyridines is distinctive, so a preferential protonation of one of the pyridine rings occurs. The total protonation of the molecule is seen after the addition of 10eq. of TFA,

where no changes in the spectra can be observed; at this point, again a multiplet is present for the 4-positions pyridine protons, indicating that they have very similar chemical shift and that the pyridine rings themselves are very similar. In total, a change of 0.76 ppm is observed in the chemical shift for the mentioned protons; this change is larger than the observed for **26e** (0.57 ppm), which indicates that the overall double charge of **26f** plays a significant role.

4.3 Aggregation Properties of the Dendrimer Series

In the course of synthesis of the compounds of the dendrimeric series, **G0** and **G1**, evidence of their aggregation, in special for **G1**, was observed. The characterization of their photophysical properties at different concentrations was then performed, since it is not well know how the environment of the aggregates leads to changes in the properties of the emitting species.[119] In the examples discussed in this work, it is not clear how the aggregate is arranged, since the molecules could be aggregating in a stacking way, where the π-systems are parallel, or the long alkyl chains could be interacting in the form of a micelle or liposome-type aggregate.

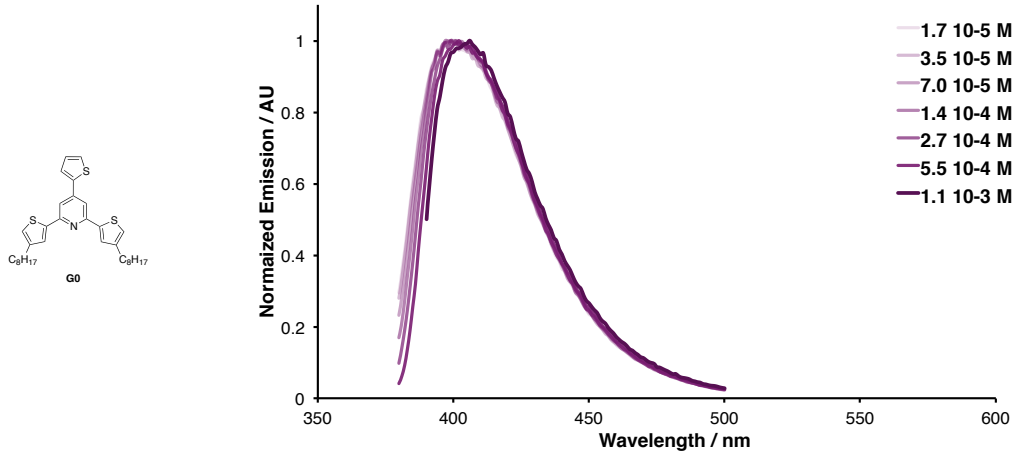

Figure 4.6: *Normalized concentration-dependent emission spectra of* ***G0*** *in* CH_2Cl_2.

The concentration-dependent emission spectra of **G0** are shown in **Figure 4.6**. From the figure, it is evident that the emission is essentially unchanged with concentration. The measurements were performed in dichloromethane, so we can conclude that aggregation is not a predominant phenomenon in this solvent; the use of solvents with more distinct character (polar or apolar) could lead to aggregation. Two possible reasons for the lack of changes in the emission will be discussed, the first deals with the size of the molecule, and since **G0** is a small molecule and exhibits a much smaller surface area when compared to **G1**, aggregation is a less

favorable process, the second hypothesis deals with the fact that, if aggregation occurs, it does not lead to considerable changes in the emission, which could also be due to the size of the fluorophore.

In the case of **G1**, a pronounced change in the photophysical properties of is visible with increasing concentration of the fluorophore, **Figure 4.7**. The change in emission is accompanied by a change in the absorption that is visible by the naked eye, but the absorption spectra of the concentrated solutions were not characterized due to the high concentrations, which lead to absorptivities that extrapolate the range of the instrument.[xi]

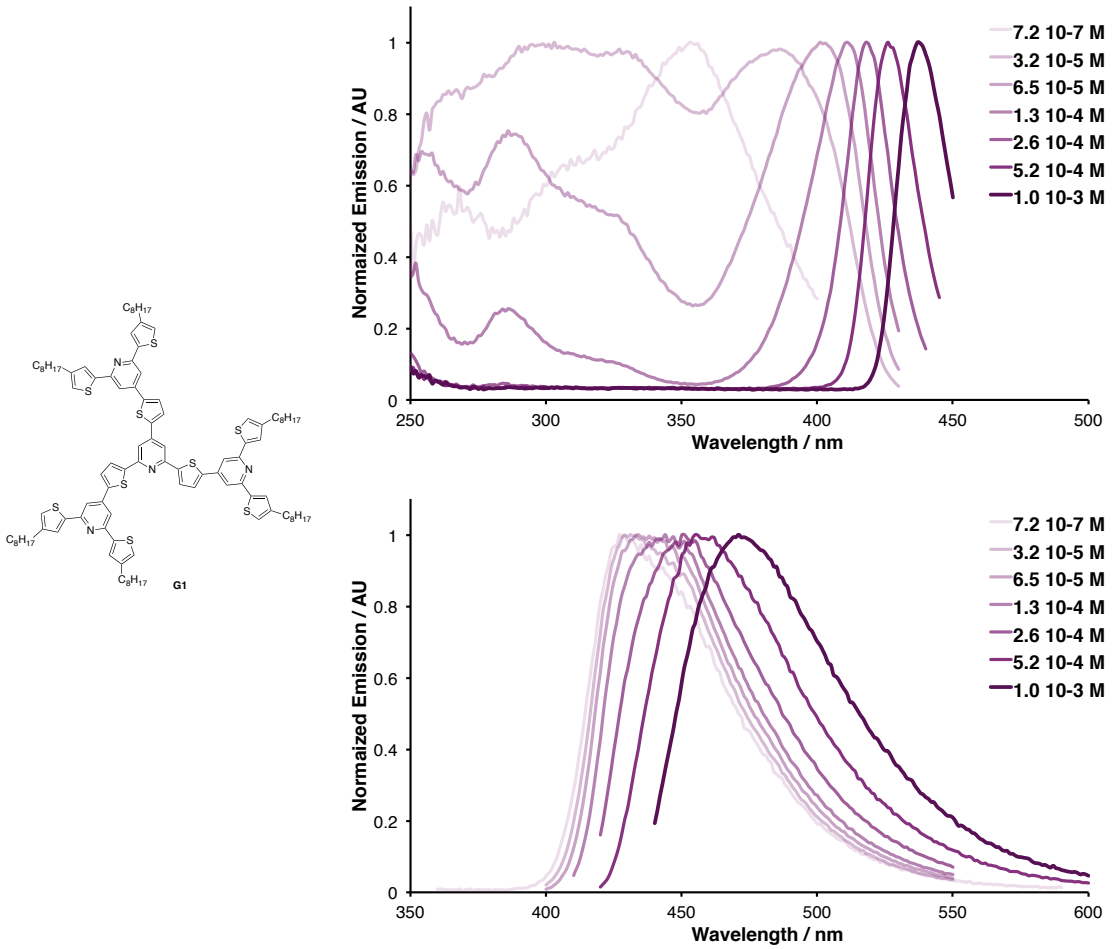

***Figure 4.7:** Concentration-dependent spectra of **G1**; excitation, top; and emission, bottom; in CH_2Cl_2.*

It is interesting to note that the changes in emission are accompanied by a change in the excitation spectra. Furthermore, the excitation spectra do not correspond to the absorption

[xi] This could have been circumvented by the use of a cuvette with very small path length, but it was not performed until the present moment.

spectra for concentrated solutions (> 10^{-5} M). In the absorption spectra, although the quality of the ones measured is not ideal, it is possible to see that the whole blue region participates in absorption processes, while the excitation is comprised of a very sharp peak. Another important point is the range of the maximum of the excitation peak, which goes from 353 nm for the most diluted to 437 nm for the most concentrated solution, a range of 84 nm.

In the case of the emission spectra, a large range in the absorption maximum is also observed, and a red shift from 435 nm for the most diluted to 471 nm for the most concentrated solution is found, a range of 36 nm. An additional aspect of the emission spectrum of high concentration solutions is the fact that they do not display any emission of the species that are present at lower concentration. One possible explanation for this observation is the assumption that a low concentration of low-order aggregates is present, which contradicts the fact that the absorption range of these species shows high absorption in solutions of high concentration. A more plausible rationalization for this is the fact that the higher order aggregate species absorb in the range where the lower order ones emit, therefore creating a silencing effect of the low order aggregates emission in solutions of high concentration.

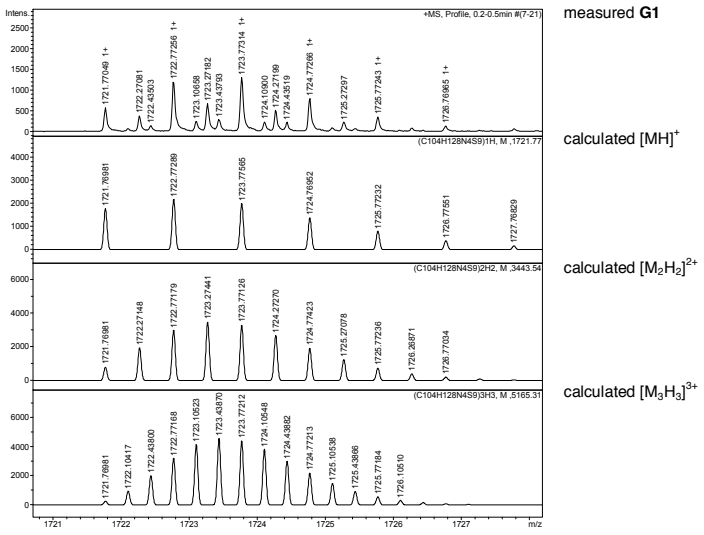

Figure 4.8: *Measured ESI high-resolution mass spectrum of* ***G1****, and calculated isolated molecule* $[MH]^+$ *and aggregates* $[M_2H_2]^{2+}$ and $[M_3H_3]^{3+}$.

The aggregation process of **G1** was also observed by HR-ESI mass spectrometry, **Figure 4.8**. In fact, the region relative to the molecular ion shows the protonated molecular ion with a 1+ charge, $[MH]^{1+}$, and peaks corresponding to the doubly protonated dimer with a 2+ charge, $[M_2H_2]^{2+}$, as well as the triply protonated trimer with a 3+ charge, $[M_3H_3]^{3+}$; which suggests that the interaction between the molecules to form aggregates is quite strong, since the

harsh conditions of the mass spectrometry measurement were not sufficient to disrupt the aggregate.

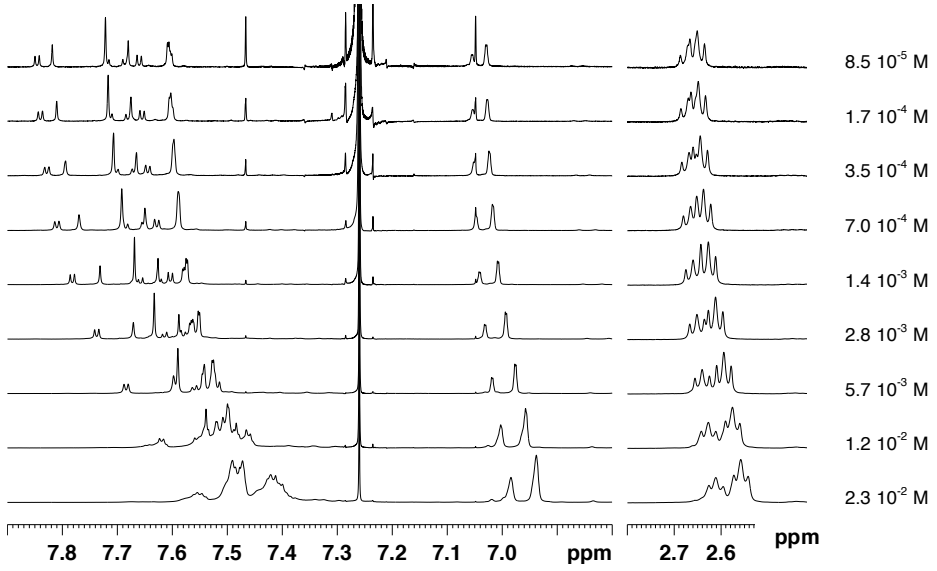

Figure 4.9: *Concentration-dependent ^{1}H-NMR of* ***G1*** *in $CDCl_3$, at 300 K, 500 MHz.*

Concentration-dependent ^{1}H-NMR was used to investigate which regions of the molecule undergo chemical shifts modifications upon aggregation, **Figure 4.9**. The ^{1}H-NMR spectrum of the most concentrated solution shows very broad signals and the individual peaks cannot be discerned. Dilution of the solution leads to distinguished sharp peaks, which can be assigned to the individual protons present in the molecule. It is also interesting that a deshielding effect can be observed with dilution, this effect is particularly evident in the signals of the protons from the heterocycles, and it is an indication that the aggregation occurs through interactions of those units.

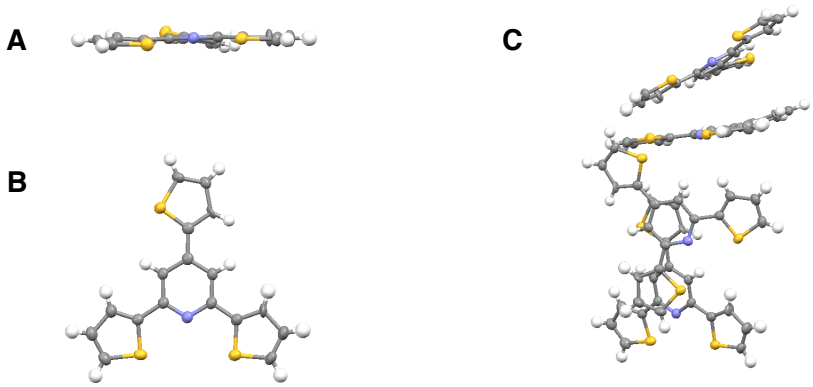

Figure 4.10: *Crystal structure of non-alkylated* ***G0, G0a****. Side view of the molecule,* ***A****, top view of the molecule,* ***B****, packing. Space group:* Pna*21. Two conformations of the molecule are found, they differ on the position of the sulfur atoms of the thiophene rings attached to the 2 and 6 positions of the pyridine ring, for clarity, only one conformation is shown here.*

A crystal structure of an unsubstituted analog of **G0** was obtained, and we can speculate that the aggregation of **G1** occurs in a similar fashion as the packing observed in the crystal, **Figure 4.10**. The side view of the molecular structure, **Figure 4.10-A**, shows a planar conformation of the 2,4,6-trithiophenylpyridine core; this indicates that a planar conformation of the core of **G1** could also be present; particularly, the aggregates are expected to have interactions that are more likely to be similar to the solid state ones, which indicates that the core could be in a planar conformation. Another interesting aspect of the crystal structure is the packing, **Figure 4.10-C**, the molecules pack in a parallel manner and the pyridine ring of one molecule appear on the top of a thiophene ring of another molecule, indicating that a donor-acceptor interaction of the conjugated rings takes place. Although it is very speculative to affirm that the same happens in the aggregates, it is conceivable that the aggregates show similar molecular interaction.

CHAPTER 5

5 EXPERIMENTAL PROCEDURES AND ANALYTICAL DATA

5.1 General Notes and Procedures

Synthetic procedures were carried out under an inert atmosphere, in dry solvent, using standard Schlenk techniques, unless otherwise noted. Dry solvents were supplied from an MBraun solvent purification system. All reagents and solvents were reagent grade and were used without further purification unless otherwise specified. Flash chromatographic purification was performed using silica gel Merck 60 (particle size 0.040–0.063 mm), or deactivated (5% water by weight) neutral aluminum oxide Sigma-Aldrich, Brockmann I, packed in glass columns; eluting solvent for each purification was determined by thin layer chromatography (TLC). Analytical thin-layer chromatography was performed using Merck TLC silica gel 60 F254 or Macherey–Nagel POLYGRAM ALOX N/UV254 and visualized using UV-lamps at 254 and 366 nm. Yields refer to chromatographically purified compounds unless noted otherwise.

^{1}H NMR spectra were obtained on Bruker AV2-400 (400 MHz) or AV2-500 (500 MHz) spectrometers. Chemical shifts are reported in parts per million (ppm) relative to the solvent residual peak ($CDCl_3$, 7.26 ppm). Multiplicities are given as: s (singlet), d (doublet), t (triplet), q (quartet), dd (doublet of doublets), m (multiplet), and the coupling constants, *J*, are given in Hz. ^{1}H-decoupled ^{13}C NMR spectra were obtained on Bruker AV2-400 (100 MHz) or AV2-500 (125 MHz) spectrometers. ^{13}C NMR chemical shifts are reported relative to the residual solvent peak ($CDCl_3$, 77.0 ppm). IR frequencies are given in cm^{-1}; the relative intensity of the bands is indicated by w (weak), m (medium) and s (strong), obtained from spectra of thin films on a Jasco FT/IR-4100 spectrometer.

The cyclic voltammetry was performed with a PGStat μ30 potentiostat (Autolab) using a standard three electrodes cell (Ar-purged). Conditions: 1mM compound, 0.1 M Bu_4NClO_4 as supporting electrolyte in THF, scan rate 50 mV s^{-1}, glassy carbon working electrode (Ø = 0.3 cm), Pt wire counter electrode, Ag/AgCl reference electrode, added ferrocene (Fc) as internal reference.

Fluorescence measurements were carried out in spectroscopic grade solvent on an Edinburgh FLS920 spectrophotometer, using 450W Xenon lamp for excitation; 1 nm

excitation and 1 nm emission slit widths. Emission spectra were obtained by exciting at the longest-wavelength absorption maxima. Quantum yields were determined by standard methods, [120] , [121] using 2,5-diphenyloxazole, PPO (ϕ = 0.94, in cyclohexane) or 9,10-diphenylanthracene DPA (ϕ = 1, in cyclohexane) as the standards.[122] Degassed samples were diluted to optical transparency (A ≤ 0.05), and the integrated emission intensity was compared to an *iso*-absorptive solution of the standards in degassed solvent. The solutions were degassed by thorough N_2 bubbling over 5 minutes.

UV/Vis measurements were carried out on a Perkin-Elmer Lambda 19 UV/VIS spectrophotometer or on an Agilent 8453 UV/VIS spectrophotometer. For extinction coefficient determination, four independent solutions of different concentrations were prepared, with absorption between 0.04-0.50 AU. The value of ε was calculated by linear least-squares fitting of plots of absorbance vs. concentration. All fits gave R^2 values of ≥0.98.

5.2 Synthetic Details and Tabulated Data

General Negishi cross coupling procedure: Flame dried flasks were used and all the solutions were handled under nitrogen. In a Schlenk flask, a THF solution (0.1-0.5M) of component A was cooled down to -78°C, using a dry ice/acetone bath, and treated with base (BuLi or LiTMP). After 40 minutes of stirring at -78°C, a THF solution of $ZnCl_2$ (0.2-0.7 M) was slowly added, the cooling bath was removed and the reaction mixture was stirred while warming up to room temperature for another 40 minutes. This mixture was then transferred via cannula to a two-neck flask equipped with a condenser and containing a THF solution of component B (0.3-0.5M) and the palladium catalyst. This final reaction mixture was heated to 60°C and stirred overnight. After cooling to room temperature, a few drops of water were added and the solvent was removed *in vacuo*. The residue was resuspended in dichloromethane, washed with saturated EDTA solution, which was extracted three times with dichloromethane and the final combined organic fractions were washed with brine, dried over Na_2SO_4 and concentrated. The crude product was purified by column chromatography.

3-Butylthiophene

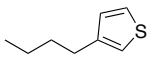

To a suspension of magnesium (79 mmol, 1.92 g) in 10 ml of diethylether, a small crystal of iodine was added; a solution of 1-bromobutane (80 mmol, 11.0 g, 8.6 mL) in 45 mL of ether was slowly added under mild reflux. The reaction mixture was stirred under reflux for 1 hour, when it was transferred *via cannula* to a suspension of 3-bromothiophene (53.4 mmol, 5.0 mL, 8.7 g) and Ni(dppp)Cl_2 (0.3 mmol, 0.16 g) in 80 mL of diethylether. The reaction mixture was heated to reflux overnight. After cooling to room temperature, the reaction mixture was quenched with ice-cold 1 M HCl solution. The aqueous phase was extracted with ether three times and the combined organic phases were washed with saturated EDTA solution and brine, dried over $MgSO_4$ and the solvent was removed *in vacuo*. The crude mixture was subjected to column chromatography (silica, AcOEt/hexane = 1:9) to give the product as a pale yellow liquid (6.86 g, 91 % yield).

^{1}H NMR (400 MHz, $CDCl_3$, δ): 7.24 (dd, *J*=4.91, 2.93, 1H), 6.94 (dd, *J*=4.91, 1.26, 1H), 6.92 (dd, *J*=2.93, 1.26, 1H), 2.64 (t, *J*=7.40, 2H), 1.61 (m, 2H), 1.37 (sextet, *J*=7.40, 2H), 0.93 (t, *J*=7.40, 3H).

^{13}C NMR (100 MHz, $CDCl_3$, 300 K, δ): 143.22, 128.29, 125.01, 119.75, 32.70, 29.96, 22.37, 13.90.

3-Octylthiophene

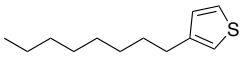

To a suspension of magnesium (79 mmol, 1.92 g) in 10 ml of diethylether, a small crystal of iodine was added; a solution of 1-bromooctane (80 mmol, 12.0 g, 10.7 mL) in 45 mL of ether was slowly added at mild reflux. The reaction mixture was stirred under reflux for 1 hour, when it was transferred *via cannula* to a suspension of 3-bromothiophene (53.4 mmol, 5.0 mL, 8.7 g) and Ni(dppp)Cl_2 (0.3 mmol, 0.16 g) in 80 mL of diethylether. The reaction mixture was heated under reflux overnight. After cooling to room temperature, the reaction mixture was quenched with ice-cold 1 M HCl solution. The aqueous phase was extracted with ether three times and the combined organic phases were washed with saturated EDTA solution and brine, dried over

$MgSO_4$ and the solvent was removed *in vacuo*. The crude mixture was subjected to column chromatography (silica, CH_2Cl_2/hexane = 1:19) to give the product as a pale yellow liquid (10.1 g, 94 % yield).

^{1}H NMR (400 MHz, $CDCl_3$, δ): 7.24 (dd, *J*=5.0, 2.9, 1H), 6.94 (dd, *J*=4.9, 1.3, 1H), 6.93 (m, 1H), 2.64 (t, *J*=7.7, 2H), 1.63 (quintet, *J*=7.7 2H), 1.31 (m, 10H), 0.90 (t, *J*=7.7, 3H).

^{13}C NMR (100 MHz, $CDCl_3$, 300 K, δ): 143.25, 128.27, 124.99, 119.73, 31.88, 30.57, 30.29, 29.43, 29.35, 29.26, 22.66, 14.09.

5.2.1 Synthesis of the 2,6-Series

6-Bromo-2-(1,1-dimethylethoxy)pyridine (1)

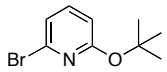

To a solution of 2,6-dibromopyridine (21.1 mmol, 5.00 g) in 75 mL of toluene was added potassium *tert*-butoxide (23.2 mmol, 2.60 g) and the reaction mixture was refluxed overnight. After cooling to room temperature, the crude mixture was filtered through celite and the solvent was removed *in vacuo*. Purification by column chromatography (silica, ethylacetate/hexanes = 1/9) afforded the product as colorless liquid (15.1 mmol, 71 % yield).

^{1}H NMR (400 MHz, $CDCl_3$, 300 K, δ): 7.34 (t, *J* = 7.8, 1H), 6.97 (d, *J* = 7.5, 1H), 6.57 (d, *J* = 8.1, 1H), 1.58 (s, 9H).

^{13}C NMR (100 MHz, $CDCl_3$, 300 K, δ): 162.97, 139.97, 137.61, 119.44, 111.42, 80.86, 28.39.

6-(4-Butylthiophen-2-yl)-2-(1,1-dimethylethoxy)pyridine (26a)

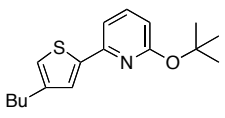

Prepared by the general Negishi cross-coupling procedure. Component A, 3-butylthiophene (12.00 mmol, 1.68 g); base, LiTMP (12.2 mmol); $ZnCl_2$ (13.5 mmol, 1.84 g); catalyst: $Pd(PPh_3)_4$ (0.4 mmol, 462 mg); component B, 2-*tert*-butoxy-6-bromopyridine **(1)** (34.33 mmol,

7.90 g). Purified by column chromatography (silica, CH_2Cl_2/hexanes = 1:9, 2:8) to afford a light yellow liquid (2.41 g, 76 %).

R_f (silica, EtOAc/hexanes = 1/9) = 0.57

^{1}H NMR (400 MHz, $CDCl_3$, 300 K, δ): 7.49 (dd, *J* = 8.1, 7.4, 1H), 7.35 (dd, *J* = 1.3, 1H), 7.14 (dd, *J* = 7.4, 0.6, 1H), 6.93 (d, *J* = 1.3, 1H), 2.61 (t, *J* = 7.6, 2H), 1.65 (s, 9H), 1.61 (m, 2H), 1.38 (sextet, *J* = 7.4, 2H), 0.94 (t, *J* = 7.4, 3H).

^{13}C NMR (100 MHz, $CDCl_3$, 300 K, δ): 163.49, 149.54, 145.26, 144.11, 138.67, 125.02, 121.70, 110.94, 110.09, 79.66, 32.62, 30.31, 28.58, 22.32, 13.88.

MS (ESI, *m/z*): 234.0 ($[M\text{-}Bu+H]^+$), 312.1 ($[M+Na]^+$).

6-(4-Butylthiophene-2-yl)pyridin-2-ol (26aOH)

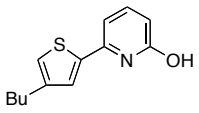

Pyridine hydrochloride (112 mmol, 13 g) was added to **(26a)** (4.5 mmol, 1.3 g) and the neat mixture was heated to 200 °C for 4 hours. The mixture was then dissolved with water, neutralized with 1M NaOH solution and extracted three times with CH_2Cl_2. The combined fractions were combined, dried over Na_2SO_4 and concentrated *in vacuo*. The crude mixture was passed through a plug of alumina (deactivated alumina, CH_2Cl_2) to afford the product (1.01 g, 96 %).

^{1}H NMR (400 MHz, $CDCl_3$, 300 K, δ): 10.76 (bs, 1H), 7.52 (d, *J* = 1.6, 1H), 7.40 (dd, *J* = 9.2, 7.2, 1H), 6.99 (dd, *J* = 2.2, 1.1, 1H), 6.45 (m, 2H), 2.63 (t, *J* = 7.48, 2H), 1.63 (m, 2H), 1.38 (m, 2H), 0.95 (t, *J* = 0.95, 3H).

^{13}C NMR (125 MHz, $CDCl_3$, 300 K, δ): 164.79, 144.93, 141.37, 141.13, 135.54, 128.32, 122.25, 118.16, 103.71, 32.38, 30.18, 22.29, 13.93.

6-(4-Butylthiophen-2-yl)pyridin-2-yl trifluoromethanesulfonate (26aTf)

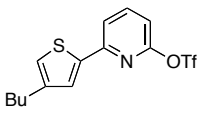

A solution of **(26aOH)** (4.32 mmol, 1.01 g) in 15 mL of CH_2Cl_2 was treated with triethylamine (4.75 mmol, 0.65 mL). the reaction mixture was cooled down to 0 °C and

trifluoromethanesulfonic anhydride (4.75 mmol, 0.80 mL) was slowly added and the cooling bath was removed. The reaction mixture was stirred for 4 hours at room temperature, when it was quenched with water. The water phase was neutralized with $NaHCO_3$ saturated solution and extracted three times with CH_2Cl_2. The combined organic fractions were dried over Na_2SO_4 and the solvent was removed *in vacuo*. The crude mixture was passed through a plug of alumina (deactivated alumina, CH_2Cl_2/hexanes = 1:1) to afford the product (1.42 g, 90 %).

^{1}H NMR (400 MHz, $CDCl_3$, 300 K, δ): 7.83 (t, *J* = 7.8, 1H), 7.61 (dd, *J* = 7.8, 0.6, 1H), 7.51 (d, *J* = 1.4, 1H), 7.05 (d, *J* = 1.4, 1H), 6.97 (dd, *J* = 7.8, 0.6, 1H), 2.63 (t, *J* = 7.6, 2H), 1.62 (m, 2H), 1.38 (m, 2H), 0.94 (t, *J* = 7.3, 3H).

^{13}C NMR (100 MHz, $CDCl_3$, 300 K, δ): 155.37, 152.61, 144.63, 141.44, 141.32, 127.92, 124.07, 118.54, 118.73 (q, J_{C-F} = 318, 1C), 112.15, 32.56, 30.15, 22.29, 13.86.

HR-MS (ESI, $C_{14}H_{14}F_3NNaO_3S_2$, $[M+Na]^+$): calculated, 388.0259; found, 388.0259.

6-{4-Butyl-6-[6-(4-butylthiophen-2-yl)pyridin-2-yl]thiophen-2-yl}-2-(1,1-dimethylethoxy)-pyridine (26b)

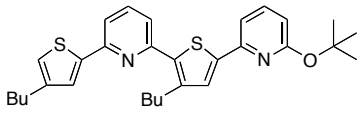

Prepared by the general Negishi cross-coupling procedure. Component A, **(26a)** (2.50 mmol, 0.723 g); base, BuLi (2.55 mmol); $ZnCl_2$ (3.25 mmol, 0.440 g); catalyst: $Pd(PPh_3)_4$ (0.150 mmol, 0.173 g); component B, **(26aTf)** (2.60 mmol, 0.950 g). Purified by column chromatography (deactivated alumina, CH_2Cl_2/hexanes = 1:9, 1:4, 3:7, 2:3) to afford a yellow solid (0.78 g, 62 %).

^{1}H NMR (400 MHz, $CDCl_3$, 300 K, δ): 7.67 (t, *J* = 7.8, 1H), 7.53-7.42 (m, 4H), 7.41 (s, 1H), 7.21 (dd, *J* = 7.5, 0.6, 1H), 7.00 (d, *J* = 1.3, 1H), 6.51 (dd, *J* = 8.2, 0.6, 1H), 3.09 (t, *J* = 7.8, 2H), 2.65 (t, *J* = 7.7, 2H), 1.77-1.62 (m, 4H), 1.68 (s, 9H), 1.50-1.35 (m, 4H), 0.96 (t, *J* = 7.3, 3H), 0.95 (t, *J* = 7.3, 3H).

^{13}C NMR (100 MHz, $CDCl_3$, 300 K, δ): 163.22, 153.34, 152.12, 149.36, 144.70, 144.43, 144.11, 143.03, 138.66, 138.14, 137.01, 127.71, 126.06, 122.55, 119.72, 115.98, 111.29, 110.33, 79.80, 32.80, 32.64, 30.33, 29.89, 28.65, 22.80, 22.35, 14.09, 13.91.

MS (ESI, *m/z*): 505.3 ($[M+H]^+$)

6-{4-Butyl-6-[6-(4-butylthiophen-2-yl)pyridin-2-yl]thiophen-2-yl}-2-(1,1-dimethylethoxy)-pyridin-2-ol (26bOH)

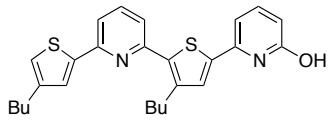

Pyridine hydrochloride (18 mmol, 2.1 g) was added to (**25a**) (0.36 mmol, 0.181 g) and the neat mixture was heated to 190 °C for 4 hours. The mixture was then dissolved in water, neutralized with 1M NaOH solution and extracted three times with CH_2Cl_2. The combined fractions with dried over Na_2SO_4 and concentrated *in vacuo*. The crude mixture was passed through a plug of alumina (deactivated alumina, CH_2Cl_2) to afford the product (155 mg, 93 %).

^{1}H NMR (500 MHz, $CDCl_3$, 300 K, δ): 13.25 (bs, 1H), 7.71 (t, *J*=8.0, 2.6, 1H), 7.65 (s, 1H), 7.54-7.49 (m, 3H), 7.39 (d, *J*=7.8, 1H), 7.02 (s, 1H), 6.67 (d, *J*=7.1, 1H), 6.56 (d, *J*=8.0, 1H), 3.02 (t, *J*=8.0, 2H), 2.65 (t, *J*=7.6, 2H), 1.60-1.74 (m, 2H), 1.68-1.62 (m, 2H), 1.50-1.45 (m, 2H), 1.42-1.38 (m, 2H), 0.99-0.94 (m, 6H).

^{13}C NMR (125 MHz, $CDCl_3$, 300 K, δ): 163.94, 152.46, 151.90, 144.28, 144.07, 142.80, 142.12, 140.77, 140.54, 137.29, 134.35, 130.39, 126.34, 122.90, 119.43, 117.82, 116.82, 105.09, 32.63, 32.32, 30.30, 29.80, 22.73, 22.34, 14.04, 13.92.

6-{4-Butyl-6-[6-(4-butylthiophen-2-yl)pyridin-2-yl]thiophen-2-yl}-2-(1,1-dimethylethoxy)-pyridin-2-yl trifluoromethanesulfonate (26bTf)

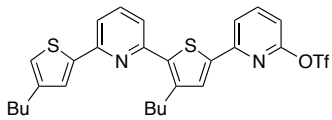

A solution of **(26bOH)** (0.37 mmol, 0.167 g) in 5 mL of CH_2Cl_2 was treated with triethylamine (0.59 mmol, 0.09 mL). The reaction mixture was cooled down to 0 °C and trifluoromethanesulfonic anhydride (0.55 mmol, 0.09 mL) was slowly added and the cooling bath was removed. The reaction mixture was stirred for 4 hours at room temperature, when it was quenched with water. The water phase was neutralized with $NaHCO_3$ saturated solution and extracted three times with CH_2Cl_2. The combined organic fractions were dried over Na_2SO_4 and the solvent was removed *in vacuo*. The crude mixture was passed through a plug of alumina (deactivated alumina, CH_2Cl_2/hexanes = 1:1) to afford the product (191 mg, 89 %).

^{1}H NMR (500 MHz, $CDCl_3$, 300 K, δ): 7.86 (t, *J*=7.8, 1H), 7.71-7.68 (m, 2H), 7.57 (s, 1H), 7.51 (d, *J*=7.9, 1H), 7.49 (d, *J*=1.3, 1H), 7.43 (d, *J*=7.8, 1H), 7.01 (d, *J*=1.1, 1H), 7.00 (d, *J*=8.0, 1H), 3.07 (t, *J*=7.8, 2H), 2.65 (t, *J*=7.7, 2H), 1.77-1.71 (m, 2H), 1.68-1.62 (m, 2H), 1.49-1.44 (m, 2H), 1.42-1.37 (m, 2H), 0.97-0.93 (m, 6H).

^{13}C NMR (100 MHz, $CDCl_3$, 300 K, δ): 155.39, 152.57, 152.33, 152.28, 144.32, 144.22, 143.09, 141.34, 140.65, 140.30, 137.22, 130.54, 126.23, 122.75, 119.78, 118.77, 118.73 (q, J_{C-F} = 320, 1C), 116.58, 114.91, 112.40, 32.67, 32.62, 30.31, 29.78, 22.78, 22.35, 14.06, 13.92.

MS (ESI, *m/z*): 603.2 ([M+Na]$^+$).

6-[4-Butyl-6-(6-{4-butyl-6-[6-(4-butylthiophen-2-yl)pyridin-2-yl]thiophen-2-yl}pyridin-2-yl)thiophen-2-yl]-2-(1,1-dimethylethoxy)pyridine (26c)

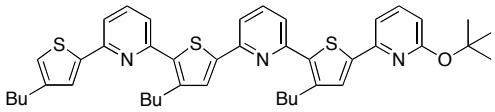

Prepared by the general Negishi cross-coupling procedure. Component A, (**26b**) (0.081 mmol, 0.040 g); base, BuLi (0.090 mmol); $ZnCl_2$ (0.100 mmol, 0.015 g); catalyst: $Pd(PPh_3)_4$ (0.013 mmol, 0.015 g); component B, (**26aTf**) (0.12 mmol, 0.043 g). Purified by column chromatography (silica, CH_2Cl_2/hexanes = 1:9, 1:4, 3:7, 2:3, 1:1) to afford a yellow waxy solid (11 mg, 20 %).

^{1}H NMR (400 MHz, $CDCl_3$, 300 K, δ): 7.69 (dd, *J* = 15.9, 7.9, 2H), 7.56 (s, 1H), 7.55-7.43 (m, 6H), 7.42 (s, 1H), 7.22 (dd, *J* = 7.5, 0.6, 1H), 3.12 (t, *J* = 7.7, 4H), 2.65 (t, *J* = 7.6, 2H), 1.81-1.73 (m, 4H), 1.69 (s, 9H), 1.67-1.62 (m, 2H), 1.53-1.46 (m, 4H), 1.43-1.36 (m, 2H), 0.98-0.95 (m, 9H).

^{13}C NMR (125 MHz, $CDCl_3$, 300 K, δ): 163.22, 153.43, 153.35, 152.19, 151.85, 149.36, 144.68, 144.48, 144.13, 143.67, 143.19, 143.16, 138.72, 138.67, 138.07, 137.03, 137.01, 128.76, 127.76, 126.06, 122.55, 119.95, 119.83, 116.14, 116.11, 111.30, 110.35, 79.80, 32.85(2C), 32.65, 30.33, 29.93, 29.69, 28.67, 22.87(2C), 22.36, 14.14, 14.11, 13.91.

MS (ESI, *m/z*): 720.5 ([M+H]$^+$), 742.4 ([M+Na]$^+$).

6-(4-Butyl-6-{6-[4-butyl-6-(6-{4-butyl-6-[6-(4-butylthiophen-2-yl)pyridin-2-yl]thiophen-2-yl}pyridin-2-yl)thiophen-2-yl]pyridin-2-yl}thiophen-2-yl)-2-(1,1-dimethylethoxy)pyridine (26d)

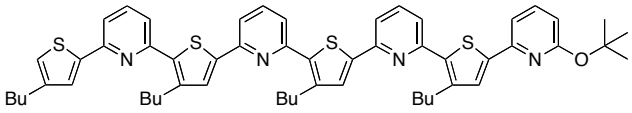

Prepared by the general Negishi cross-coupling procedure. Component A, **(26b)** (0.21 mmol, 0.106 g); base, BuLi (0.22 mmol); $ZnCl_2$ (0.25 mmol, 0.034 g); catalyst: (SIPr)Pd(cin)Cl (0.010 mmol, 0.007 g); component B, **(26bTf)** (0.19 mmol, 0.111 g). Purified by column chromatography (deactivated alumina, CH_2Cl_2/hexanes = 1:9, 1:4, 3:7, 2:3, 1:1) to afford a yellow waxy solid (44 mg, 25 %).

^{1}H NMR (400 MHz, $CDCl_3$, 300 K, δ): 7.75-7.67 (m, 3H), 7.60-7.44 (m, 11H), 7.24 (d, *J* = 7.2, 1H), 7.02 (d, *J* = 0.8, 1H), 6.54 (d, *J* = 8.0, 1H), 3.21-3.13 (m, 6H), 2.67 (t, *J* = 7.6, 2H), 1.84-1.78 (m, 6H), 1.71 (s, 9H), 1.68-1.64 (m, 2H), 1.58-1.52 (m, 6H), 1.50-1.42 (m, 2H), 1.02-0.96 (m, 12H).

^{13}C NMR (125 MHz, $CDCl_3$, 300 K, δ): 163.21, 153.45, 153.42, 153.34, 152.17, 151.93, 151.84, 149.35, 144.68, 144.47, 144.13, 143.70, 143.66, 143.36, 143.22, 143.18, 138.77, 138.68, 138.60, 138.06, 137.05, 128.81, 128.75, 127.79, 126.07, 122.54, 120.11, 119.95, 119.89, 116.26, 116.15, 111.31, 110.36, 79.81, 32.93, 32.89, 32.86, 32.65, 30.34, 30.01, 29.94, 28.67, 22.95, 22.89, 22.37, 14.18, 14.15, 14.13, 13.93.

MS (ESI, *m/z*): 720.5 ($[M+H]^+$), 957.4 ($[M+Na]^+$).

5.2.2 Synthesis of the 2,5-Series

5-Bromo-2-(1,1-dimethylethoxy)pyridine (1)

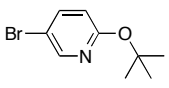

To a solution of 2,5-dibromopyridine (21.1 mmol, 5.00 g) in 40 mL of toluene was added potassium *tert*-butoxide (30.0 mmol, 3.30 g) as a solid and the reaction mixture was refluxed for 2.5 hours. After cooling down to room temperature, the crude mixture was filtered through celite and the solvent was removed. Purification by column chromatography (silica,

ethylacetate/hexanes = 1/19, 1/9) afforded the product as a colorless liquid (15.1 mmol, 52 % yield).

R_f (silica, CH_2Cl_2/hexanes = 1/9) = 0.13

^{1}H NMR (400 MHz, $CDCl_3$, δ): 8.15 (dd, *J*=2.6, 0.6, 1H), 7.57 (dd, *J*=8.7, 2.6, 1H), 6.55 (dd, *J*=8.7, 0.6, 1H), 1.56 (s, 9H).

^{13}C NMR (100 MHz, $CDCl_3$, 300 K, δ): 162.62, 147.04, 140.67, 114.96, 111.28, 80.19, 28.50.

5-(4-Butylthiophen-2-yl)-2-(1,1-dimethylethoxy)pyridine (25a)

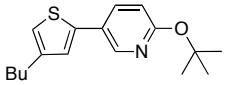

Prepared by the general Negishi cross-coupling procedure. Component A, 3-butylthiophene (41.20 mmol, 5.78 g); base, LTMP (41.50 mmol); $ZnCl_2$ (51.50 mmol, 7.02 g); catalyst: in situ mixture of $Pd_2(dba)_3$ (1.02 mmol, 0.592 g), IPr.HCl (2.04 mmol, 0.867 g) and KO*t*Bu (2.04 mmol, 0.228 g); component B, 2-*tert*-butoxy-5-bromopyridine **(1)** (34.33 mmol, 7.90 g). Purified by column chromatography (deactivated alumina, CH_2Cl_2/hexanes = 1:95) to afford a light yellow liquid (7.15 g, 72 %).

R_f (alumina, CH_2Cl_2/hexanes = 1/9) = 0.25

^{1}H NMR (400 MHz, $CDCl_3$, 300 K, δ): 8.37 (d, *J*=2.6, 1H), 7.70 (dd, *J*=8.6, 2.5, 1H), 7.04 (d, *J*=1.2, 1H), 6.84 (d, *J*=0.8, 1H), 6.65 (d, *J*=8.6, 1H), 2.61 (t, *J*=7.6, 2H), 1.63 (m, 2H), 1.59 (s, 9H), 1.39 (sextet, *J*=7.5, 2H), 0.94 (t, *J*=7.3, 3H).

^{13}C NMR (100 MHz, $CDCl_3$, 300 K, δ): 163.21, 144.23, 143.44, 140.71, 135.81, 124.07, 123.74, 119.03, 113.27, 79.85, 32.57, 30.26, 28.71, 22.37, 13.91.

IR (thin film, cm-1): 2958 (w), 2928 (w), 2858 (w), 1601 (m), 1557 (w), 1491 (s), 1389 (m), 1362 (s), 1307 (m), 1243 (m), 1172 (s), 1128 (m), 1022 (w), 931 (m), 910 (m), 827 (m), 733 (w), 668 (w).

MS (ESI, m/z): 312.2 ([M+Na]+), 301.1 ([M-Me+Na]+), 256.0 ([M-Bu+Na]+), 234.0 ([M-Bu+H]+).

HR-MS (ESI, $C_{17}H_{23}NNaOS$, $[M+Na]^+$): calculated, 312.1398; found, 312.1394.

5-(4-Butylthiophene-2-yl)pyridin-2-ol (25aOH)

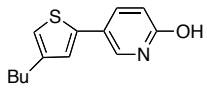

Pyridine hydrochloride (2.60 mmol, 30 g) was added to **(25a)** (10.4 mmol, 3 g) and the neat mixture was heated to 200 °C for 4 hours. The mixture was then dissolved with water, neutralized with 1M NaOH solution and extracted three times with CH_2Cl_2. The combined fractions with dried over Na_2SO_4 and concentrated *in vacuo*. The crude mixture was passed through a plug of alumina (deactivated alumina, CH_2Cl_2) to afford the product (2.32 g, 95 %).

R_f (alumina, MeOH/EtOAc = 1/9) = 0.42

^{1}H NMR (400 MHz, $CDCl_3$, 300 K, δ): 13.19 (bs, 1H), 7.73 (dd, *J*=9.4, 2.6, 1H), 7.62 (d, *J*=2.5, 1H), 6.93 (d, *J*=1.4, 1H), 6.81 (d, *J*=1.2, 1H), 6.64 (dd, *J*=9.4, 0.5, 1H), 2.59 (t, *J*=7.6, 2H), 1.61 (m, 2H), 1.38 (sextet, *J*=7.4, 2H), 0.94 (t, *J*=7.3, 3H).

^{13}C NMR (125 MHz, $CDCl_3$, 300 K, δ): 164.40, 144.36, 140.65, 138.78, 130.62, 124.07, 120.36, 118.87, 115.95, 32.52, 30.20, 22.33, 13.88.

IR (thin film, cm^{-1}): 2959 (w), 2931 (w), 2860 (w), 2359 (w), 1581 (w), 1478 (m), 1420 (s), 1305 (w), 1207 (s), 1167 (s), 1135 (s), 1027 (w), 885 (s), 832 (m), 788 (w), 749 (w), 700 (w), 605 (m), 574 (w), 521 (w).

MS (ESI, *m/z*): 256.1 ($[M+Na]^+$), 234.1 ($[M+H]^+$)

HR-MS (ESI, $C_{13}H_{15}NNaOS$, $[M+Na]^+$): calculated, 256.0772; found, 256.0769.

5-(4-Butylthiophen-2-yl)pyridin-2-yl trifluoromethanesulfonate (25aTf)

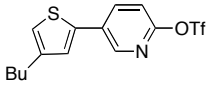

A solution of **(25aOH)** (9.94 mmol, 2.32 g) in 20 mL of CH_2Cl_2 was treated with triethylamine (10.93 mmol, 1.52 mL). the reaction mixture was cooled down to 0 °C and trifluoromethanesulfonic anhydride (10.93 mmol, 1.84 mL) was slowly added. The reaction mixture was stirred for 4 hours, when it was quenched with water. The water phase was neutralized with $NaHCO_3$ saturated solution and extracted three times with CH_2Cl_2. The combined organic fractions were dried over Na_2SO_4 and the solvent was removed *in vacuo*. The

crude mixture was passed through a plug of alumina (deactivated alumina, CH_2Cl_2/hexanes = 1:1) to afford the product (3.50 g, 96 %).

R_f (alumina, CH_2Cl_2/hexanes = 1/1) = 0.67

^{1}H NMR (400 MHz, $CDCl_3$, 300 K, δ): 8.57 (d, *J*=2.5, 1H), 8.00 (dd, *J*=8.5, 2.5, 1H), 7.21 (d, *J*=1.3, 1H), 7.17 (d, *J*=8.5, 1H), 7.00 (d, *J*=0.9, 1H), 2.64 (t, *J*=7.7, 2H), 1.64 (m, 2H), 1.39 (sextet, *J*=7.4, 2H), 0.96 (t, *J*=7.4, 3H).

^{13}C NMR (100 MHz, $CDCl_3$, 300 K, δ): 154.47, 145.03, 144.95, 137.58, 137.46, 131.81, 126.65, 121.85, 118.67 (q, *J*=319), 115.23, 32.53, 30.13, 22.32, 13.84.

IR (thin film, cm^{-1}): 2959 (w), 2931 (w), 2859 (w), 2365 (w), 1581 (w), 1478 (m), 1420 (s), 1361 (w), 1305 (w), 1206 (s), 1166 (s), 1135 (s), 1027 (w), 883 (s), 831 (m), 788 (m), 708 (w), 638 (w), 603 (s), 574 (m), 521 (m).

HR-MS (ESI, $C_{14}H_{14}F_3NNaO_3S_2$, $[M+Na]^+$): calculated, 388.0265; found, 388.0265.

5-{4-Butyl-5-[5-(4-butylthiophen-2-yl)pyridin-2-yl]thiophen-2-yl}-2-(1,1-dimethylethoxy)-pyridine (25b)

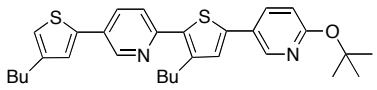

Prepared by the general Negishi cross-coupling procedure. Component A, **(25a)** (2.87 mmol, 0.835 g); base, BuLi (2.93 mmol); $ZnCl_2$ (3.56 mmol, 0.485 g); catalyst: $Pd(PPh_3)_4$ (0.176 mmol, 0.196 g); component B, **(25aTf)** (2.74 mmol, 1.00 g). Purified by column chromatography (deactivated alumina, CH_2Cl_2/hexanes = 1:9, 1:4, 3:7, 2:3) to afford a yellow solid (1.09 g, 79 %).

R_f (alumina, CH_2Cl_2/hexanes = 1/1) = 0.41

^{1}H NMR (500 MHz, $CDCl_3$, 300 K, δ): 8.87 (d, *J*=2.0, 1H), 8.44 (d, *J*=2.6, 1H), 7.86 (dd, *J*=8.3, 2.3, 1H), 7.76 (dd, *J*=8.6, 2.6, 1H), 7.53 (d, *J*=8.2, 1H), 7.22 (d, *J*=1.0, 1H), 7.10 (s, 1H), 6.94 (d, *J*=0.7, 1H), 6.67 (d, *J*=8.5, 1H), 2.92 (t, *J*=7.8, 2H), 2.65 (t, *J*=7.7, 2H), 1.74–1.63 (m, 4H), 1.60 (s, 9H), 1.48–1.36 (m, 4H), 0.96 (t, *J*=7.3, 3H), 0.95 (t, *J*=7.3, 3H).

^{13}C NMR (125 MHz, $CDCl_3$, 300 K, δ): 163.45, 151.75, 146.41, 144.64, 143.46, 141.95, 140.81, 140.01, 136.62, 135.65, 133.03, 128.12, 126.48, 125.25, 123.32, 120.99, 120.49, 113.33, 79.99, 32.57, 32.51, 30.23, 29.68, 28.70, 22.70, 22.36, 13.95, 13.89.

IR (thin film, cm^{-1}): 2956 (m), 2927 (m), 2858 (w), 2360 (w), 2337 (w), 1600 (m), 1558 (m), 1479 (s), 1447 (m), 1389 (m), 1361 (m), 1309 (m), 1291 (s), 1244 (w), 1172 (s), 1129 (w), 1027 (w), 931 (m), 910 (m), 827 (s), 740 (w).

HR-MS (ESI, $C_{30}H_{37}N_2OS_2$, $[M+H]^+$): calculated, 505.2341; found, 505.2343.

5-[4-Butyl-5-(5-{4-butyl-5-[5-(4-butylthiophen-2-yl)pyridin-2-yl]thiophen-2-yl}pyridin-2-yl)thiophen-2-yl]-2-(1,1-dimethylethoxy)pyridine (25c)

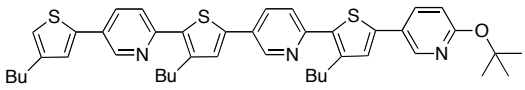

Prepared by the general Negishi cross-coupling procedure. Component A, **(25b)** (0.877 mmol, 0.443 g); base, BuLi (0.895 mmol); $ZnCl_2$ (1.14 mmol, 0.156 g); catalyst: $Pd(PPh_3)_4$ (0.053 mmol, 0.062 g); component B, **(25aTf)** (0.92 mmol, 0.331 g). Purified by column chromatography (deactivated alumina, CH_2Cl_2/hexanes = 1:9, 1:4, 3:7, 2:3, 1:1) to afford a yellow waxy solid (0.453 g, 72 %).

R_f (alumina, CH_2Cl_2/hexanes = 2/1) = 0.53

^{1}H NMR (400 MHz, $CDCl_3$, 300 K, δ): 8.92 (d, *J*=2.2, 1H), 8.88 (d, *J*=2.3, 1H), 8.44 (d, *J*=2.5, 1H), 7.91 (dd, *J*=8.3, 2.4, 1H), 7.87 (dd, *J*=8.3, 2.4, 1H), 7.76 (dd, *J*=8.6, 2.6, 1H), 7.55 (d, *J*=8.3, 1H), 7.54 (d, *J*=8.4, 1H), 7.27 (s, 1H), 7.23 (s, 1H), 7.10 (s, 1H), 6.95 (s, 1H), 6.68 (d, *J*=8.5, 1H), 2.96–2.91 (m, 4H), 2.65 (t, *J*=7.7, 2H), 1.76–1.63 (m, 6H), 1.61 (s, 9H), 1.51–1.36 (m, 6H), 0.99–0.94 (m, 9H).

^{13}C NMR (100 MHz, $CDCl_3$, 300 K, δ): 163.45, 151.97, 151.40, 146.43, 146.31, 144.66, 143.44, 142.12, 142.11, 140.90, 139.87, 139.86, 138.13, 136.60, 135.62, 133.03, 132.87, 128.39, 127.69, 127.65, 126.50, 125.34, 123.29, 121.05, 120.97, 120.61, 113.32, 79.98, 32.55, 32.49, 30.21, 29.71, 29.69, 28.69, 22.71, 22.70, 22.35, 13.95, 13.94, 13.89.

IR (thin film, cm^{-1}): 2955 (m), 2927 (m), 2869 (w), 2365 (w), 1600 (m), 1559 (m), 1473 (s), 1447 (s), 1389 (m), 1361 (m), 1308 (m), 1290 (s), 1244 (w), 1172 (s), 1129 (m), 1028 (w), 930 (m), 910 (m), 827 (s), 739 (w).

HR-MS (ESI, $C_{43}H_{50}N_3OS_3$, $[M+H]^+$): calculated, 720.3110; found, 720.3118.

5-(4-Butyl-5-{5-[4-butyl-5-(5-{4-butyl-5-[5-(4-butylthiophen-2-yl)pyridin-2-yl]thiophen-2-yl}pyridin-2-yl)thiophen-2-yl]pyridin-2-yl}thiophen-2-yl)-2-(1,1-dimethylethoxy)pyridine (25d)

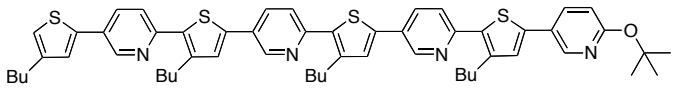

Prepared by the general Negishi cross-coupling procedure. Component A, **(25c)** (0.355 mmol, 0.251 g); base, BuLi (0.360 mmol); $ZnCl_2$ (0.450 mmol, 0.062 g); catalyst: $Pd(PPh_3)_4$ (0.021 mmol, 0.023 g); component B, **(25aTf)** (0.37 mmol, 0.135 g). Purified by column chromatography (deactivated alumina, CH_2Cl_2/hexanes = 1:9, 1:4, 3:7, 2:3, 1:1) to afford a yellow waxy solid (84 mg, 25 %).

R_f (alumina, CH_2Cl_2/hexanes = 2/1) = 0.26

^{1}H NMR (500 MHz, $CDCl_3$, 300 K, δ): 8.92–8.91 (m, 2H), 8.87 (d, *J*=1.8, 1H), 8.44 (d, *J*=2.6, 1H), 7.89–7.86 (m, 2H), 7.84 (dd, *J*=8.3, 2.3, 1H), 7.75 (dd, *J*=8.5, 2.6, 1H), 7.53–7.49 (m, 3H), 7.25 (s, 1H), 7.24 (s, 1H), 7.21 (d, *J*=1.2, 1H), 7.08 (s, 1H), 6.94 (d, *J*=1.0, 1H), 6.67 (d, *J*=8.5, 1H), 2.94–2.89 (m, 6H), 2.63 (t, *J*=7.7, 2H), 1.73–1.63 (m, 8H), 1.61 (s, 9H), 1.49–1.36 (m, 8H), 0.99–0.97 (m, 12H).

^{13}C NMR (125 MHz, $CDCl_3$, 300 K, δ): 163.40, 151.89, 151.55, 151.29, 146.33, 146.23, 146.20, 144.61, 143.38, 142.23, 142.09, 142.07, 140.82, 139.88, 139.81, 139.65, 138.21, 138.06, 136.57, 135.56, 132.93, 132.75, 128.34, 127.88, 127.68, 127.62, 127.59, 126.46, 125.28, 123.25, 120.96, 120.94, 120.85, 120.57, 113.27, 79.93, 32.51, 32.43, 32.42, 30.18, 29.74, 29.72, 29.70, 29.65, 28.66, 22.71, 22.70, 22.69, 22.34, 13.94, 13.93, 13.87.

IR (thin film, cm^{-1}): 2955 (m), 2922 (s), 2853 (m), 2364 (w), 1730 (w), 1588 (w), 1560 (w), 1466 (m), 1456 (m), 1389 (w), 1376 (w), 1290 (m), 1172 (w), 1129 (w), 1026 (w), 827 (m), 798 (w), 742 (w).

HR-MS (ESI, $C_{56}H_{63}N_4OS_4$, $[M+H]^+$): calculated, 935.3879; found, 935.3878.

5.2.3 Synthesis of the Dendrimeric Series

2,6-Dichloro-4-iodopyridine

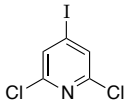

2,6-Dichloro-4-iodopyridine was prepared according to the literature.[123] Neat 2,2,6,6-tetramethyl piperidine (17.6 mmol, 2.49 g, 3 mL) was added to a solution of *iso*-propylmagnesium chloride lithium chloride complex (1.3 M, 17.1 mmol, 13.1 mL, THF) at room temperature and stirred for 48 hours. The final solution was then slowly added to a solution of 2,6-dicholoropyridine (1 M, 11.0 mmol, 1.63 g, THF) at room temperature and allowed to stir for 10 minutes; when a solution of iodine (1 M, 12.1 mmol, 3.07 g, THF) was slowly added and allowed to react for 20 minutes. The final reaction mixture was quenched with NH_4Cl saturated solution and extracted three times with ethylacetate, the combined organic phases was washed with brine, dried over $MgSO_4$ and the solvent was removed *in vacuo* to afford the title compound as a colorless solid (2.55 g, 85 %).

^{1}H NMR (500 MHz, $CDCl_3$, 300 K, δ): 7.66 (s, 2H)

^{13}C NMR (125 MHz, $CDCl_3$, 300 K, δ): 150.67, 131.48, 107.54.

2,6-Dichloro-4-(thiophen-2-yl)pyridine

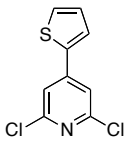

Prepared by the general Negishi cross-coupling procedure. Component A, thiophene (*C_4H_4S*, 4.38 mmol, 368 mg); base, BuLi (*C_4H_9Li*, 4.38 mmol, 3.10 mL, 1.40 M); zinc chloride (*$ZnCl_2$*, 5.47 mmol, 745 mg); catalyst, $Pd(PPh_3)_4$ (*$C_{72}H_{60}P_4Pd$*, 0.18 mmol, 21 mg); component B, 2,6-dichloro-4-iodopyridine (*$C_5H_2Cl_2IN$*, 1.73 mmol, 300 mg), reaction conditions: 1 hour, at room temperature. Purified by column chromatography (deactivated alumina, CH_2Cl_2/hexane = 1:9) to give a white solid (790 mg, 94 % yield).

^{1}H NMR (500 MHz, $CDCl_3$, 300 K, δ): 7.53 (dd, *J*=3.7, 1.2, 1H), 7.50 (dd, *J*=5.0, 1.1, 1H), 7.44 (s, 2H), 7.16 (dd, *J*=5.0, 3.7, 1H).

^{13}C NMR (125 MHz, $CDCl_3$, 300 K, δ): 151.21, 146.61, 138.35, 128.92, 128.77, 126.99, 118.75.

2,6-Bis(4-octylthiophen-2-yl)-4-(thiophen-2-yl)pyridine

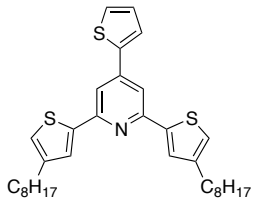

Prepared by the general Negishi cross-coupling procedure. Component A, 3-octylthiophene (10.9 mmol, 2.13 g); base, LiTMP (11.1 mmol); $ZnCl_2$ (13.0 mmol, 1.77 g); catalyst: Pd-PEPPSI-IPr (0.22 mmol, 150 mg); component B, 2,6-dichloro-4-(thiophen-2-yl)pyridine (4.3 mmol, 1.0 g). Purified by column chromatography (deactivated alumina, CH_2Cl_2/hexanes = 1:19, 1:9) to afford a light yellow solid (2.11 g, 88 %).

^{1}H NMR (400 MHz, $CDCl_3$, 300 K, δ): 7.61 (s, 2H), 7.58 (dd, *J*=3.5, 1.1, 1H), 7.54 (d, *J*=1.4, 2H), 7.44 (dd, *J*=5.0, 1.1, 1H), 7.17 (dd, *J*=5.0, 3.6, 1H), 7.01 (d, *J*=1.3, 2H), 2.65 (t, *J*=7.5, 4H), 1.67 (quintet, *J*=7.5, 4H), 1.36-1.26 (m, 20H), 0.89 (t, *J*=7.1, 6H).

^{13}C NMR (100 MHz, $CDCl_3$, 300 K, δ): 152.89, 144.24, 144.10, 142.74, 141.51, 128.32, 126.94, 126.30, 125.36, 122.75, 113.01, 31.89, 30.66, 30.52, 29.44, 29.32, 29.28, 22.67, 14.10.

HR-MS (ESI, $C_{33}H_{44}NS_3$, $[M+H]^+$): calculated, 550.2630; found, 550.2628.

2,6-Dichloro-4-{5-[2,6-bis(4-octylthiophen-2-yl)pyridine-4-yl]thiophen-2-yl}pyridine

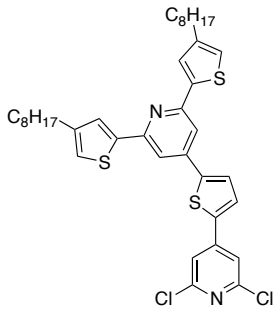

Prepared by the general Negishi cross-coupling procedure. Component A, 2,6-bis(4-octylthiophen-2-yl)-4-(thiophen-2-yl)pyridine (0.91 mmol, 500 mg); base, LTMP (0.92

mmol); zinc chloride (1.26 mmol, 172 mg); catalyst, $Pd(PPh_3)_4$ (0.025 mmol, 29 mg); component B, 2,6-dichloro-4-iodopyridine (0.84 mmol, 230 mg), reaction conditions: 1 hour, at room temperature. Purified by column chromatography (deactivated alumina, CH_2Cl_2/hexane = 1:2, 1:1) to give a yellow solid (443 mg, 76 % yield).

^{1}H NMR (500 MHz, $CDCl_3$, 300 K, δ): 7.58 (d, *J*=3.9, 1H), 7.57 (s, 1H), 7.54 (d, *J*=3.9, 1H), 7.53 (d, *J*=1.3, 2H), 7.47 (s, 2H), 7.03 (d, *J*=1.3, 2H), 2.64 (t, *J*=7.5, 4H), 1.67 (quintet, *J*=7.5, 4H), 1.37-1.27 (m, 20H), 0.89 (t, *J*=7.2, 6H).

^{13}C NMR (125 MHz, $CDCl_3$, 300 K, δ): 153.16, 151.36, 145.83, 144.64, 144.36, 143.68, 141.38, 139.02, 127.94, 126.57, 126.51, 123.13, 118.56, 112.54, 31.89, 30.65, 30.52, 29.45, 29.33, 29.29, 22.68, 14.12.

HR-MS (ESI, $C_{38}H_{45}Cl_2N_2S_3$, $[M+H]^+$): calculated, 695.2116; found, 695.2114.

2,4,6-Tris{5-[2,6-bis(4-octylthiophen-2-yl)pyridin-4-yl]thiophen-2-yl}pyridine

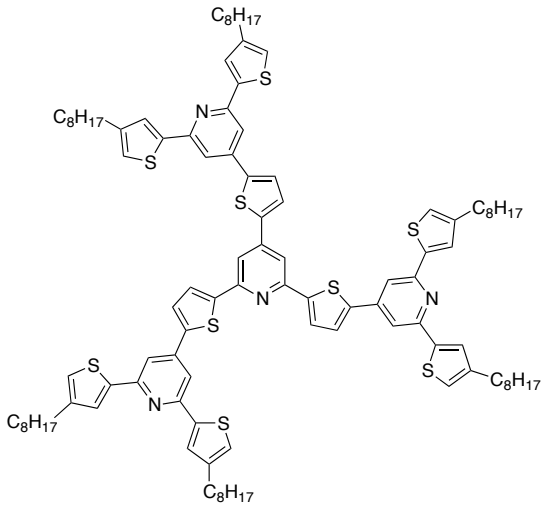

Prepared by the general Negishi cross-coupling procedure. Component A, 2,6-bis(4-octylthiophen-2-yl)-4-(thiophen-2-yl)pyridine (1.25 mmol, 687 mg); base, LTMP (1.28 mmol); $ZnCl_2$ (1.71 mmol, 233 mg); catalyst: Pd-PEPPSI-IPr (0.028 mmol, 19 mg); component B, 2,6-dichloro-4-{5-[2,6-bis(4-octylthiophen-2-yl)pyridine-4-yl]thiophen-2-yl}pyridine (0.57 mmol, 400 mg). Purified by three consecutive column chromatographies (deactivated alumina, gradient of CH_2Cl_2/hexanes = 1:99, 1:19, 1:9, 1:6, 1:4, 1:3, 1:2) to afford a yellow solid (520 mg, 53 %).

^{1}H NMR (400 MHz, $CDCl_3$, 300 K, δ): 0.085 mM solution; 7.85 (d, *J*=3.9, 2H), 7.82 (s, 2H), 7.72 (s, 4H), 7.71 (d, *J*=3.9, 1H), 7.68 (s, 2H), 7.68 (d, *J*=3.8, 1H), 7.65 (d, *J*=3.9, 2H), 7.61 (d,

J=1.5, 4H), 7.60 (d, *J*=1.1, 2H), 7.05 (d, *J*=1.1, 2H), 7.03 (d, *J*=1.4, 4H), 2.69-2.64 (m, 12H), 1.72-1.67 (m, 12H), 1.37-1.26 (m, 60H), 0.88 (t, *J*=6.3, 18H).

^{13}C NMR (125 MHz, $CDCl_3$, 300 K, δ): 152.93, 152.82, 152.30, 145.30, 144.28, 144.24, 143.99, 143.89, 143.45, 142.96, 142.28, 142.11, 141,71, 126.61, 126.43, 126.41, 126.33, 126.21, 126.16, 122.88, 122.64, 113.14, 112.56, 112.39, 31.91, 31.90, 30.70, 30.67, 30.52, 30.45, 29.50, 29.49, 29.42, 29.41, 29.34, 29.33, 22.70, 22.69, 14.14, 14.13.

HR-MS (ESI, $C_{104}H_{129}N_4S_9$, $[M+H]^+$): calculated, 1721.7698; found, 1721.7705.

2,6-Bis{5-[2,6-bis(4-octylthiophen-2-yl)pyridin-4-yl]thiophen-2-yl}-4-(thiophen-2-yl)pyridine

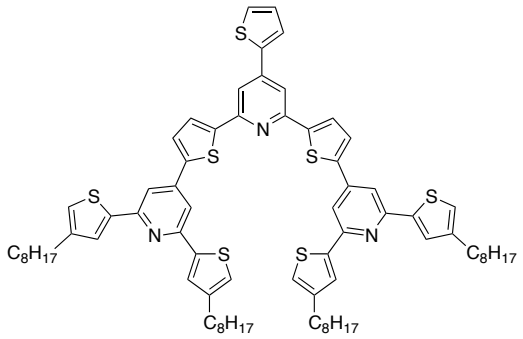

Prepared by the general Negishi cross-coupling procedure. Component A, 2,6-bis(4-octylthiophen-2-yl)-4-(thiophen-2-yl)pyridine (0.91 mmol, 500 mg); base, LTMP (0.92 mmol); $ZnCl_2$ (1.08 mmol, 147 mg); catalyst: Pd-PEPPSI-IPr (0.014 mmol, 9 mg); component B, 2,6-dichloro-4-(thiophen-2-yl)pyridine (0.36 mmol, 83 mg). Purified by column chromatography (deactivated alumina, gradient of CH_2Cl_2/hexanes = 1:99, 1:33, 1:19, 1:9, 1:6, 1:4, 1:3, 1:2, 1:1) to afford a yellow solid (230 mg, 50 %).

^{1}H NMR (400 MHz, $CDCl_3$, 300 K, δ): 7.66 (d, *J*=4.0, 2H), 7.61 (s, 2H), 7.60 (s, 4H), 7.57 (dd, *J*=3.6, 1.1, 1H), 7.53 (d, *J*=1.1, 4H), 7.52 (d, *J*=3.8, 2H), 7.44 (dd, *J*=5.0, 1.1, 1H), 7.15 (dd, *J*=5.0, 3.6, 1H), 6.99 (d, *J*=1.0, 4H), 2.61 (t, *J*=7.7, 8H), 1.66 (quintet, *J*=7.7, 8H), 1.35-1.27 (m, 40H), 0.88 (t, *J*=7.1, 12H).

^{13}C NMR (125 MHz, $CDCl_3$, 300 K, δ): 152.79, 152.20, 145.46, 144.21, 144.05, 143.24, 142.88, 142.38, 140.85, 128.45, 127.31, 126.36, 126.16, 126.08, 125.69, 122.64, 113.65, 112.62, 31.89, 30.66, 30.47, 29.47, 29.38, 29.31, 22.68, 14.13.

HR-MS (ESI, $C_{75}H_{90}N_3S_7$, $[M+H]^+$ and $C_{75}H_{91}N_3S_7$, $[M+2H]^{2+}$): calculated, 1256.5174 and 628.7623; found, 1256.5150 and 628.7620.

2,6-Dichloro-4-[5-(2,6-bis{5-[2,6-bis(4-octylthiophen-2-yl)pyridin-4-yl]thiophen-2-yl}pyridin-4-yl)thiophen-2-yl]pyridine

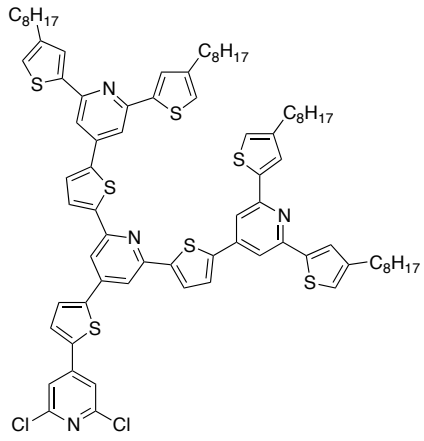

Prepared by the general Negishi cross-coupling procedure. Component A, 2,6-bis{5-[2,6-bis(4-octylthiophen-2-yl)pyridin-4-yl]thiophen-2-yl}-4-(thiophen-2-yl)pyridine (0.040 mmol, 50 mg); base, LTMP (0.044 mmol); zinc chloride (0.052 mmol, 7.1 mg); catalyst, $Pd(PPh_3)_4$ (1.2 μmol, 1.4 mg); component B, 2,6-dichloro-4-iodopyridine (0.052 mmol, 14 mg), reaction conditions: 20 hours, at room temperature. Purified by column chromatography (deactivated alumina, gradient of CH_2Cl_2/hexanes = 1:99, 1:33, 1:19, 1:9, 1:6, 1:4, 1:3, 1:2, 1:1) to afford a yellow solid (25 mg, 45 %).

^{1}H NMR (500 MHz, $CDCl_3$, 300 K, δ): 7.65 (d, *J*=3.8, 2H), 7.56 (s, 4H), 7.54 (s, 2H), 7.52-7.51 (m, 7H), 7.42 (d, *J*=3.8, 1H), 7.37 (s, 2H), 6.99 (d, *J*=1.1, 4H), 2.62 (t, *J*=7.7, 8H), 1.66 (quintet, *J*=7.7, 8H), 1.36-1.27 (m, 40H), 0.88 (t, *J*=7.1, 12H).

^{13}C NMR (125 MHz, $CDCl_3$, 300 K, δ): 152.77, 152.17, 151.20, 145.30, 145.06, 144.28, 143.91, 143.48, 143.37, 142.05, 141.36, 139.31, 127.76, 126.58, 126.45, 126.13, 125.97, 122.62, 118.35, 112.82, 112.25, 31.92, 30.70, 30.44, 29.50, 29.48, 29.34, 22.69, 14.10.

HR-MS (ESI, $C_{80}H_{91}Cl_2N_4S_7$, $[M+H]^+$ and $C_{80}H_{92}Cl_2N_4S_7$, $[M+2H]^{2+}$): calculated, 1401.4660 and 701.2366; found, 1401.4662 and 701.2353.

2,5-Bis{5-[2,6-bis(4-octylthiophen-2-yl)pyridin-4-yl]thiophen-2-yl}pyridine

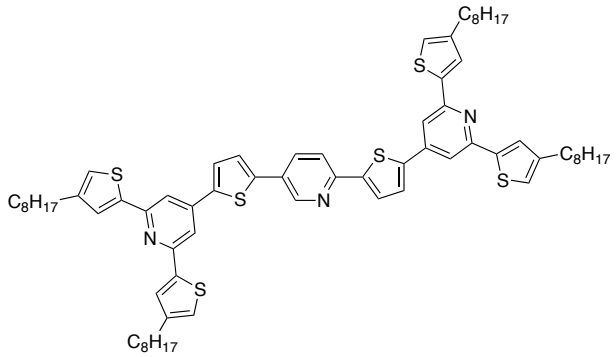

Prepared by the general Negishi cross-coupling procedure. Component A, 2,6-bis(4-octylthiophen-2-yl)-4-(thiophen-2-yl)pyridine (0.26 mmol, 143 mg); base, LTMP (0.27 mmol); $ZnCl_2$ (0.33 mmol, 45 mg); catalyst: Pd-PEPPSI-IPr (4.4 μmol, 3 mg); component B, 2,5-dibromopyridine (0.11 mmol, 26 mg). Purified by column chromatography (deactivated alumina, gradient of CH_2Cl_2/hexanes = 1:9, 1:4, 1:3, 1:2, 1:1) to afford a yellow solid (79 mg, 61 %).

^{1}H NMR (400 MHz, $CDCl_3$, 300 K, δ): 8.91 (dd, *J*=3.0, 0.5, 1H), 7.96 (dd, *J*=8.5, 2.4, 1H), 7.74 (d, *J*=8.5, 1H), 7.72 (d, *J*=3.7, 1H), 7.66 (s, 2H), 7.61 (s, 2H), 7.60 (d, *J*=3.8, 1H), 7.59 (d, *J*=3.8, 1H), 7.57 (d, *J*=1.3, 2H), 7.56 (d, *J*=1.3, 2H), 7.44 (d, *J*=3.8, 1H), 7.03 (d, *J*=1.1, 2H), 7.02 (d, *J*=1.1, 2H), 2.68-2.64 (m, 8H), 1.69 (quintet, *J*=7.0, 8H), 1.39-1.29 (m, 40H), 0.89 (t, *J*=6.7, 12H).

^{13}C NMR (125 MHz, $CDCl_3$, 300 K, δ): 153.05, 153.03, 151.13, 146.57, 145.53, 144.32, 144.29, 144.11, 144.04, 143.38, 142.33, 142.15, 141.83, 141.55, 133.37, 128.50, 126.53, 126.44, 126.41, 126.28, 125.59, 125.16, 122.89, 122.81, 118.70, 112.60, 112.59, 31.91, 30.70, 30.54, 30.53, 29.47, 29.37, 29.29, 22.68, 14.09.

HR-MS (ESI, $C_{71}H_{88}N_3S_6$, $[M+H]^+$ and $C_{71}H_{89}N_3S_6$, $[M+2H]^{2+}$): calculated, 1174.5297 and 587.7685; found, 1174,5280 and 587.7678.

5-{5-[2,6-Bis(4-octylthiophen-2-yl)pyridin-4-yl]thiophen-2-yl}-2,2'-bipyridyl

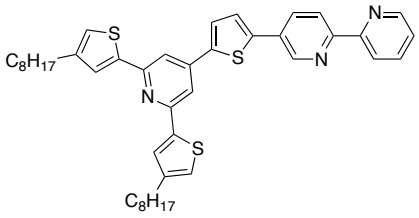

Prepared by the general Negishi cross-coupling procedure. Component A, 2,6-bis(4-octylthiophen-2-yl)-4-(thiophen-2-yl)pyridine (1.0 mmol, 550 mg); base, LTMP (1.05 mmol); $ZnCl_2$ (1.5 mmol, 205 mg); catalyst: Pd-PEPPSI-IPr (0.03 mmol, 20 mg); component B, 5-bromo-2,2'-bipyridyl (1.1 mmol, 148 mg). Purified by column chromatography (deactivated alumina, gradient of CH_2Cl_2/hexanes = 1:9, 1:4, 1:3, 1:2, 1:1) to afford a yellow solid (235 mg, 33 %).

^{1}H NMR (400 MHz, $CDCl_3$, 300 K, δ): 9.00 (d, *J*=8.0, 1H), 8.71 (d, *J*=4.1, 1H), 8.49 (d, *J*=8.3, 1H), 8.46 (d, *J*=8.0, 1H), 8.06 (dd, *J*=8.3, 2.3, 1H), 7.86 (td, *J*=7.7, 1.4, 1H), 7.62 (s, 2H), 7.61 (d, *J*=3.7, 1H), 7.56 (d, *J*=0.5, 2H), 7.48 (d, *J*=3.7, 1H), 7.35 (dd, *J*=6.9, 5.1, 1H), 7.03 (d, *J*=0.5, 2H), 2.65 (t, *J*=7.9, 4H), 1.68 (quintet, *J*=7.9, 4H), 1.36-1.29 (m, 20H), 0.89 (t, *J*=7.0, 6H).

^{13}C NMR (125 MHz, $CDCl_3$, 300 K, δ): 155.27, 154.98, 152.96, 149.04.146.10, 144.29, 143.96, 142.12, 141.90, 141.63, 137.26, 133.68, 129.79, 126.52, 126.38, 125.44, 123.93, 122.89, 121.23, 121.22, 112.55, 31.89, 30.66, 30.52, 29.45, 29.33, 29.28, 22.67, 14.12.

HR-MS (ESI, $C_{43}H_{50}N_3S_3$, $[M+H]^+$): calculated, 704.3161; found, 704.3160.

5.3 Photophysical Data

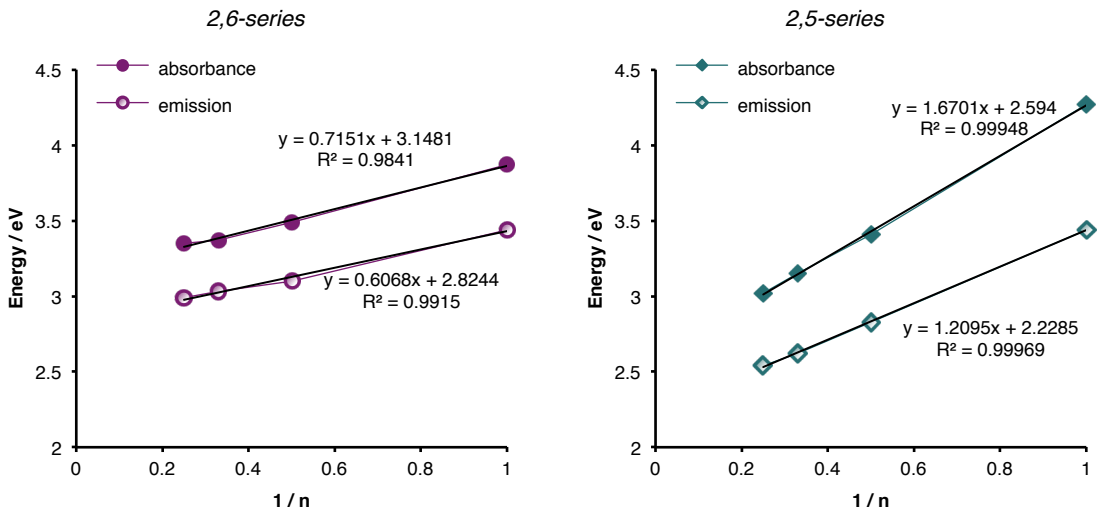

Figure 5.1: Plot of energy versus the inverse chain length and least square linear fits with the respective equations.

5.4 Crystal structure

Crystals suitable for X-ray crystallographic analyses were obtained for **G0a**. The ORTEP plots of the two conformations observed are shown in **Figure 5.2** and the crystallographic data is given in **Table 5.1**.

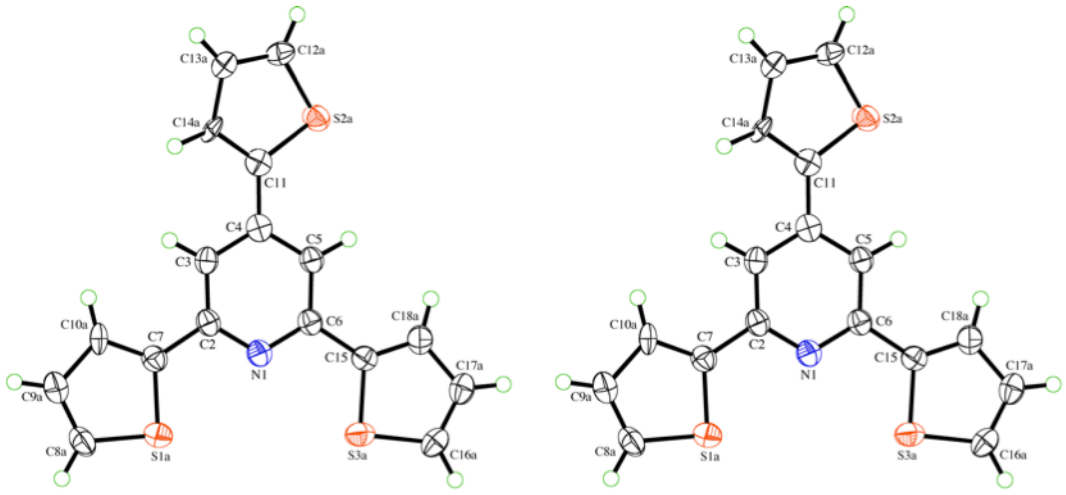

*Figure 5.2: ORTEP representation of the two conformations of the molecule, **G0a** (50% probability ellipsoids; H-atoms given arbitrary displacement parameters for clarity).*

Table 5.1: *Crytallographic data of* ***G0a****.*

Crystallised from		hexane / EtOAc
Empirical formula		$C_{17}H_{11}NS_3$
Formula weight [g mol^{-1}]		325.46
Crystal colour, habit		colourless, prism
Crystal dimensions [mm]		0.20 × 0.20 × 0.25
Temperature [K]		160(1)
Crystal system		orthorhombic
Space group		*Pna*2$_1$ (#33)
Z	4	
Reflections for cell determination		36216
2θ range for cell determination [°]		4–55
Unit cell parameters	a [Å]	10.4570(2)
	b [Å]	11.4169(2)
	c [Å]	12.6533(2)
	α [°]	90
	β [°]	90
	γ [°]	90
	V [Å^3]	1510.63(5)
F(000)		672
D_x [g cm^{-3}]		1.431
μ(Mo $K\alpha$) [mm^{-1}]		0.481
Scan type		ϕ and ω
2θ(max) [°]		55
Transmission factors (min; max)		0.815; 0.910
Total reflections measured		23271
Symmetry independent reflections		3434
R_{int}	0.058	
Reflections with $I > 2\sigma(I)$		2984
Reflections used in refinement		3433
Parameters refined; restraints		301; 331
Final $R(F)$ [$I > 2\sigma(I)$ reflections]		0.0397
$wR(F^2)$ (all data)		0.0959
Weights:	$w = [\sigma^2(F_o^2) + (0.0481P)^2 + 0.5797P]^{-1}$ where $P = (F_o^2 + 2F_c^2)/3$	
Goodness of fit		1.046
Final Δ_{max}/σ		0.001
$\Delta\rho$ (max; min) [e Å^{-3}]		0.19; -0.31
$\sigma(d(C–C))$ [Å]		0.003 – 0.006

CURRICULUM VITAE

Silvia Veleirinho de Oliveira Rocha

Sex: Female **Date of Birth:** January 15th, 1982 **Nationality:** Brazilian / Portuguese

---

EDUCATION

July 2010:	University of Zurich, Zurich, Switzerland – *M.Sc. In Chemistry* "*Synthesis and Photophysical Properties of Donor–Acceptor–Donor Chromophores Containing Thiophene and Pyridine Units* Advisor: PD Dr. Nathaniel S. Finney
2005:	University of São Paulo (USP), São Paulo, Brazil – *B.Sc. in Chemistry*
2004:	University of São Paulo (USP), São Paulo, Brazil – *B.Sc. in Molecular Sciences*

WORK EXPERIENCE

April 2006 – today:	University of Zurich, Zurich, Switzerland Graduate research fellow Advisor: PD Dr. Nathaniel S. Finney
2004:	Institute of Chemistry, Inorganic Chemistry Department, USP, Brazil Undergraduate research fellow from CNPq (National Council for Scientific and Technological Development) Advisor: Prof. Henrique Eise Toma
2003:	Institute of Chemistry, Biochemistry Department, USP, São Paulo, Brazil Undergraduate research fellow from CNPq Advisor: Prof. Etelvino J. H. Bechara

---

PUBLICATIONS, PRESENTATIONS AND POSTERS

Publications	Rocha, S. V., Finney, N. S. Synthesis and Photophysical Properties of Donor–Acceptor–Donor Chromophores Containing Thiophene and Pyridine Units, *manuscript in preparation*.
	Rocha, S. V., Finney, N. S. Alternating 2,6-Linked Pyridine–Thiophene Oligomers: Synthesis and Properties, *manuscript in preparation*.

Rocha, S. V., Finney, N. S. Synthesis and Evaluation of 2,5-Linked Alternating Pyridine–Thiophene Oligomers, *Organic Letters*, 2010, *12*, 2598–2601.

Adriaenssens, L., Severa, L., Salova, T., Cisarova, I., Pohl, R., Saman, D., Rocha, S. V., Finney, N. S., Pospisil, L., Slavice, P., Teply, F. Helquats: a Facile, Modular, Scalable Route to Novel Helical Dications, *Chemistry - A European Journal*, 2009, *15*, 1072–1076.

Engelmann, F. M., Rocha, S. V. O., Toma, H. E., Araki, K., Baptista, M. S. Determination of *n*-Octanol/Water Partition and Membrane Binding of Cationic Porphyrins, *International Journal of Pharmaceutics*, 2007, *329*, 12–18.

Oral presentation Swiss Chemical Society Meeting, Lausanne, Switzerland, 2009

2009-DokTag, PhD Students Day of the Organic Chemistry Institute of the University of Zurich, Zurich, Switzerland, 2009

Poster presentation ISNA-14 International Symposium on Novel Aromatic Compounds, Eugene (OR), United States, 2011

EuCheMS Chemistry Congress, Nuremberg, Germany, 2010

ISNA-13 International Symposium on Novel Aromatic Compounds, Luxembourg, Luxembourg, 2009

2nd and 3rd Dorothy Crowfoot Hodgkin Symposium, Zurich, Switzerland, 2007 and 2008

EuCheMS Chemistry Congress, Torino, Italy, 2008

Swiss Chemical Society Meeting, Lausanne, Switzerland, 2007

12th Brazilian National Journey of Undergraduate Research, Fortaleza, Brazil, 2005

57th Annual Meeting of the Brazilian Society for the Science Progress (SBPC), Fortaleza, Brazil, 2005

13th International Symposium of Undergraduate Research of the University of São Paulo, São Paulo, Brazil, 2004

AWARDS

SCNAT Travel Award – Swiss Academy of Sciences, 2009

Honorable Mention – 13th International Symposium of Undergraduate Research of University of São Paulo, 2004

REFERENCES

1. IUPAC. Compendium of Chemical Terminology, 2nd ed. (the "Gold Book"). Compiled by A. D. McNaught and A. Wilkinson. Blackwell Scientific Publications, Oxford (1997). XML on-line corrected version: http://goldbook.iupac.org (2006-) created by M. Nic, J. Jirat, B. Kosata; updates compiled by A. Jenkins. ISBN 0-9678550-9-8. doi:10.1351/goldbook.

2. Chiang, C. K.; Fincher, C. R., Jr.; Park, Y. W.; Heeger, A. J.; Shirakawa, H.; Louis, E. J.; Gau, S.C.; MacDiarmid, A. G. *Phys. Rev. Lett.* **1977**, *39*, 1098.

3. Sirringhaus, H.; Tessler, N.; Friend, R. H. *Science* **1998**, *280*, 1741.

4. Yugeng, W.; Liu, Y. *Adv. Mater.* **2010**, *22*, 1.

5. György, I. *Conducting Polymers*; Springer: Berlin, 2008.

6. Thomas III, S. W.; Joly, G. D.; Swager, T. M. *Chem. Rev.* **2007**, *107*, 1339.

7. The original reference where Hückel first describes systems containing double bonds: Hückel, E. *Z. Physik A-Hardon Nucl.* **1930**, *60*, 423.

8. Reference where Hückel describes benzene: Hückel, E. *Z. Physik A-Hardon Nucl.* **1931**, *70*, 204.

9. Many textbooks present a treatment of the Hückel Molecular Orbitals, the one shown here is mainly based on: Carroll, F. A. *Perspectives on Structure and Mechanism in Organic Chemistry*, 2nd edition, John Wiley & Sons, Inc.: Hoboken, 2010; Chapter 4.

10. Rauk, A. *Orbital Interaction Theory of Organic Chemistry*, 2nd edition, John Wiley & Sons, Inc.: New York, 2001.

11. McQuarrie, D. A.; Simon, J. D. *Physical Chemistry: A Molecular Approach* University Science Books: Sausalito, 1997; Chapter 7.

12. Brown, R. D. *Q. Rev. Chem. Soc.* **1952**, *6*, 63.

13. *SHMO Simple Hückel Molecular Orbital Calculator*, version 20111118; SHMO is an interactive program to perform electronic structure calculations within the "Simple Hückel Molecular Orbital" approximations; programmed by Hans-Ulrich Wagner in Java language: available online http://wchem.cup.lmu.de/SHMO/ (accessed Mar 19, 2012).

14. There are many textbooks presenting details about symmetry point groups and irreducible representations, the mainly source consulted by this author was: Bishop, D. M. *Group Theory and Chemistry* Dover Publications, Inc.: New York, 1973.

15. Van-Catledge, F. A. *J. Org. Chem.* **1980**, *45*, 4801.

16. *Handbook of Oligo- and Polythiophenes*; Fichou, D., Ed.; Wiley-VCH: Weinheim, 1999.

17. Osaka, I.; McCullough, R. D. *Acc. Chem. Res.* **2008**, *41*, 1202.

18. Edwards, P.P.; Johnston, R. L.; Rao, C. N. R.; Tunstall, D. P.; Hensel, F. *Philos. Trans. R. Soc. London, Ser. A* **1996**, *356*, 5.

19. Roncali, J. *Chem. Rev.* **1997**, *97*, 173.

20. Zhang, Q. T.; Tour, J. M. *J. Am. Chem. Soc.* **1998**, *120*, 5355.

21. Furukawa, Y. Electronic Spectra of Conjugated Polymers and Oligomers. In *Handbook of Advanced Electronic and Photonic Materials and Devices – Volume 8: Conducting Polymers*; Nalwa, H. S., Ed.; Academic Press, San Diego, 2001, pp. 303–320.

22. Cheng, Y.-J.; Yang, S.-H.; Hsu, C.-S. *Chem. Rev.* **2009**, *109*, 5868.

23. Botiz, I.; Schaller, R. D.; Verduzco, R.; Darling, S. B. *J. Phys. Chem. C* **2011**, *115*, 9260.

24. Yuen, J. D.; Fan, J.; Seifter, J.; Lim, B.; Hufschmid, R.; Heeger, A. J.; Wudl, F. *J. Am. Chem. Soc.* **2011**, *133*, 20799.

25. Letizia, J. A.; Salata, M. R.; Tribout, C. M.; Facchetti, A.; Ratner, M. A.; Marks, T. J. *J. Am. Chem. Soc.* **2008**, *130*, 9679.

26. Mullekom, H. A. M.; Vekemans, J. A. J. M.; Havinga, E. E.; Meijer, E. W. *Mat Sci. Eng.* **2001**, *32*, 1.

27. Alam, M. M.; Jenekhe, S. A. *Chem. Mater.* **2004**, *16*, 4647.

28. Kulkarni, A. P.; Tonzola, C. J.; Babel, A.; Jenekhe, S. A. *Chem. Mater.* **2004**, *16*, 4556.

29. Yamamoto, T.; Maruyama, J. T.; Zhou, Z.; Ito, T.; Fukuda, T.; Yoneda, Y.; Begum, F.; Ikeda, T.; Sasaki, S.; Takezoe, H.; Fukuda, A.; Kubotall, K. *J. Am. Chem. Soc.* **1994**, *116*, 4832.

30. Wang, C.; Kilitziraki, M.; McBride, J. A. H.; Bryce, M. R.; Horsburgh, L. E.; Sheridan, A. K.; Monkman, A. P.; Samuel, I. D. *Adv. Mater.* **2000**, *12*, 217

31. Effect of protonation in pyridine-containing polymers: Monkman, A. P.; Halim, M.; Samuel, I. D. W.; Horsburgh, L. E. *J. Chem. Phys.* **1998**, *109*, 10372.

32. Effect of protonation–deprotonation processes in pyridine-containing polymers: Eichen, Y.; Nakhmanovich, G.; Gorelik, V.; Epshtein, O.; Poplawski, J. M.; Ehrenfreund, E. *J. Am. Chem. Soc.* **1998**, *120*, 10463.

33. For a review about metallosupramolecular polymers containing pyridine ligands, see: Schubert, U. S.; Eschebaumer, C. *Angew. Chem. Int. Ed.* **2002**, *41*, 2892.

34. Example where bipy ligand units were introduced directly into the conjugated polymer backbone and polymeric ruthenium complexes are reported: Zhu, S. S.; Swager, T. M. *Adv. Mater.* **1996**, *8*, 497.

35. Izuhara, D.; Swager, T. M. *J. Am. Chem. Soc.* **2009**, *131*, 17724.

36. Izuhara, D.; Swager, T. M. *Macromolecules* **2011**, *44*, 2678.

37. Facchetti, A. *Chem. Mater.* **2011**, *23*, 733.

38. Mishra. A.; Ma, C.-Q.; Bäuerle, P. *Chem. Rev.* **2009**, *109*, 1141.

39. Murphy, A. R.; Fréchet, J. M. J. *Chem. Rev.* **2007**, *107*, 1066.

40. Meier, H.; Stalmach, U.; Kolshorn, H. *Acta Polymer.* **1997**, *48*, 379.

41. Bäuerle, P. *Advanced Materials* **1992**, *4*, 102.

42. Lo. S.; Burn, P. L. *Chem. Rev.* **2007**, *107*, 1097.

43. Astruc, D.; Boisselier, E.; Ornelas, C. *Chem. Rev.* **2010**, *110*, 1857.

44. Bosman, A. W.; Janssen, H. M.; Meijer, E. W. *Chem. Rev.* **1999**, *99*, 1665.

45. Zeng, F.; Zimmerman, S. C. *Chem. Rev.* **1997**, *97*, 1681.

46. Moore, J. S. *Acc. Chem. Res.* **1997**, *30*, 402.

47. Devadoss, C.; Bharathi, P.; Moore, J. S. *J. Am. Chem. Soc.* **1996**, *118*, 9635.

48. Hecht, S.; Fréchet, J. M. J. *Angew. Chem. Int. Ed.* **2001**, *40*, 74.

49. Wang, J.; Yan, J.; Tang, Z.; Xiao, Q.; Ma, Y.; Pei, J. *J. Am. Chem Soc.* **2008**, *130*, 9952.

50. Ma. C.; Mena-Osteritz, E.; Debaerdemaeker, T.; Wienk, M. M.; Janssen, R. A.; Bäuerle, P. *Angew. Chem. Int. Ed.* **2007**, *46*, 1679.

51. Feller, F.; Monkman, A. P. *Synth. Met.* **2001**, *116*, 149.

52. Wang, C.; Kilitziraki, M.; McBride, J. A. H.; Bryce, M. R.; Horsburgh, L. E.; Sheridan, A. K.; Monkman, A. P.; Samuel, I. D. *Adv. Mater.* **2000**, *12*, 217.

53. Zhou, Z.; Maruyama, T.; Kanbara, T.; Ikeda, T.; Ichimura, K.; Yamamoto, T.; Tokuda, K. *Chem. Commun.* **1991**, 1210.

54. Perepichka, I. F.; Perepichka, D. F.; Meng, H.; Wudl, F. *Adv. Mater.* **2005**, *17*, 2281.

55. Takahashi, A.; Lin, C.-J.; Ohshimizu, K.; Higashihara, T.; Chen, W.-C.; Ueda, M. *Polym. Chem.* **2012**, *3*, 479.

56. Yamamoto, T.; Zhou, Z.; Kanbara, T.; Kizu, K.; Tsukasa Maruyama, T.; Yoshiyuki Nakamura, Y.; Lee, B.-L.; Ooba, N.; Tomaru, S.; Kurihara, T.; Kaino, T.; Kubota, K.; Sasaki, S. *J. Am. Chem. Soc.* **1996**, *118*, 10389.

57. Trouillet, L.; Nicola, A. D.; Guillerez, S. *Chem. Mater.* **2000**, *12*, 1611.

58. DuBois, C. J.; Reynolds, J. R. *Adv. Mater.* **2002**, *14*, 1844.

59. Jenkins, I. H.; Salzner, U.; Pickup, P. G. *Chem. Mater.* **1996**, *8*, 2444.

60. Irvin, D. J.; DuBois, C. J., Jr.; Reynolds, J. R. *Synth. Met.* **2001**, *119*, 321.

61. Lee, B.-L.; Yamamoto, T. *Macromolecules* **1999**, *32*, 1375.

62. Yue, W.; Tian, H.; Hu, N.; Geng, Y.; Wang, F. *Cryst. Growth Des.* **2008**, *8*, 2352

63. Chevallier, F.; Charlot, M.; Katan, C.; Mongin, F.; Blanchard-Desce, M. *Chem. Commun.* **2009**, 692.

64. Ortiz, R. P.; Casado, J.; Hernandez, V.; Navarrete, J. T. L.; Letizia, J. A.; Ratner, M. A.; Facchetti, A.; Marks, T. J. *Chem.—Eur. J.* **2009**, *15*, 5023.

65. Fukumoto, H.; Kumagai, A.; Fujiwara, Y.; Koinuma, H.; Yamamoto, T. *Heterocycles* **2006**, *68*, 1349.

66. Kumagai, A.; Fukumoto, H.; Yamamoto, T. *J. Phys. Chem. B* **2007**, *111*, 8020.

67. Mello, J. V.; Finney, N. S. *Angew. Chem., Int. Ed.* **2001**, *40*, 1536.

68. Fang, A. G.; Mello, J. V.; Finney, N. S. *Org. Lett.* **2003**, *5*, 967.

69. Mello, J. V.; Finney, N. S. *J. Am. Chem. Soc.* **2005**, *127*, 10124.

70. Newkome, G. R.; Paudler, W. W. *Contemporary Heterocyclic Chemistry*; John Wiley: New York, 1982.

71. Clayden, J.; Greeves, N.; Warren, S.; Wothers, P. *Organic Chemistry*, Oxford University Press: Oxford, 2001, pp. 555-560.

72. Isaacs, N. S. *Physical Organic Chemistry*, 2nd edition, Addison Wesley Longman: London, 1995, pp. 153-154.

73. Ingold, C. K.; Ingold, E. H. *J. Chem. Soc.* **1926**, 1310.

74. The Nobel Prize in Chemistry 2010". Nobelprize.org, accessed on 25 April 2012. http://www.nobelprize.org/nobel_prizes/chemistry/laureates/2010/

75. Wu, X.; Anbarasan, P.; Neumann, H.; Beller, M. *Angew. Chem. Int. Ed.* **2010**, *48*, 9047.

76. Hantzsch, A. *Chem. Ber.* **1881**, *14*, 1637–1638.

77. Tschitschibabin, A. E. *J. Prakt. Chem.* **1924**, *107*, 122–128.

78. Paal, C. *Ber. Dtsch. Chem. Ges.* **1884**, *17*, 2756.

79. Knorr, L. *Ber. Dtsch. Chem. Ges.* **1884**, *17*, 2863.

80. Gronowitz, S.; Hörnfeldt, A.-B. *Thiophenes* Elsevier, 2004.

81. Hinsberg, O. *Ber.* **1910**, *43*, 901.

82. Beny, J.-P.; Dhawan, S. M.; Kagan, J.; Sundlass, S. *J. Org. Chem.* **1982**, *47*, 2201.

83. Kozhushkov, S.; Haumann, T.; Boese, R.; Knieriem, B.; Scheib, S.; Bäuerle, P.; de Meijere, A. *Angew. Chem. Int. Ed. Engl.* **1995**, *34*, 781.

84. King, A. O.; Okukado, N.; Negishi, E. *J. Chem. Soc., Chem. Commun.* **1977**, *19*, 683.

85. Milne, J. E.; Buchwald, S. L. *J. Am. Chem. Soc.* **2004**, *126*, 13028.

86. Sase, S.; Jaric, M.; Metzger, A.; Malakhov, V.; Knochel, P. *J. Org. Chem.* **2008**, *73*, 7380.

87. Negishi, E.; Hu, Q.; Huang, Z.; Qian, M.; Wang, G. *Aldrichimica Acta* **2005**, *38*, 71.

88. Echavarren, A. M.; Cárdenas, D. J. *Mechanistic Aspects of Metal-Catalyzed C,C- and C,X-Bond-Forming Reactions* in *Metal-Catalyzed Cross-Coupling Reactions (2nd Edition)* (Eds: A. De Meijere, F. Diederich), WILEY-VCH Verlag GmbH & Co. KGaA, Weinheim, **2004**, pp. 1-40.

89. Hegedus, L. S. *Transition Metals in the Synthesis of Complex Organic Molecules*; University Science Books: Mill Valley, 1994; pp 87–102.

90. Ortiz, R. P.; Casado, J.; Hernandez, V.; Lopez Navarrete, J. T.; Letizia, J. A.; Ratner, M. A.; Facchetti, A.; Marks, T. J. *Chem. Eur. J.* **2009**, *15*, 5023.

91. Mei, J.; Graham, K. R.; Stalder, R.; Reynolds, J. R. *Org. Lett.* **2010**, *12*, 660.

92. van Mullekom, H. A. M.; Vekemans, J. A. J. M.; Meijer, E. W. *Chem. Eur. J.* **1998**, *4*, 1235.

93. Jones, R. A.; Civcir, P. U. *Tetrahedron* **1997**, *53*, 11529.

94. Grayson, S. M.; Frechet, J. M. J. *Chem. Rev.* **2001**, *101*, 3819.

95. Smith, K.; Barratt, M. L. *J. Org. Chem.* **2007**, *72*, 1031.

96. Rocha, S. V.; Finney, N. S. *Org. Lett.* **2010**, *12*, 2598.

97. Zoltewicz, J. A.; Smith, C. L. *Tetrahedron* **1969**, *25*, 4331.

98. *Glossary of Terms Used in Photochemistry*, 2nd Ed., March 1996, IUPAC, Organic Chemistry Division, Commission on Photochemistry.

99. Cowan, D. O., Drisko, R. L. *Elements of Organic Photochemistry*; Plenum Press: New York, 1976.

100. Original reference where Kasha's rule is postulated: Kasha, M. *Faraday Discuss.* **1950**, *9*, 14.

101 . Rohatgi-Mukherjee. K. K. *Fundamentals of Photochemistry*, 2nd Ed.; New Age International Publishers: New Delhi, 1986, p. 95.

102. de Silva, A. P.; Gunaratne, H. Q. N.; Gunnlaugsson, T.; Huxley, A. J. M.; McCoy, C. P.; Rademacher, J. T.; Rice, T. *Chem Rev.* **1997**, *97*, 1515.

103. Gabrowski, Z. R.; Rotkiewicz, K.; Rettig, W. *Chem. Rev.* **2003**, *103*, 3899

104. Reichardt, C. *Chem. Rev.* **1994**, *94*, 2319.

105. Dimroth, K.; Reichardt, C.; Siepmann, T.; Bohlmann, F. *Justus Liebigs Ann. Chem.* **1963**, *661*, 1.

106. Ten Hoeve, W.; Wynberg, H.; Havinga, E. E.; Meijer, E. W. J. Am. Chem. Soc. **1991**, 113, 5887.

107. Meier, H.; Stalmach, U.; Kolshorn, H. *Acta Polym.* **1997**, *48*, 379.

108. Dennler, G.; Scharber, M. C.; Brabec, C. *J. Adv. Mater.* **2009**, *21*, 1323.

109. Englman, R.; Jortner, J. *J. of Lumin.* **1970**, *1-2*, 134.

110. Guo, X.; Ortiz, R. P.; Zheng, Y.; Hu, Y.; Noh, Y.; Baeg, K.; Facchetti, A.; Marks, T. J. *J. Am. Chem. Soc.* **2011**, *133*, 1405.

111. Garcia, P.; Pernaut, J. M.; Hapiot, P.; Wintgens, V.; Valat, P.; Garnier, F.; Delabouglise, D. *J. Phys. Chem.* **1993**, *97*, 513.

112. This field was the theme of a dedicated issue on *Chemical Reviews* in 2007, entitled *Organic Electronics and Optoelectronics*: Forrest, S. R.; Thompson, M. E. (Guest Editors) *Chem. Rev.* **2007**, *107*, 923.

113. Evans, D. H. *Chem. Rev.* **2008**, *108*, 2113.

114. Cardona, C. M.; Li, W.; Keifer, A. E.; Stockdale, D.; Bazan, G. C. *Adv. Mater.* **2011**, *23*, 2367.

115. Connelly, N. G.; Geiger, W. E. *Chem. Rev.* **1996**, *96*, 877.

116. Yue, W.; Tian, H.; Hu, N.; Geng, Y.; Wang, F. *Cryst. Growth Des.* **2008**, *8*, 2352.

117. Yoon, M.-H.; DiBenedetto, S. A.; Russell, M. T.; Facchetti, A.; Marks, T. J. *J. Am. Chem. Soc.* **2005**, *127*, 1348.

118. Yoon, M.-H.; DiBenedetto, S. A.; Russell, M. T.; Facchetti, A.; Marks, T. J. *J. Am. Chem. Soc.* **2007**, *19*, 4864.

119. Davis, B. L.; Melinger, J. S.; McMorrow, D.; Peng, Z.; Pan, Y. *J. Lumin.* **2004**, *106*, 301.

120. Lakowicz, J.R. Principles of Fluorescent Spectroscopy, 2nd ed.; Kluwer Academic: New York, 1999.

121. Demas, J. M.; Grosby, G. A. J. Phys. Chem., 1975, 75, 991.

122. Berlman, I. B. Handbook of Fluorescent Spectra. Academic Press: New York, NY, 1965.

123. Rohbogner, C. J.; Wunderlich, S. H.; Clososki, G. C.; Knochel, P. *Eur. J. Org. Chem.* **2009**, 1781.